# Chemotherapy Induced Sensory Neuropathy Depends on Non-Linear Interactions with Cancer

A Dissertation
Presented to
The Academic Faculty

By

Dr. Stephen Nicholas Housley, PT, DPT
B.S. University of Georgia, 2013
D.P.T. Georgia State University, 2016

In Partial Fulfilment
Of the Requirements for the Degree of
Doctor of Philosophy in
Applied Physiology

Georgia Institute of Technology
May, 2020

# Chemotherapy Induced Sensory Neuropathy Depends on Non-Linear Interactions with Cancer

Approved by:

Dr. T. Richard Nichols
School of Biological Sciences
*Georgia Institute of Technology*

Dr. Tim C. Cope, Advisor
School of Biological Sciences and
Coulter Department of Biomedical Engineering
*Georgia Institute of Technology*

Dr. Peter Wenner
Department of Physiology
*Emory University*

Dr. John F. McDonald
School of Biological Sciences
*Georgia Institute of Technology*

Dr. Edward Balog
School of Biological Sciences
*Georgia Institute of Technology*

Date Approved: [March 09, 2020]

*This work is dedicated to my wife, Emily.*

*You empower me to be my best in all endeavors.*
*This work would not be possible without you.*

*I owe you a lifetime of gratitude*
*For your unwavering love and support.*

# ACKNOWLEDGMENTS

None of the work in this dissertation would have been possible without the mentorship, patience, generosity, and support of Dr. Timothy C. Cope. You have been invaluable to my education and have made an enormous impression on my professional and personal development. It has been an honor to work alongside you and learn from you. I look forward to continuing our productive relationship for many years to come as I aim to become an independent investigator. I will be forever grateful for mentorship and friendship.

I would like to thank Paul Nardelli, your unwavering support from day one and countless hours of instruction have left me with innumerable scientific and problem-solving abilities. I would also like to thank Dr. Dario Carrasco and Dr. Travis Rotterman for contributing to my scientific development and for providing vital feedback during our many discussions, you all have helped push me towards my long-term goals.

I would also like to thank Dr. John F. McDonald and all the members of your lab for being so inviting and providing such an enriching environment for me to develop new skills and appreciation for new areas of scientific discovery. These opportunities have provoked exciting questions that will hopefully establish my scientific career going forward.

I would like to thank Dr. Mark M. Rich and Dr. Randy Powers for being such wonderful collaborators. It has been a privilege to learn from your expertise. Your unique insights have inspired me to approach science questions from novel directions.

I would like to thank Dr. Thomas Burkholder for delivering the single most challenging yet enjoyable course of my graduate career. Thankfully, your mentorship persisted

throughout my training and has left an indelible impact on my scientific process, thank you.

I would also like to thank the Georgia Institute of Technology, specifically the Applied Physiology Ph.D. program for giving me this opportunity, Eric Woods and Walter Henderson, members of the Materials Characterization Facility for introducing me to novel analytic approaches and the Physiological Research Laboratory for your dedication to animal care.

I would like to thank my committee members for their dedication, time, and mentorship as I have progressed through this my program. I would also like to thank all my friends and family for their support through the years. I would also like to collectively thank all lab members of the Cope Lab and our collaborators, for making me feel like family.

Lastly, I would like to thank my wife, Emily for her support and for always reminding me of and pushing me to pursue my goals. I simply could not have done this without you, thank you.

## Table of Contents

# List of Tables

# List of Figures

# Summary

For the constellation of neurological disorders known as chemotherapy induced neuropathy, mechanistic understanding, and treatment remain deficient. In **project one**, I leveraged a multi-scale experimental approach to provide the first evidence that chronic sensory neuropathy depends on non-linear interactions between cancer and chemotherapy. Global transcriptional profiling of dorsal root ganglia revealed amplified differential expression, notably in regulators of neuronal excitability, metabolism and inflammatory responses, all of which were unpredictable from effects observed with either chemotherapy or cancer alone. Systemic interactions between cancer and chemotherapy also determined the extent of deficits in sensory encoding *in vivo* and ion channel protein expression by single mechanosensory neurons, with the potassium ion channel Kv3.3 emerging as candidate mechanisms explaining sensory neuron dysfunction. The sufficiency of this novel molecular mechanism was tested in an *in silico* biophysical model of mechanosensory function. Finally, validated measures of sensorimotor behavior in awake behaving animals confirmed that dysfunction after chronic chemotherapy treatment is exacerbated by cancer. Notably, errors in precise fore-limb placement emerged as a novel behavioral deficit unpredicted by our previous study of chemotherapy alone. These original findings identify novel contributors to peripheral neuropathy, and emphasize the fundamental dependence of neuropathy on the systemic interaction between chemotherapy and cancer across multiple levels of biological control.

In **project two**, I extend study to multiple classes of mechanosensory neurons that are necessary for generating the information content (population code) needed for proprioception. I first tested the hypothesis that exacerbated neuronal dysfunction is conserved across multiple classes of mechanosensory neurons. Results revealed co-

suppression of specific signaling parameters across all neuronal classes. To understand the consequences of corrupt population code, I employed a long-short-term memory neural network (LSTM), a deep-learning algorithm, to test how decoding of spatiotemporal features of movement are altered after chemotherapy treatment of cancer. Results indicate that spiking activity from the population of neurons in animals with cancer, treated by chemotherapy contain significantly less information about key features of movement including, e.g. timing, magnitudes, and velocity. I then modeled the central nervous systems (CNS) capacity to compensate for this information loss. Even under optimal learning conditions, the inability to fully restore predictive power suggests that the CNS would not be able to compensate and restore full function. Our results support our proposal that lasting deficits in mobility and perception experienced by cancer survivors can originate from sensory information that is corrupted and un-interpretable by CNS neurons or networks.

Collectively, I present the first evidence that chronic cancer neuropathy cannot be explained by the effects of chemotherapy alone but instead depend on non-linear interactions with cancer. This understanding is a prerequisite for designing future studies and for developing effective treatments or preventative measures.

# CHAPTER 1. INTRODUCTION

### *Societal Burden of Cancer*

Cancer diagnoses represent an ever-increasing burden on global society which is expected to grow to over 20 million new cases annually by 2025 (Ferlay, Soerjomataram *et al.* 2015). While the incidence of cancer diagnoses expands (Center, Jemal *et al.* 2009), increased screening and advanced treatment strategies, such as chemotherapies are extending disease-free lifespans (André, Boni *et al.* 2004; Edwards, Ward *et al.* 2010; Bosetti, Levi *et al.* 2011; Avan, Postma *et al.* 2015).

### *Chemotherapy's Benefit to Survival*

One such example, platinum-based chemotherapies, are central pillars of contemporary cancer treatment. Oxaliplatin (OX), a third-generation platinum-based agent, has been shown to extend lifespans by improving disease free survival up to 80%, reduce toxicity and improve tolerability, especially for older patients (Galanski, Jakupec *et al.* 2005; Montagnani, Turrisi *et al.* 2011; Johnstone, Park *et al.* 2014). This superior efficacy as a first-line treatment for the 1.4 million new diagnoses of colorectal cancer (Torre, Bray *et al.* 2015) and adjunctive therapy for millions of bladder, ovarian and testicular cancers patients (Andre et al 2009; de Gramont, Et al 2000; Taylor et al 2014; Fu et al 2006) helps explain why it is estimated that approximately 50% of all patients diagnosed with cancer undergoing chemotherapeutic treatment receive a platinum-based chemotherapy such as OX (Galanski, Jakupec et al. 2005; (Johnstone, Park et al. 2014).

### *Dark side of chemotherapy*

Despite impressive efficacy, nearly all patients treated with OX and other platinum-based drugs are afflicted by severe off-target, neurotoxic side-effects such as pain, sensory

abnormalities, fatigue, mobility and balance deficits (Bennett, Park *et al.* 2012). This constellation dose-limiting side effects is collectively referred to as Chemotherapy-Induced Peripheral Neuropathy (CIPN), diminishes quality of life and limits functional capacity (Cavaletti, Bogliun *et al.* 1995; Quasthoff and Hartung 2002; André, Boni *et al.* 2004; Argyriou, Polychronopoulos *et al.* 2008; Alcindor and Beauger 2011; Mols, Beijers *et al.* 2013; Tofthagen, Donovan *et al.* 2013; Argyriou, Kyritsis *et al.* 2014; Beijers, Mols *et al.* 2014; Avan, Postma *et al.* 2015). While, *acute* CIPN symptoms may decline after caseation of treatment, they frequently persist, leaving many patients with *chronic* CIPN that does not improve even years after treatment (Dietrich, Han *et al.* 2006; Park, Lin *et al.* 2011; Park, Goldstein *et al.* 2013; Aaronson, Mattioli *et al.* 2014; Seretny, Currie *et al.* 2014; Marshall, Zipp *et al.* 2017).

***Seeking Treatments for CIPN***

Various approaches to prevent *acute* and ameliorate *chronic* CIPN have been attempted (Adelsberger, Quasthoff *et al.* 2000; Webster, Brain *et al.* 2005; Ishibashi, Okada *et al.* 2010; Saif, Syrigos *et al.* 2010; Sittl, Lampert *et al.* 2012; Kagiava, K Kosmidis *et al.* 2013). However, these approaches have yet to show efficacy in large randomized control trials, leaving cancer patients' symptoms essentially unabated (Loprinzi, Qin *et al.* 2013; Hershman, Lacchetti *et al.* 2014; Sisignano, Baron *et al.* 2014). Given the lack of supporting evidence, The American Society of Clinical Oncologists recently published clinical practice guidelines that concluded, few, if any, therapeutic strategies are recommended (Hershman, Lacchetti *et al.* 2014).

***Knowledge gaps and motivations***

Abject failure of these clinical trials to lessen symptoms of CIPN present prima fascia evidence of knowledge gaps (Hershman, Lacchetti *et al.* 2014), promulgated by problems with preclinical study we correct in this work, notably 1) focus on transient

(*acute*) CIPN signs and symptoms at the expense of understanding lasting *chronic* effects, 2) flawed experimental methodologies, and 3) failure to consider role of cancer in pathophysiology of CIPN.

*Focus on Acute CIPN*

While it is clear that platinum-based drugs have the potential to disrupt neuronal excitability (Sittl, Lampert *et al.* 2012), the majority of studies have focused on elucidating underlying mechanisms of *acute* CIPN symptomology that do not persist, e.g. cold-induced pain, muscle spasms and cramps (Alcindor and Beauger 2011; Seretny, Currie *et al.* 2014). *Acute* CIPN symptoms that are readily attributable to neural hyper-excitability. This has been verified by axon-excitability testing in peripheral nerves (Quasthoff and Hartung 2002; Krishnan, Goldstein *et al.* 2006; Argyriou, Polychronopoulos *et al.* 2008; Alcindor and Beauger 2011; Seretny, Currie *et al.* 2014) along with numerous demonstrations of disrupted ion channels, e.g. Na, K, and Ca ion channels, Ca chelation, and TRP channels, all of which have the potential in increase neuronal excitability (Grolleau, Gamelin *et al.* 2001; Sittl, Lampert *et al.* 2012; Sittl, Lampert *et al.* 2012; Kagiava, K Kosmidis *et al.* 2013; Sisignano, Baron *et al.* 2014; Kanat, Ertas *et al.* 2017).

However, many fewer studies have examined *chronic* CIPN, which results in lasting impairments to cancer survivors. These impairments are associated with functional movement disorders e.g. reduced sensation, impaired balance, discoordination (Saif, Syrigos *et al.* 2010; Marshall, Zipp *et al.* 2017) and are commonly attributed to dying-back, length-dependent axon degeneration (Argyriou, Kyritsis *et al.* 2014; Avan, Postma *et al.* 2015). However, given that physical evidence from nerve-conduction studies suggest that axon degeneration is typically minimal <25% (Burakgazi, Messersmith *et al.* 2011), additional mechanisms must be at play. Chronic CIPN can occur even in cases

where no detectable reduction in either nerve-evoked action potentials or epidermal nerve density exist (Burakgazi, Messersmith *et al.* 2011). Based on reports from our lab (Vincent, Wieczerzak *et al.* 2016), we speculated that rather than by structural degeneration alone, chronic CIPN symptoms might depend on functional impairment of sensory neurons attributable to neuronal hypo-excitability based on a failure to maintain firing in response to fixed levels of stimulation (Vincent, Nardelli *et al.* 2015; Vincent, Wieczerzak *et al.* 2016). Discovering no receptor or axonal degeneration provides further evidence for this hypothesis, despite this being the pervasive explanation in the literature (Vincent, Nardelli *et al.* 2015; Vincent, Wieczerzak *et al.* 2016).

*Methodology*

Another limitation is that the effects of platinum-based chemotherapy on neuronal excitability have been examined almost exclusively using experimental methodologies, which themselves alter neuronal excitability (Button, Kalmar *et al.* 2008; Yamamoto, Tsuboi *et al.* 2016; Yamamoto, Ono *et al.* 2016). With neuronal excitability influenced by a myriad of factors (Desai, Rutherford *et al.* 1999; Rekling, Funk *et al.* 2000; Kuo, Siddique *et al.* 2005; Grubb and Burrone 2010; Panatier and Robitaille 2012), experimental effects confound identification of the actual mechanisms by which platinum-based chemotherapy alone alter neuronal excitability (Devor, Govrin-Lippmann *et al.* 1993). For example, neuronal excitability is altered by damage, which is an inevitable consequence with tissue extraction used during in vitro study, a common experimental approach utilized and a likely contributor to abnormal neuronal excitability without platinum-based chemotherapy (Tulleuda, Cokic *et al.* 2011). Investigations also fall short when failing to reproduce the in vivo milieu, including interaction with systemic changes induced by platinum-based chemotherapy, e.g. inflammatory and oxidative responses known to impact excitability (Pardillo-Díaz, Carrascal *et al.* 2015; Vezzani and

Viviani 2015; Barbosa, Xiao *et al.* 2017; Tzour, Leibovich *et al.* 2017; Wang, Zhang *et al.* 2017).

*Cancer*

Experimental investigations of CIPN also fall short when failing to reproduce the clinically relevant condition when platinum-based chemotherapy effects coexist cancer effects (Cain, Wacnik *et al.* 2001; Klampfer 2011; Zheng, Fang *et al.* 2012; Cai, Fang *et al.* 2015; Pardillo-Díaz, Carrascal *et al.* 2015; Vezzani and Viviani 2015; West, McCuaig *et al.* 2015; Mager, Wasmer *et al.* 2016; Barbosa, Xiao *et al.* 2017; Kovalchuk, Ilnytskyy *et al.* 2017; Tzour, Leibovich *et al.* 2017; Wang, Zhang *et al.* 2017).

To date, cancer is excluded in preclinical studies of CIPN. However, since the clinical utility of chemotherapy rest solely on treating cancer, we must consider how cancer contributes to CIPN independent of or in combination with chemotherapy (Ahles 2012; Boyette-Davis, Eng *et al.* 2012; van Erning, Janssen-Heijnen *et al.* 2016). Patients with tumors located outside the nervous system can exhibit subclinical peripheral neuropathy even before chemotherapy or surgical intervention (Ahles 2012; Boyette-Davis, Eng *et al.* 2012; van Erning, Janssen-Heijnen *et al.* 2016). These observations are consistent with cancer's effect on signaling pathways known to affect neuronal excitability (Cain, Wacnik *et al.* 2001; Klampfer 2011; Zheng, Fang *et al.* 2012; Cai, Fang *et al.* 2015; Pardillo-Díaz, Carrascal *et al.* 2015; Vezzani and Viviani 2015; West, McCuaig *et al.* 2015; Mager, Wasmer *et al.* 2016; Barbosa, Xiao *et al.* 2017; Kovalchuk, Ilnytskyy *et al.* 2017; Tzour, Leibovich *et al.* 2017; Wang, Zhang *et al.* 2017). Several signaling pathways intersect with ones affected by chemotherapy, thereby opening the possibility for dynamical interaction. For example, the frequency and gain of neuronal repetitive firing is impaired by oxidative stress (Pardillo-Díaz, Carrascal *et al.* 2015). Because colorectal cancer and chemotherapy treatment each induce oxidative stress (Boyette-

Davis, Walters *et al.* 2015), their combination may amplify neuronal dysfunction. The prototypical inflammatory cytokines, e.g. IL-1β, TNF-α, IL-6 are activated by chemotherapy and colorectal cancer (Klampfer 2011; West, McCuaig *et al.* 2015; Mager, Wasmer *et al.* 2016). These pathways present additional sites where dynamical interactions may disrupt neuronal excitability (Vezzani and Viviani 2015; Barbosa, Xiao *et al.* 2017; Tzour, Leibovich *et al.* 2017). Alternatively, cancer and chemotherapy may act through pathways that are hidden from investigations of chemotherapy alone. These data provide strong rationale to suspect that cancer and chemotherapy may dynamically interact to exacerbate CIPN. While chemotherapy alone may be necessary to induce neuronal dysfunction in preclinical models, it may not be sufficient to capture the mechanistic underpinnings of the clinically relevant CIPN condition when cancer is present (Sisignano, Baron *et al.* 2014).

***Overall Objectives***

My overall objective was to investigate the role of cancer in the development of chronic neuropathy in living animals. By doing so, I correct many of the limitations of previous preclinical studies to gain mechanistic understanding of the clinically relevant *chronic* CIPN to meet the urgent and unmet need of cancer survivors globally. To accomplish these objectives, I employed a multi-scale experimental approach centered on *in vivo* electrophysiologic recordings from intact neurons. Further utilization of high-throughput, whole transcriptome analysis, protein expression studies, validated measures of sensorimotor behavior in awake behaving animals, *in silico* biophysical modeling, and deep-learning decoding algorithms afforded comprehensive insight into establishing the independent and combinatorial effects of chemotherapy and cancer on the sensory nervous system.

# CHAPTER 2. GENERAL METHODS

### *Animal Care*

All procedures and experiments were approved by the Georgia Institute of Technology Institutional Animal Care and Use Committee. Adult male rats (250-350g) were studied in terminal experiments only and were not subject to any other experimental procedures. All animals were housed in clean cages and provided food and water ad libitum in a temperature- and light-controlled environment in Georgia Institute of Technology's Animal facility.

### *Rat model of Colorectal Cancer*

We studied the rat model of colorectal cancer developed in Fisher 344 (F344) rats and known as polyposis in rat colon ($Apc^{Pirc/+}$) (Amos-Landgraf, Kwong *et al.* 2007). Pirc rats were generated from a germline mutation in the Apc gene ($Apcam^{1137/+}$). This mutation is shared by 80% of patients with colorectal cancer (Kwong and Dove 2009). We studied age-matched male rats (4 months). This age has been previously validated to result in 100% incidence of animals (Irving, Yoshimi *et al.* 2014) developing colon cancer and was consistent with our population. $Apc^{Pirc/+}$ rats exhibit: regional distribution of tumors that best represents that seen in human colorectal cancer (Irving, Yoshimi *et al.* 2014); histopathology and morphology closely resembling human tumors (adenocarcinomas) (Washington, Powell *et al.* 2013; Femia, Luceri *et al.* 2015), up-regulation of well-established pro-growth factors, e.g. β-catenin and EGFR and proliferative makers Ki-67 seen in human carcinogenesis (Amos-Landgraf, Kwong *et al.* 2007), dramatic increases in Wnt signaling believed to be a key factor in human colorectal carcinogenesis (Bienz and Clevers 2000), presence of apoptotic resistant cells unique to carcinogenesis (Figure 1) (Amos-Landgraf, Kwong *et al.* 2007; Irving, Yoshimi *et al.* 2014), oxaliplatin

(OX)-induction of apoptosis in colon tumors, survivability (12-15 months) enabling long-term investigation of OX's chronic effects (Amos-Landgraf, Kwong *et al.* 2007).

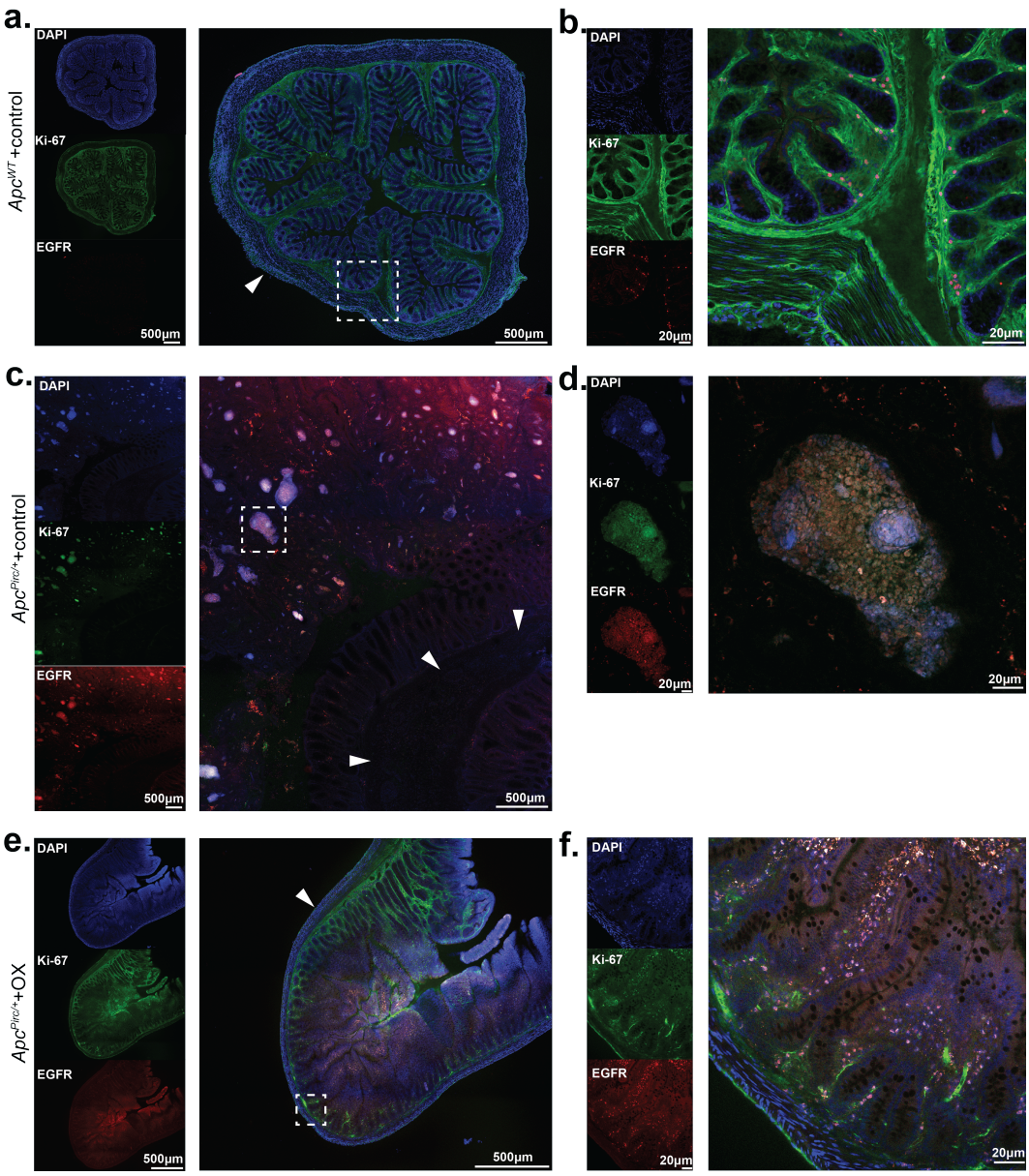


**Figure 1.**

**Immunohistochemical and morphological analyses of healthy and tumor bearing colons. a-f,** Confocal images of a colon from *Apc*$^{WT}$ +control rat (**a, b**) and colon and colon tumors from *Apc*$^{Pirc/+}$+control (**c, d**) and *Apc*$^{Pirc/+}$+ OX rats (**e, f**). Immunolabeling shows expression of DAPI and Ki-67, and EGFR a measure proliferative growth associated with tumor progression. White dotted boxes in wide-field images (**a, c, e**) outline region of interest (**b, d, f**). White arrows indicate smooth muscle boundary used as anatomical reference.

***Chemotherapy treatment***

OX (Cyclohexane-1,2-diamine; oxalate; platinum(2+)) was injected intraperitoneal (i.p.) once a week (10mg/Kg, 1 ml 5% dextrose in DMSO ) in aged matched rats (4 months) to achieve a cumulative dose of 70 mg/Kg over 7 weeks, which scales to a human dose of 420mg/m2 (conversion based on rat body surface area and Km= 6) (Reagan-Shaw, Nihal *et al.* 2008; Nair and Jacob 2016). Further, this dose minimizes nerve degeneration in patients (Grisold, Cavaletti *et al.* 2012; Park, Goldstein *et al.* 2013). Rats in each group were randomized to receive injections of oxaliplatin (OX), a platinum based compound known to induce neuropathy in patients with cancer and shown in our previous studies to induce chronic movement disorders (Vincent, Wieczerzak *et al.* 2016). OX was administered by intraperitoneal injection on a human-scaled dose schedule (Vincent, Wieczerzak *et al.* 2016). The OX treatment schedule resulted in four experimental groups used for all studies: $Apc^{WT}$+control, $Apc^{WT}$+OX, $Apc^{Pirc/+}$+control and $Apc^{Pirc/+}$+ OX (Figure 2).

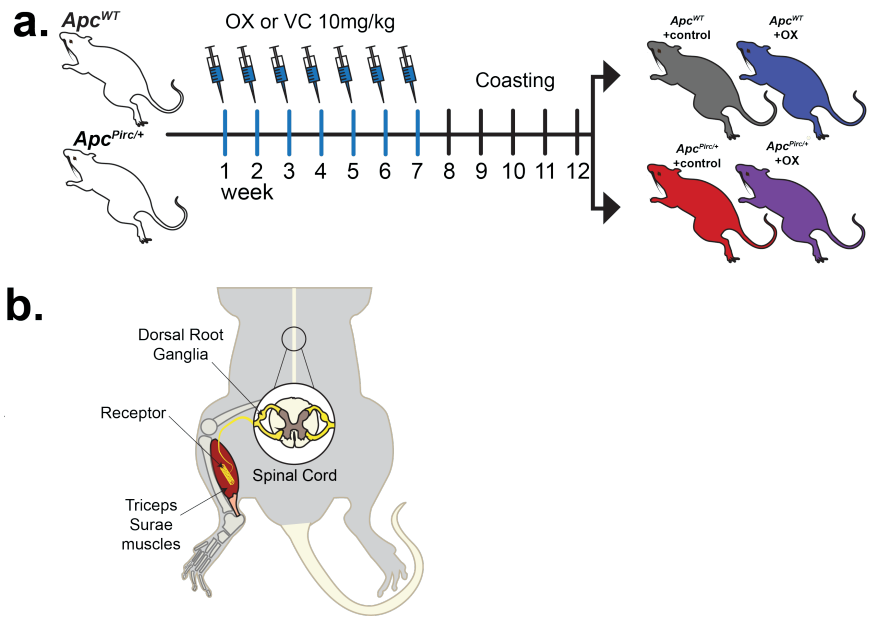


***Figure 2.***

**Treatment Schedule and Targets.** a, Schematic of treatment schedule of oxaliplain (OX) and vehicle control (VC) generating four independent experimental groups in wild-type (*Apc*$^{WT}$) and autosomal dominant mutation of the adenomatous polyposis coli gene (*Apc*$^{Pirc/+}$): *Apc*$^{WT}$+control, *Apc*$^{WT}$+OX, *Apc*$^{Pirc/+}$+control, and *Apc*$^{Pirc/+}$+OX rats. b, Diagram of experimental targets of lumbosacral dorsal root ganglia (DRG) and muscle for assaying transcriptomes and/or cell-specific protein expression in rat models.

Clinical dose extrapolation, e.g. converting human OX doses to rat OX doses was based on body surface area, which is a better representation of metabolic rate than mass. Metabolic rate is a key determinant of drug pharmacokinetic and pharmacodynamics and scales non-linearly with animal size, e.g. the body surface area in relation to body weight decreases. In other words, larger animals have lower specific metabolic rate (the metabolic rate per unit mass) whereas metabolic rate to surface area remains relatively conserved (Sharma and McNeill 2009; Nair and Jacob 2016).

Throughout treatment, rats were frequently monitored for pain or distress. No individual rat reached set criteria established for early removal from the study: greater than 10% weight loss, pain or distress assessed by vocalization, absence of grooming, and rats show normal exploratory and feeding behaviors.

***Surgical Procedures***

Terminal in vivo experiments were performed 5 weeks after achieving clinically relevant chemotherapy doses. They were designed to measure the firing of individual intact sensory neurons in response to physiologically relevant muscle contraction and stretch with electrophysiological techniques. All in vivo procedures are well established in our lab and have been extensively described in previous publications (Haftel, Bichler *et al.* 2004; Bullinger, Nardelli *et al.* 2011; Vincent, Wieczerzak *et al.* 2016; Nardelli, Powers *et al.* 2017; Vincent, Gabriel *et al.* 2017). Briefly, rats were deeply anesthetized by inhalation of isoflurane (5% in 100% $O_2$), intubated via a tracheal cannula, then maintained for the remainder of the experiment (up to 12 hours by 1.5–2.5% in 100% O2). Respiratory rate, $pCO_2$, core temperature, pulse rate and $pO_2$ were continuously monitored and maintained by adjusting anesthesia and adjusting heat sources. Dorsal roots (lumbar L4–6), muscles, and nerves in the left hindlimb were prepared for stimulation and recording with the rat fixed in a rigid frame at the snout, vertebral bodies, distal tibia, and distal femur (knee angle 120°). Triceps surae muscles (lateral and medial gastrocnemii and soleus) were partially freed of surrounding connective tissue and marked for their resting length ($L_o$) at ankle angle 90° before their common Achilles tendon was severed at the calcaneus and tied directly to the lever arm of a force- and length-sensing servomotor (model 305B-LR; Aurora Scientific). Triceps surae nerves were loosely positioned in continuity on a unipolar silver stimulating electrode, and all other hindlimb nerves were crushed to reduce extraneous neuronal activity. Dorsal

rootlets were freed in continuity from overlying connective tissue and supported on bipolar hook electrodes positioned close to the rootlet's entry into the dorsal spinal cord. Exposed tissues were covered with warm mineral oil in pools formed by attaching the edges of severed skin to the recording frame (*Figure 3*).

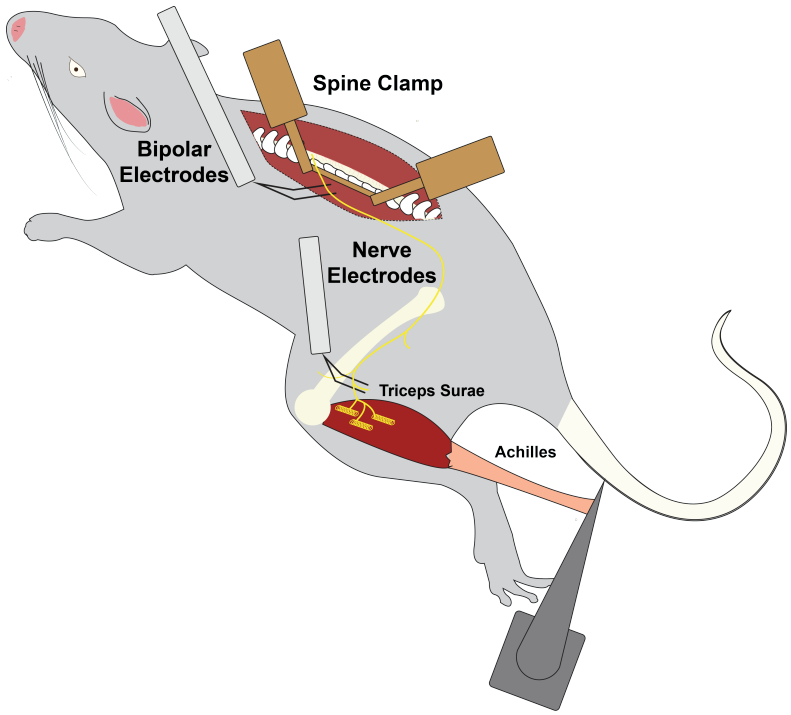


**Figure 3.**

**In Vivo Design**. Diagram of anesthetized rat stabilized in spine clamps for physiological recordings. Experiments focus on the triceps surae muscles (soleus and medial and lateral gastrocnemius), triceps surae nerves, and intra-axonally from single sensory neurons in dorsal roots in the lumbosacral (L4-S2) spinal cord.

### *Bayesian Data Analysis*

*General Approach*

To determine the effect of cancer and/or chemotherapy on various parameters, e.g. neuronal signaling, sensorimotor behavioral factors, etc., we employed Bayesian data

analytic approaches to empirically derive the full joint posterior probability distribution of parameters on which inferences were applied. Bayesian analytic techniques were chosen because they present noteworthy advantages over frequentist analysis such as null hypothesis statistical testing e.g. *t*-test and ANOVA. Bayesian analytics do not require making assumptions that traditional ANOVA necessitates (e.g. normally distributed data, heteroscedasticity, multiple-test correction) (Kruschke 2013; Kruschke 2014). There is no need to generate sampling distributions, e.g. *t*, *F*, $x^2$, and determine whether the probability that fictitious data generated from the null distribution would be more extreme than the observed data i.e. formal definition of *p*-values. In addition to their ambiguity, *p* values provide an incoherent framework for reallocation of evidential support because of their high sensitivity to stopping and testing intentions (Wagenmakers 2007; Kruschke 2013). Instead, Bayesian estimation derives the entire joint posterior distribution of all parameters simultaneously (Eq. 1) and provides the ability to examine individual parameters, such as the threshold of spindle firing and peak firing rate in chemotherapy treated animals compared to control without the need to correct for multiple tests on the data. In other words, there is no need for *p* values and *p* value-based confidence intervals (e.g. 95%CI). Instead, Bayesian inference and decision making provides a simpler and more intuitive interpretation of the evidence by directly examining the posterior distribution to see which parameter values and ranges are most credible. Further, unlike null hypothesis statistical testing, that can only reject or fail to reject a null hypothesis, by reallocating credibility across the parameter space, Bayesian inference generates evidence and uncertainty in that evidence to support *or* refute the null *or* alternative hypothesis (when a region of practical equivalence (ROPE) is defined). While parameter estimation is not unique to Bayesian approaches (e.g. maximum likelihood estimation) uncertainty in parameter

estimates are typically expressed in the form of confidence intervals which rests on the *p* value along with the limitations discussed above.

$$P(\theta|x) = \frac{P(x|\theta)\,P(\theta)}{P(x)}\,, \qquad \theta_j \sim N(\mu,\sigma)\,,\; x_{i,j} \sim f(\theta_j)$$

Where $\theta = (\mu, \sigma)$ is a set of all unknown model parameters as defined above, $x$ denotes a set of mean-centered and standardized dynamic conditioned stretch reflex (cSR) response measurements. The conditional distribution of $\theta$ given data (i.e. $P(\theta|x)$) denotes the posterior distribution. The $P(x|\theta)$ is the distribution of $x$, which is a likelihood function when viewed as a function of model parameters, assuming that $\theta$ is known. The $P(\theta)$ is the distribution of $\theta$ without any knowledge on data, referred to as a prior distribution. The equation above demonstrates that the posterior distribution of $\theta$ is proportional to the product of the likelihood of $\theta$ given $x$ and the prior distribution of $P(\theta)$.

*Inferences*

Bayesian inference, e.g. analogous to traditional hypothesis testing, was performed by analyzing the probability mass of the parameter region in question we defined as the 95% highest posterior density interval (HDI) hereinafter referred to as the HDI. Value contained within the HDI are more credible than values outside. The HDI was used to make unbiased inferences by directly comparing the posterior probability distributions between two (or more) contrasts of interests e.g. mean-comparisons testing. For example, when performing a mean comparison test, an HDI of a credible difference distribution that does not span zero indicates that the model predictions for the two conditions of interest are different from each other. This provides strong unbiased evidential support to simultaneously support the alternative and refute the null hypothesis that the parameters for both populations are equal. Alternatively, if an HDI of

a credible difference distribution spans zero, that indicates the model predictions for the two conditions do not differ. Unlike null hypothesis statistical testing, Bayesian techniques afford the ability to accept the null hypothesis by defining a ROPE (region of practical equivalence) range, e.g. values between -0.1 and 0.1. When the 95% HDI falls completely within the ROPE region we declare the ROPE value accepted. We report the expected value for the parameter alongside 95% credible intervals using the HDI unless otherwise noted.

*Models*

All models were developed in a fully hierarchal Bayesian framework with the *rstanarm* package (2.18.1) (Gabry and Goodrich 2018) in the R environment (3.5.0) (Team 2018). *Rstanarm* implements regression models in *stan* (Carpenter, Gelman *et al. 2017)*, which are fit using Hamiltonian Markov Chain Monte Carlo sampling to compute credible parameter values (Brooks, Gelman *et al.* 2011; Hoffman and Gelman 2014). For intercepts and predictors, we use Student's *t*-distribution with mean zero and four degrees of freedom as the prior distribution. The scale of the prior distribution is 10 for the intercept and 2.5 for the predictors. Each model was run with four independent chains for 400 warm-up, 4,000 sampling steps and every second sample (thinning) was discarded. For all parameters, the number of effective (*n_eff*) samples was >500. Convergence was assessed and assumed to have reached the stationary distribution by ensuring that the Gelman–Rubin shrinkage statistic (rhat, $\hat{R}$) statistic for all reported parameters was <1.05 and Monte Carlo standard error of the parameter means was <0.002 (Gelman and Rubin 1992) . We report the expected mean parameter values alongside 95% credible intervals using the HDI. For clarity, an example 'Kruschke style' hierarchical model diagram is included and should be interpreted as the graphical representation of mathematical model used for analysis (*Figure 4*). Reading the

diagrams should start at the bottom with a description and nature of the data being modeled, then described the likelihood function, then described the prior (top). Diagrams were created in LibreOffice (Version: 6.0.6.2).

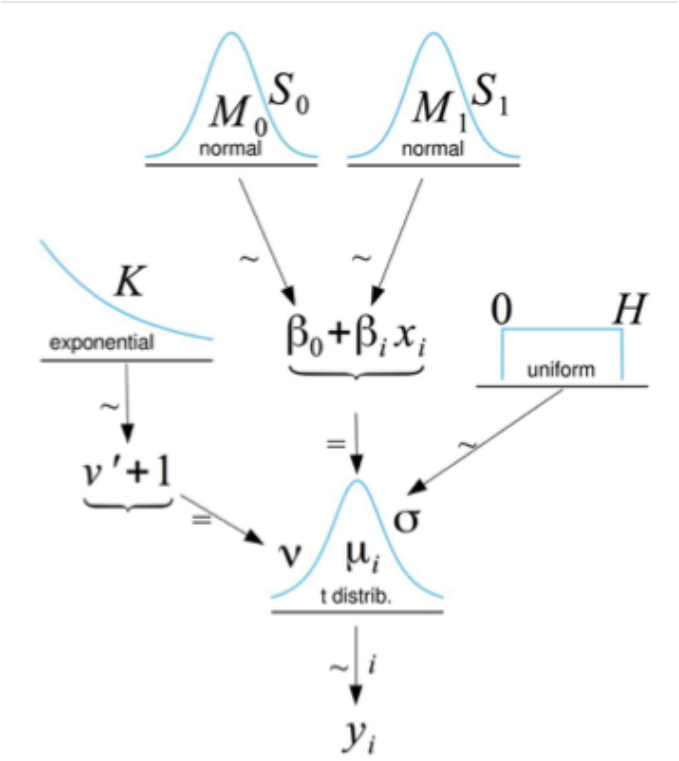


**Figure 4.**

**'Kruschke style' hierarchical model graphical diagram.** Robust Bayesian linear regression was used to model the data $y_i$ as a t-distributed random value around the central tendency $\mu_i = \beta_0 + \beta_1 x_i$. The intercept $\beta_0$ and slope $\beta_1$ were given broad normal priors that are vague to the scale of data. $\sigma$ was given an uninformative uniform prior, and the normality parameter v was given a broad exponential prior.

*Model Validation*

To estimate and validate model performance of our fitted Bayesian models, for the purposes of model comparison and model selection (Geisser and Eddy 1979; Vehtari and Lampinen 2002; Ando and Tsay 2010; Vehtari and Ojanen 2012), we estimated the

out-of-sample predictive accuracy (Figure 5) using Pareto-smoothed importance sampling (PSIS (Vehtari, Gelman *et al.* 2017)) to perform leave-one-out cross (LOO) validation. Exact cross-validation requires refitting models with different training data; however, one can approximate LOO by importance sampling (Gelfand, Dey *et al.* 1992; Gelfand 1996). Importance sampling is a simple statistical procedure for computing/estimating expectations, e.g. of a particular distribution, while only having samples generated from a different, approximating distribution than from the target distribution. Expectations with respect to the target distribution can be estimated by weighting the importance samples by the ratio of their densities. However, importance sampling can result in noisy estimates (Epifani, MacEachern *et al.* 2008), when the approximating distribution is narrower than the target distribution or when the approximating distribution is a poor fit, resulting in the distribution having a heavy right tail and unstable estimates.

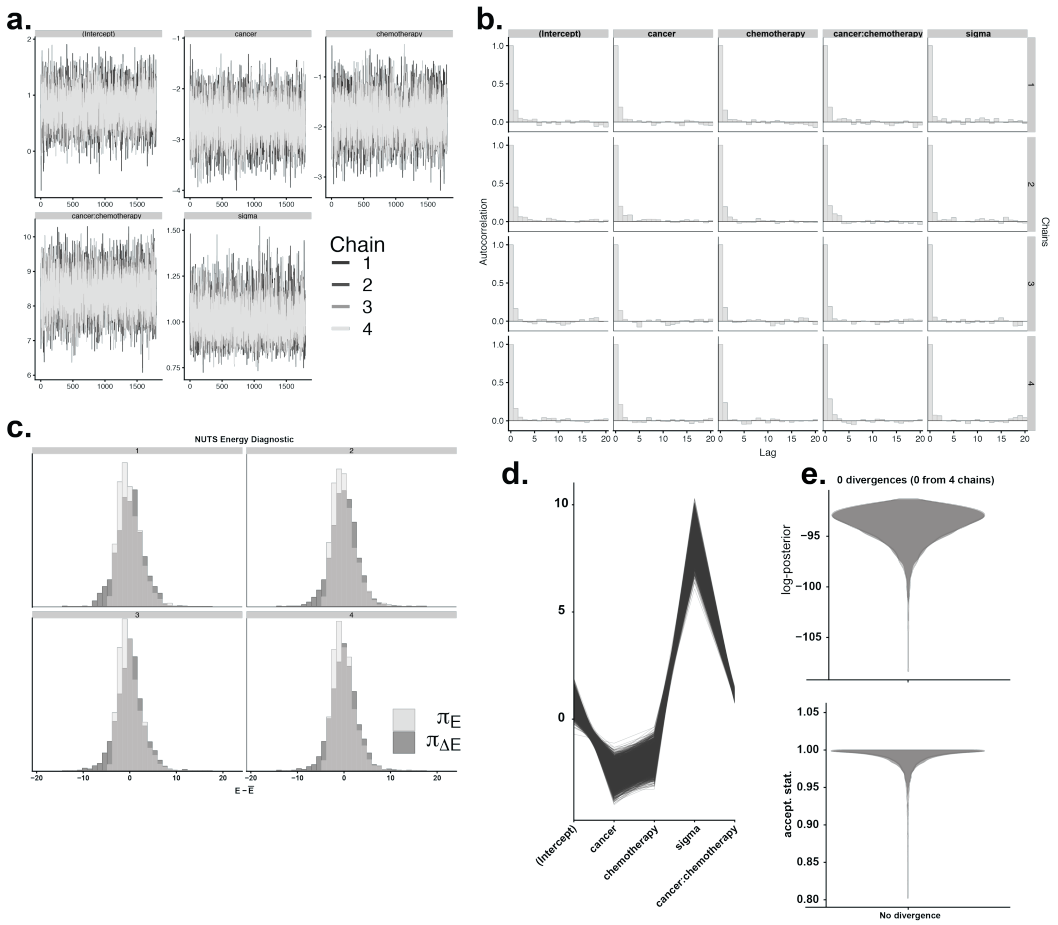


## ***Figure 5.***

**Exemplar Graphical Bayesian Model Validation. a,** Time series trace plot of the Markov chains (n=4 overlaid) shows the evolution of parameter (n=5) vectors over the all iterations and indicate chains explored the full parameter space. **b,** Autocorrelation of paramters (columns) illustrate the degree of correlation between MCMC samples separated by different lags (x-axis). For example, a lag of 0 represents the degree of correlation between each MCMC sample and itself (correlation of 1). A lag of 1 represents the degree of correlation between each Markov chain Monte Carlo (MCMC) sample and the next sample along the chains (rows). Independent (uncorrelated) samples (autocorrelation of 0) indicate unbiased estimates of parameters. No parameters violate autocorrelation. **c,** Shows overlaid histograms of the (centered) marginal energy distribution $\pi_E$ and the first-differenced distribution $\pi_{\Delta E}$. The MCMC No-U-Turn Sampler (NUTS) Energy diagnostic identifies overly heavy tails that are also challenging for sampling and quantifies the heaviness of the tails of the posterior distribution. The two distributions are well-matched, meaning the random walk will explore the marginal energy distribution extremely efficiently. **d,** Plot shows one line per

iteration connecting parameter values at iterations and identifies global patterns to detect divergences if present (divergences will be colored in the plot (by default in red). No divergent transitions were detected. **e,** NUTS divergence plot in the top panel shows the distribution of the log-posterior and indicates no divergences for all chains. This provides evidential support that chains adequately explore all parts of the posterior. The bottom panel shows the distribution of NUTS acceptance statistic approaches 1.

PSIS is a new approach that provides a more accurate and reliable estimate by fitting a Pareto distribution to the upper tail of the distribution of the importance weights. PSIS allows the computation of LOO using importance weights that would otherwise be unstable (PSIS-LOO). Although alternative validation strategies, e.g. Watanabe-Akaike information criterion (Watanabe 2010), are asymptotically equal to LOO, PSIS-LOO provides a more accurate and stable estimate of model performance and is more robust in the finite cases with diffuse priors (weakly informative), as is true for models in this proposal when little is known previously about the cancer and chemotherapy interactions.

PSIS-LOO was quantified by computing standard errors for predictions and for comparison of predictive errors between models to definitively test and rank models based on predictive accuracy (*elpd* = expected log pointwise predictive density) (Vehtari, Gelman *et al.* 2017).

# CHAPTER 3. PROJECT 1

## Introduction

Chemotherapy can achieve high rates of survival in patients with common cancers (André, Boni *et al.* 2004) but often causes severe side effects, including neuropathy, that can limit its use (Cavaletti and Marmiroli 2010; Alcindor and Beauger 2011; Stone and DeAngelis 2016). Debilitating sensory disorders, including pain, paraesthesia, and somatosensory loss, reduce quality of life for many patients and can persist for months or years after discontinuing chemotherapy (Quasthoff and Hartung 2002; Seretny, Currie *et al.* 2014; Sisignano, Baron *et al.* 2014). These neurological disorders occur for up to 80% of patients receiving commonly used antineoplastic agents, notably antitubulins and proteasome inhibitors, as well as platinum-based compounds (Sisignano, Baron *et al.* 2014; Avan, Postma *et al.* 2015), which are the prescribed adjuvant treatment in 50% of cancer cases worldwide (Galanski, Jakupec *et al.* 2005; Johnstone, Park *et al.* 2014). There are few options available for the prevention or treatment of sensory disorders and those that exist largely focus on symptomatic management (Hershman, Lacchetti *et al.* 2014). Thus, there is an urgent need to better understand the pathogenesis of sensory dysfunction to aid development of mechanism-based therapies.

Preclinical studies of chronic neuropathy in experimental models of cancer are unavailable, possibly because of presumption that chemotherapy alone is sufficient to explain the neuropathology. A recently published meta-analysis identified 341 preclinical studies of chemotherapy induced neuropathy, and none assessed interaction between chemotherapy and cancer (Currie, Angel-Scott *et al.* 2018). Omitting cancer from preclinical study produces a fundamental gap in knowledge that may explain why treatments for neuropathic side effects of chemotherapy have been unsuccessful in

patients with cancer. Cancerous tumors located outside the nervous system can induce cognitive disability and peripheral nervous system dysfunction independent of chemotherapy, surgery, or co-morbidities (Ahles 2012; Boyette-Davis, Eng *et al.* 2012). Moreover, cancer provokes dysregulation in immune, metabolic, oxidative and neuronal excitability (Reuter, Gupta *et al.* 2010; Zheng, Fang *et al.* 2012), all of which are identified as targets through which chemotherapy produces neuropathy (Cavaletti and Marmiroli 2010). Convergence of cancer and chemotherapy on the same biological processes seems likely to yield non-linear interactions, leading us to hypothesize that clinically relevant neuropathy emerges from codependent actions of cancer and chemotherapy.

We tested our hypothesis by uncoupling the independent and combinatorial effects of cancer and chemotherapy on sensory neurons in studies of rats that are not feasible in human patients. Here we present original findings to show that sensory neuropathy depends on complex systemic interactions between cancer and chemotherapy. By combining cancer and chemotherapy, we reproduce the relevant clinical condition in preclinical study of rats to produce the first transcriptional profile of nervous tissue, to discover recurrent metabolic reprogramming and perturbed inflammatory and ion channel processes distinct from the independent effects of cancer or chemotherapy. Parallel codependency is found in novel neuropathic responses of mechanosensory neurons, both in their immunohistochemistry for selected voltage-gated potassium ion channels and in electrophysiological measures of encoding naturalistic stimuli *in vivo*. Collectively, our data show for the first time that sensory neuropathy emerges from codependencies between the systemic effects of cancer and chemotherapy. Apart from identifying new molecular targets for restoring function to mechanosensory neurons, our findings provide the fundamental insight that accounting for chemotherapy-cancer

combinatorial effects on the somatosensory nervous system is prerequisite for developing meaningful treatment or prevention of neuropathy.

## Aim 1: Test the hypothesis that cancer exacerbates chemotherapy induced gene dysregulation in the sensory nervous system.

### *Aim 1 Introduction*

To gain comprehensive and unbiased understanding of treatment effects, we first profiled the transcriptomes of lumbosacral (L4-S1) dorsal root ganglia, where sensory neurons (Figure 2b) are known to be particularly vulnerable to chemotherapy (Cavaletti and Marmiroli 2010). We studied wild-type ($Apc^{WT}$) rats and rats carrying an *Apc gene* mutation ($Apc^{Pirc/+}$) (Amos-Landgraf, Kwong *et al.* 2007) associated with development of colon cancer (Kwong and Dove 2009), not only in these rats, but also in 80% of patients with colorectal cancer (Kwong and Dove 2009). This allowed us to simulate clinical treatment of colorectal cancer in a rat model. We employed the standard-of-care, platinum-based chemotherapy agent oxaliplatin (OX), in a human-scaled, dose-equivalent treatment schedule. This experimental approach provided the best available approximation of human colorectal cancer treatment, while enabling controlled experimental manipulations and analysis of molecular and functional properties of sensory neurons (Irving, Yoshimi *et al.* 2014).

### *Aim Specific Methods*

*Tissue Collection*

At the conclusion of in vivo experiments, three to four animals from each of four groups were selected for whole-transcriptome analysis alone and did not undergo further

analysis. Dorsal root ganglia (DRG) from the lumbosacral (L5-S2) spinal cord were surgically removed (4-6 per animal), washed with sterile saline and immediately flash frozen (fresh) in 2-methylbutane (isopentane) pre-chilled in liquid nitrogen. DRG were then stored at -80°C for further analysis (see below).

*RNA Extraction and Amplification*

RNA extraction and amplification were performed according to our previously described methods (Lili, Matyunina *et al.* 2013). Briefly, RNAs were isolated and purified from sensory neurons of DRG (L5-S2) using the mRNeasy Micro KIT (Qiagen, Germantown, MD). Total RNA concentration and integrity was assessed on the Bioanalyzer RNA Pico Chip (Agilent Technologies, Santa Clara, CA). Labeling of RNAs was performed with the FlashTag Biotin HSR RNA Labeling Kit (Affymetrix, ThermoFisher). Gene expression was determined by microarray analysis on the Affymetrix platform (Rat Transcriptome Array 2.0).

*Microarray data analysis*

In total, 13 (four groups with biologic triplicates per group (4 biologic replicates from $Apc^{Pirc/+}$+OX group) global transcriptional expression data sets were generated in this study. Raw mRNA expression data were processed using Affymetrix Expression Console (EC) software Version 1.4. Raw data probes were normalized using SST-RMA algorithm. Differentially expressed genes (DEG) were determined through a linear fixed effects model (*limma (Smyth 2004; Smyth 2005)*) with a robust empirical Bayes (eBayes) framework(Phipson, Lee *et al.* 2016) to moderate the residual variances *(Smyth 2004; Smyth 2005)*. This has the effect of increasing the effective degrees of freedom by which gene-wise variances are estimated, thus reduces the number of false

positives for genes with small variances and improves power to detect DEG with larger variances (Ritchie, Silver *et al.* 2007).

*Unsupervised multivariate analysis*

DEGs were subjected to paired multivariate analyses to discover latent data structure. We serially linking two analytic techniques, Principal Components Analysis (PCA) and Hierarchical clustering. This stabilized clustering performance and reduced dimensionality to a more tractable number of continuous variables containing the most important information on which clustering algorithms are focused which leads to a better clustering solution (Husson, Josse *et al.* 2010; Argüelles, Benavides *et al.* 2014). PCA and visualization was applied to DEGs with the *factoextra (Kassambara and Mundt 2016)* and *FactoMineR (Husson, Josse et al. 2010)* packages. PCs capturing high-level structure were then employed to drive hierarchical clustering. Hierarchical clustering and heatmaps were visualization with the *gplots* package (*heatmap.2*) (Warnes, Bolker *et al.* 2016) in the R environment (3.5.0) (Team 2018). Hierarchical-clustering, using the ward.D2 method (Murtagh and Legendre 2014) were applied to the eBayes-filtered gene set to obtain unsupervised visualization of the gene clusters coordinately expressed among the different experimental groups. Prior to hierarchical clustering, genes were standardized across the samples to a mean of zero and an s.d. of 1. Subclusters were derived using the R function *cutree (Becker, Chambers et al. 1988)*.

*Pathway and Gene Set Enrichment Analysis*

To extract biological meaning from large lists of differentially expressed genes acquired through high-throughput technologies, e.g. transcriptomics, one must utilize bioinformatic support. Pathway enrichment analysis is one such analytic approach through which high-throughput, typically -omics, data are analyzed to uncover a variety of biological

mechanisms associated with a physiological process, e.g. diseases, development, etc. Detailed descriptions and protocols have been described previously (Huang, Sherman *et al.* 2008; Huang, Sherman *et al.* 2008); therefore, only a brief description follows.

Pathway enrichment analysis was conducted on subclusters of named genes using DAVID (Database for Annotation, Visualization, and Integrated Discovery) and g:Profiler to pinpoint significantly enriched pathways or biological processes (Huang, Sherman *et al.* 2008; Huang, Sherman *et al.* 2008). Biological processes and pathways are composed of group of genes as opposed to individual genes and are derived from the collective knowledgebase of published literature e.g. annotation database Gene Ontology (GO). Biological processes link individual genes to a broader biological concept or pathway and typically contain many tens to hundreds of genes. It should be noted that different biological processes can have some degree of redundancy of their composition.

The foundations of pathway enrichment analysis rest on the idea that if a biological process or pathway is truly abnormal in a disease, the co-functioning genes should have a higher potential to be selected for as a relevant group by the high-throughput screening technologies as opposed to studying individual genes. This shift from focus on individual genes to large gene lists increases the likelihood of identifying correct biological processes most pertinent to the disease or biological phenomena under study and reduces the likelihood of false positive findings. We further increase statistical power by submitting subclusters, co-regulated (up or down) probe sets, for testing that were previously separated during our initial multivariate approach (Hong, Zhang *et al.* 2014). All biological processes with adjusted $P < 0.05$ were considered significantly enriched. g:Profiler 3-500 (min-max) Benjamini Hochberg FDR correction intersection terms (2) only annotated genes were searched.

Parallel identification of pathways enrichment was performed by GSEA (gene-set enrichment analysis). GSEA underlying statistical construct is independent of DAVID. GSEA can uncover novel sets of functionally related genes by focusing on all detected (above-background) genes. GSEA is unbiased in this regard in that is reduces arbitrary cut-off factors in the typical gene selection step utilized in traditional analyses; and it uses all information by allowing genes with even minimal change that would otherwise not pass the selection threshold. These advantages afford the detection of even subtle enrichment signals. GSEA accomplishes this by leveraging list rank information without using a threshold typically applied in overlap statistics like hypergeometric testing to define genes as members at the top or bottom of a ranked list of genes.

The Molecular Signature Database v 6.2 (C2-CP: canonical pathways; C3- MIR: microRNA targets; C3- TFT: transcription factor targets; C5-BP: GO biological process; C5- CC: GO cellular component; C5- MF: GO molecular function C7: immunologic signatures gene sets) with the permutation type set to ‘gene set,’ 15-500 (min-max), to calculate statistical significance, as suggested for fewer than seven replicates; default settings were applied to all the other options. For GSEA, a false discovery rate (FDR) of <0.2 was considered statistically significant. Selecting appropriate reference background for pathway analyses is a potential pitfall since the different gene reference background settings may greatly impact the enrichment scores. Even though there is no ‘gold’ standard for the reference background, we followed the widely utilized procedure of setting the reference background to the pool of genes that could be potentially be selected, e.g. total genes evaluated in an -omics study. Specifically, all pathway analyses performed utilized the same Affymetrix platform Rat Transcriptome Array 2.0 as the background list of genes.

*Targeted Transcriptional Analysis*

Complementary supervised analysis of DEGs leveraged knowledge of proteins known to be expressed at sensory neuron receptor endings that directly (Simon, Shenton *et al.* 2010; Woo, Lukacs *et al.* 2015; Carrasco, Vincent *et al.* 2017) or indirectly (Bewick and Banks 2015; de Nooij, Simon *et al.* 2015) regulate excitability. In addition, due to incomplete knowledge of the full suite of proteins that are necessary and sufficient for normal function (Bewick and Banks 2015), we expand targeted transcriptional analysis to incorporate gene families, including: ion channels, GPCRs, and channel regulators.

***Results***

*Transcriptional profiling of sensory neurons*

We employed an empirical Bayesian (eBayes) linear model *(Smyth 2004)* to modify residual variances on a total of 31,042 (22,875 named) genes and identified 3,426 differentially expressed genes (DEG) across all groupwise contrasts ($P_{\text{eBayesAdj}} < 0.005$). Subsequent *post hoc* analysis identified DEG from all possible contrasts (fold-change (FC) ≥1.2 and ≤-1.2). Overlap between DEGs retrieved from individual comparisons is illustrated in (Figure 6a). In keeping with the notion that chemotherapy and cancer act through similar molecular mechanisms, we found overlap of 112 DEG affected independently by cancer and chemotherapy (Figure 6a). Of note, we found that 73.8% (n=1,704) of all DEG (n=2,307) were uniquely affected when cancer and chemotherapy interacted ($Apc^{Pirc/+}$+OX) Figure 6a). This finding demonstrates the first evidence that cancer exacerbates genetic dysregulation induced by chemotherapy, unmasking a more than four-fold increase in DEG.

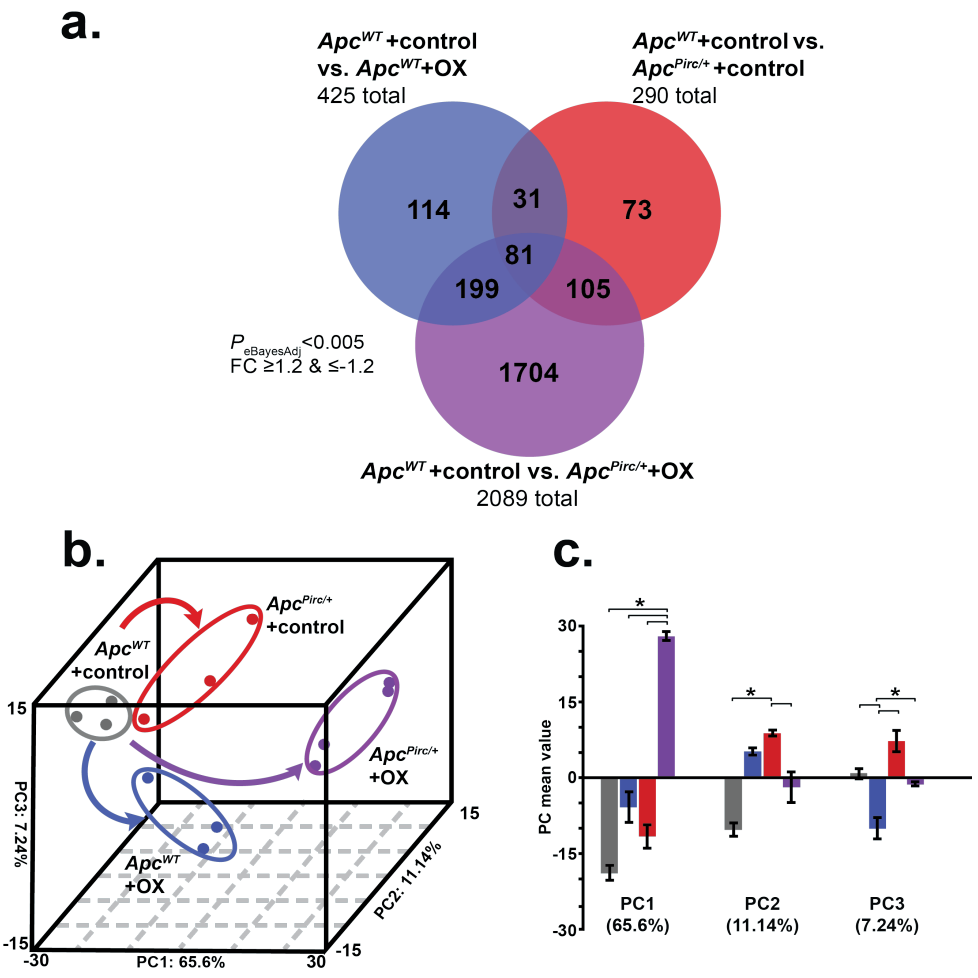


## ***Figure 6.***

**Cancer-chemotherapy codependence amplifies transcriptional dysregulation.** c, Venn-diagram distribution of significantly differentially expressed genes from the lumbosacral DRG among all groupwise contrasts. Significance determined by both P<0.005 and fold-change (FC) ≥1.2 and ≤-1.2 using a Bayesian moderated linear fixed effects model ($eBayes_{Adj}$). d, Group correlation determined by principal-component (PC) analysis of significantly differentially expressed genes. Genes were visualized in the new 3D composite space created by PC1-3. Effects of independent chemotherapy (*Apc*$^{WT}$+OX) or cancer (*Apc*$^{Pirc/+}$+control) and their combinatorial (*Apc*$^{Pirc/+}$+OX) treatment are indicated by curved arrows; dots represent individual animals. e, Bar graphs of the mean values of PC1, PC2, and PC2. Error bars represent s.e.m. * indicates statistically significant differences between experimental groups as empirically derived from hierarchical Bayesian model (stan_glm).

Next, we performed two independent downstream analyses (Figure 7) to test for interaction and determine which biologic processes might be involved in pathogenesis of sensory disorders. First, we subjected the eBayes filtered database to unsupervised principal component (PC) analysis. DEG were visualized in the new 3D composite space created by PC1-3 (Figure 6b) that explained 83.98% of the variance and clearly segregated the four experimental groups. Inspection of individual PCs revealed significant evidence of non-linear interactions between cancer and chemotherapy captured in PC1 (65.6% of explained variance), whereas PC2 (11.14%) and PC3 (7.24%) separated the effects of cancer and chemotherapy, respectively (Figure 6c). Second, we drove unsupervised hierarchical clustering onto the PC1 solution to identify groups of coregulated genes that express interaction (Argüelles, Benavides *et al.* 2014) (Figure 8a). Analysis identified two clusters of genes displaying distinct, but internally consistent expression profiles clearly representing patterns of interaction (Figure 8a, C1 and C2; Table 1).

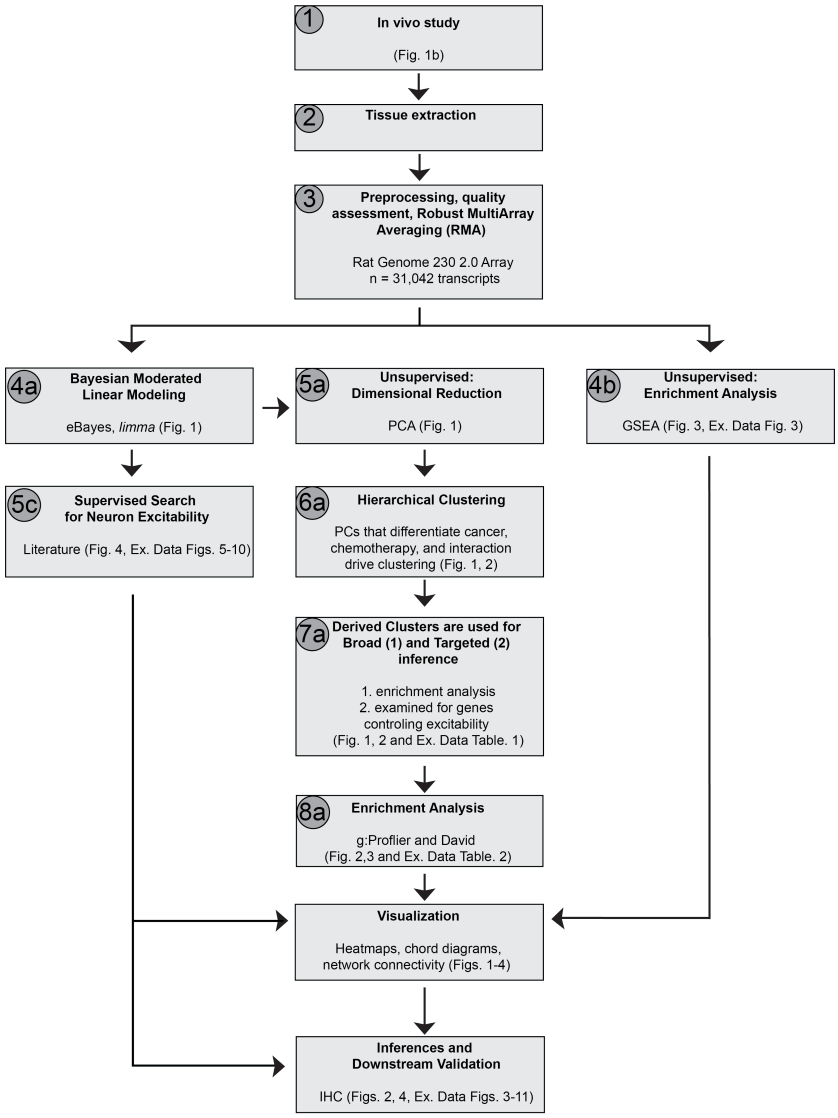


## ***Figure 7.***

**Steps outlining parallel independent transcriptome analyses.** Data analysis flowchart depicts the multi-step (split into a, b, and c streams) approach utilized for transcriptome analysis, inferences and downstream protein level validation. A detailed description of each step is available in the **Online Methods Sections.** Each box highlights specific analytic techniques, statistical packages (when relevant), and corresponding figures as reference. Principal component analysis, PCA; gene set enrichment analysis, GSEA; principal components, PC; Database for Annotation, Visualization and Integrated Discovery, DAVID; immunohistochemistry, IHC.

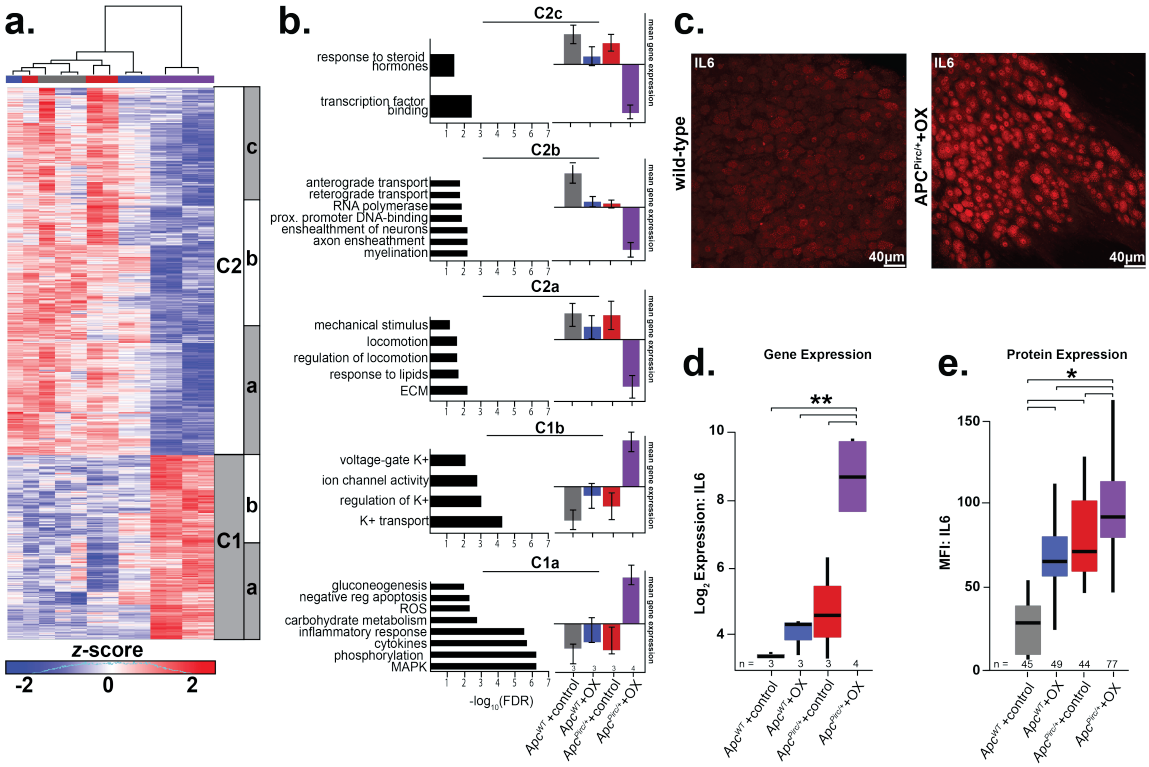


***Figure 8.***

**Cancer-chemotherapy interaction disrupts distinct biological processes.** a, Heatmap of the top differentially expressed genes in the sensory neurons identified by PC1 driven hierarchical-clustering (biological triplicates n= 3 for Apc$^{WT}$+control, , *Apc$^{WT}$*+OX, *Apc$^{Pirc/+}$*+control and four biologic replicates for *Apc$^{Pirc/+}$*+OX). Data were mean-centered and s.d. normalized before clustering; upregulated and downregulated genes (row) are shown in red and blue, respectively. White and grey bars (C1 and C2 respectively) display the main clusters from gene level hierarchical-clustering and were chosen for clarity, while subclusters (a-c) highlight unique biologic characteristics within the main clusters. b, Clusters showing distinct up- or downregulation of key biological processes (Gene Ontology (GO) terms) and pathways (Kyoto Encyclopedia of Genes and Genomes (KEGG)). Selected pathway and gene ontology terms significantly associated (false discovery rate [FDR] ≤ 0.25) with misregulated transcripts in individual clusters are listed on the left of each gene cluster with significance indicated by horizontal bars (-log$_{10}$(FDR)). The vertical bar graphs on the right compare mean±s.d. of gene expression levels in each subcluster (Table S1). c, Confocal image of a dorsal root ganglia immunostained against interleukin 6 (IL6). Scale bar, 40 μm. Gene expression (d) and receptor protein expression (e, mean fluorescence intensity (MFI)) of IL6 as determined by transcriptional profiling and cell-specific immunohistochemistry of large diameter sensory neurons

(>30μm). Numbers (n) identify sample size for each group. * indicates statistically significant differences between experimental groups as empirically derived from hierarchical Bayesian model (stan_glm). ** indicates $eBayes_{Adj}$<0.005 and fold-change (FC) >1.5 using a Bayesian moderated linear fixed effects model. Data presented as mean±s.d.

We then subjected clusters of named genes (Table S1) to pathway-enrichment analysis (Reimand, Kull *et al.* 2007; Huang, Sherman *et al.* 2008) and identified unique subclusters (Figure 8a) expressing dysregulation in distinct biological processes (Figure 8b, see Methods: *Pathway and Gene Set Enrichment Analysis*). In keeping with the notion that combinatorial effects of cancer and chemotherapy (OX) reflect convergence onto shared signaling pathways, genes mediating inflammatory response, e.g. interleukin 6 (*Il6)* ($P_{eBayesAdj}$=7.82× $10^{-6}$), *Ptgs2* ($P_{eBayesAdj}$=0.0028) and *Cxcr4* ($P_{eBayesAdj}$=3.74× $10^{-7}$), and reactive oxygen species processes, e.g. *Hmbox1* ($P_{eBayesAdj}$=0.001), were found to be among the most upregulated in cluster 1a (C1a) (Figure 8b). Notably, we observed substantial induction of genes encoding glycolytic and carbohydrate metabolic processes (FDR ≤ 1.83x$10^{-3}$, C1a; Figure 8b) in the $Apc^{Pirc/+}$+OX neurons. Coincident with these changes was a statistically significant down-regulation of genes mediating lipid metabolism (C2a), suggestive of pervasive metabolic dysfunction beyond the small subset of dysregulated mitochondrial related processes that we found in response to $Apc^{WT}$+OX or $Apc^{Pirc/+}$+control alone (Figure 8b; Figure 9a,b) and similar to dysfunctional effects previously suggested (Cavaletti and Marmiroli 2010). Among additional unique transcripts downregulated in $Apc^{Pirc/+}$+OX neurons, Figure 8b highlights multiple deficits in processes related to extracellular matrix control, mechanical stimulus transduction (C2a), DNA-binding, RNA polymerization (C2b), transcription factor activity, hormone signal transduction (C2c and Table. S1). Furthermore, we observed genes in C1b and 2a that represent specific dysregulation of neuronal and sensorimotor function,

e.g. ion-channel genes determining neuronal excitability along with coincident down-regulation of locomotion. These data provide the first evidence that codependent neuropathy induces broad metabolic reprogramming, e.g. increased glycolytic and decreased lipid metabolism, consistent with cancers capacity to corrupt metabolic processes (DeBerardinis, Lum *et al.* 2008; Hay 2016), which extends knowledge beyond the limited impairment observed in mitochondria.

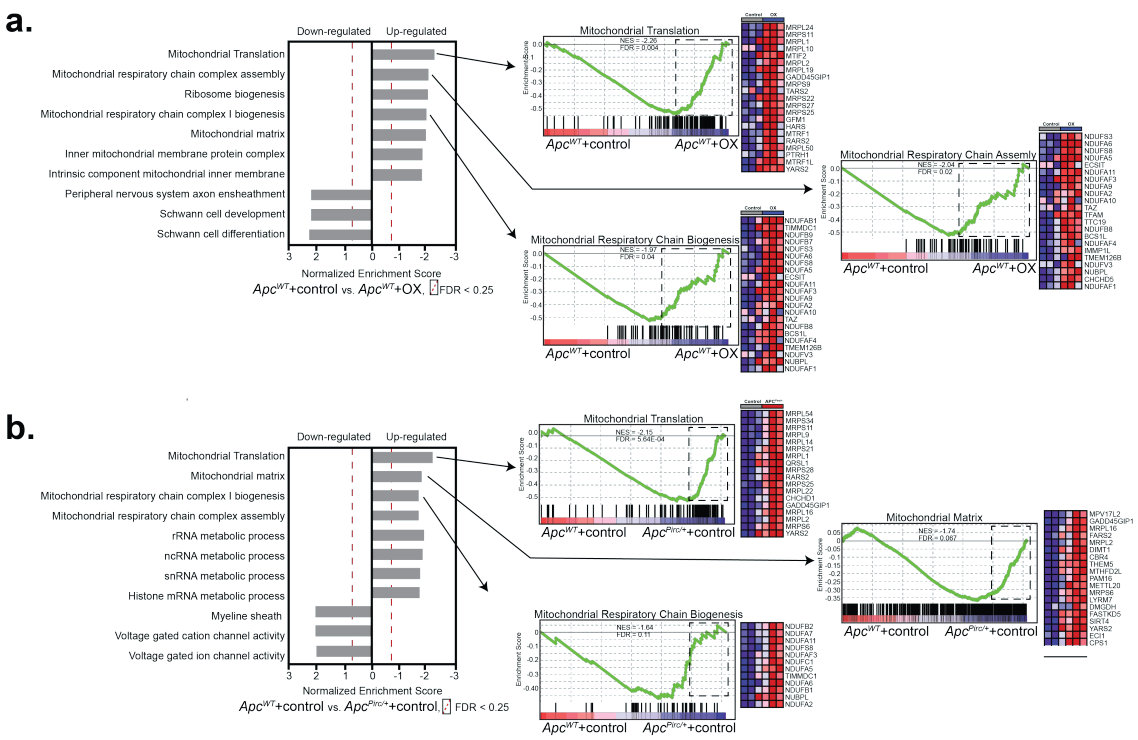


## ***Figure 9.***

**Pathway analysis and GSEA based comparison of the independent effects of cancer and chemotherapy show convergence of mitochondrial dysfunction.** List of enriched gene sets in sensory neurons identified by GSEA (queried against MSigDB, C2-CP: canonical pathways; C3- MIR: microRNA targets; C3- TFT: transcription factor targets; C5-BP: GO biological process; C5- CC: GO cellular component; C5- MF: GO molecular function C7: immunologic signatures gene sets from the comparison of a, Apc$^{WT}$+control and *Apc$^{WT}$*+OX and b, Apc$^{WT}$+control and *Apc$^{Pirc/+}$*+control groups. Individual frames identify functional relatedgroups of gene sets expressing distinct up- or downregulation as compared with control. Representative enrichment plots are shown on the right. Heat-map representation of leading-edge genes are shown on the right of each enrichment plot highlight key mitochondrion-related proc, such as translation and biogenesis in both *Apc$^{WT}$*+OX and *Apc$^{Pirc/+}$*+control neurons, and key neuron myelinatio- related processes. Statistical signifi- cance was determined by permutation testing with normalized enrichment score (NES) and Benjamini–Hochberg false discovery rate (FDR) < 0.25.

Markers for nerve degeneration, inconsistently observed in patients treated with antineoplastic drugs (Burakgazi, Messersmith *et al.* 2011) exhibited mixed results. While we observed few significantly downregulated genes associated with myelination processes (C2b; $P \leq 7.12 \times 10^{-3}$, Figure 8b), we also found significant induction of processes involved in the preservation of neurons (e.g. enrichment of negative regulation of apoptosis $P \leq 5.96 \times 10^{-3}$) in C1a that is related to the synergistic effects of cancer and chemotherapy, i.e. where cancer and chemotherapy impart influence in the same direction. Mixed results from these data suggests heterogeneous neuronal populations in the DRG may contain discrete subpopulations with selective vulnerability whereas others are resistant to degeneration, which is consistent with mixed results seen in human studies (Burakgazi, Messersmith *et al.* 2011) and highlights the need for future cell-type specific investigations that are currently unavailable.

*Global dysregulation of neuron transcriptomes*

We then used gene-set enrichment analysis (GSEA) as a second independent tool to investigate the cellular processes underlying codependent neuropathy. We initially focused on the comparison of $Apc^{WT}$+OX and $Apc^{Pirc/+}$+OX (Figure 10a: how cancer alters the independent effects of chemotherapy) and $Apc^{Pirc/+}$+control and $Apc^{Pirc/+}$+OX (Figure 10b: how chemotherapy alters the independent effects of cancer) and interrogated entire data sets against the Molecular Signatures Database (Table S2). Two novel conclusions can be drawn from the GSEA findings. First, GSEA independently validated codependencies of cancer and chemotherapy in the DEG identified by transcriptional profiling using paired unsupervised analysis (Figure 10a, b). GSEA corroborated downregulation of lipid metabolic pathways (normalized enrichment score (NES)=1.73) and upregulation of glycolytic pathways (NES=−1.94) in $Apc^{Pirc/+}$+OX sensory neurons when compared with either chemotherapy (Figure 10a) or cancer alone

(Figure 10b). Focusing analysis on pathways directly involved in neuronal signaling confirmed dysfunction in peripheral neuron ensheathment in the absence of evidence supporting neuron specific apoptotic response (FDR>0.83) (Figure 10a). Second, GSEA exposed dysregulation of genes relevant to neuronal excitability particularly potassium ion channels and transporters, and others participating in synaptic communication, e.g. SNARE and glutamatergic transmission (Figure 10a, b). Dysregulation of these and other gene sets (e.g. proinflammatory chemokines) was not predicted from the independent effects of cancer or chemotherapy alone. (Table S2). Unlike previous studies that consistently report dysregulated voltage-gated sodium channels (Sittl, Lampert *et al.* 2012), we find little evidence of differentially expressed sodium channels or disrupted regulatory pathways (Sittl, Lampert *et al.* 2012). Instead, we find targeted DEG related to potassium ion channels unlike those previously identified. We draw two conclusions from these data. First, ion channel clusters are differentially vulnerable to codependent neuropathy. Second, chronic neuropathy may be mechanistically linked to dysregulation of ion channels distinct from those identified in acute preparations.

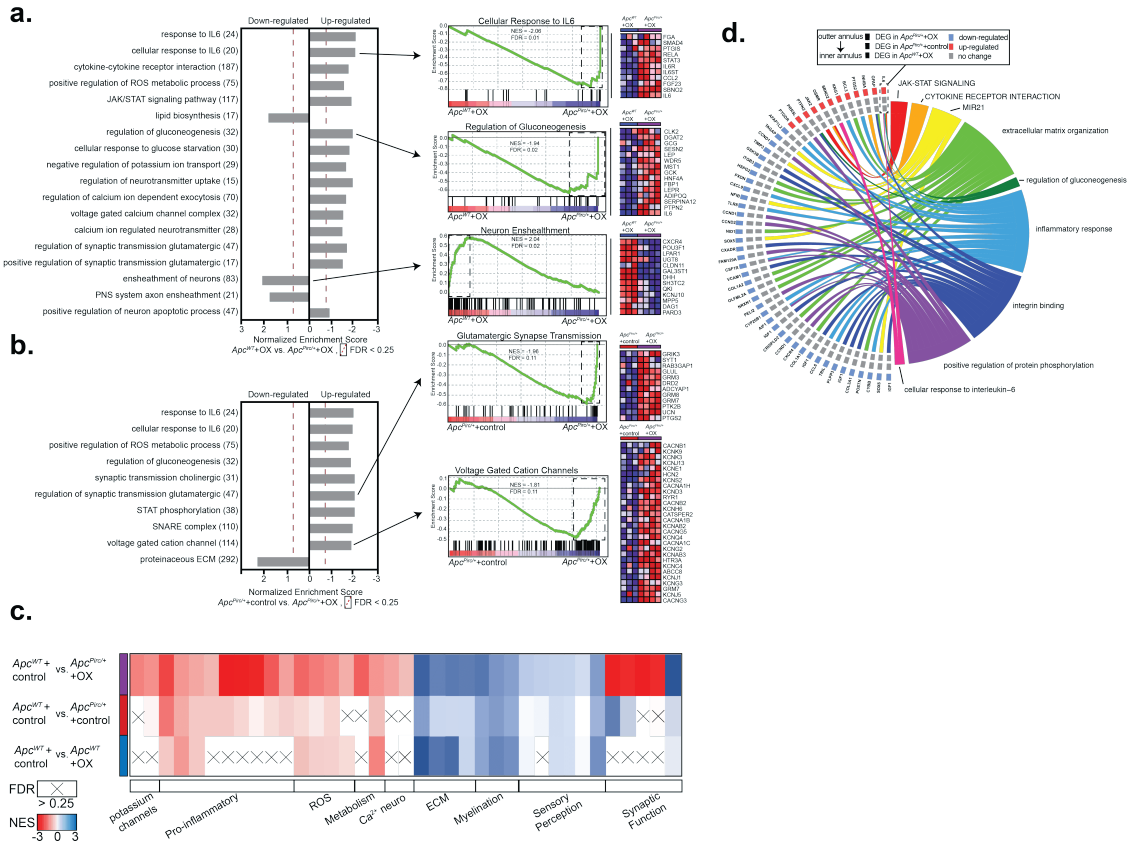


## ***Figure 10.***

**GSEA and pathway analyses test codependence of cancer and chemotherapy.** Enriched gene sets in sensory neurons identified by gene set enrichment analysis (GSEA: MSigDB, C2-CP: canonical pathways; C3- MIR: microRNA targets; C3- TFT: transcription factor targets; C5-BP: GO biological process; C5- CC: GO cellular component; C5- MF: GO molecular function C7: immunologic signatures gene sets from the comparison of a, *Apc*$^{WT}$+OX and *Apc*$^{Pirc/+}$+OX and b, *Apc*$^{Pirc/+}$+control and *Apc*$^{Pirc/+}$+OX groups. Individual frames (horizontal grey bars) identify functional related (internally consistent) groups of gene sets expressing distinct up- or downregulation as compared with *Apc*$^{WT}$+OX. Number of overlapping genes displayed in parentheses to the right of the corresponding GO term. Representative enrichment plots are shown in the middle column. Heat-map representation of leading-edge genes is shown on right. c, Heat-map representation of enriched individual gene sets, identified by GSEA, in sensory neurons for chemotherapy (bottom rown), cancer (middle row), and the combination of cancer (Apc$^{Pirc/+}$) and chemotherapy (OX) (top row). Gene sets are grouped into functionally related cohorts. Gene sets not reaching statistical significance indicated by (X). d, Chord diagram shows enriched pathways (Database for Annotation, Visualization, and

Integrated Discovery; DAVID) on the right, and genes contributing to enrichment are shown on the left. Squares on left indicate genes differentially expressed in $Apc^{WT}$+OX, $Apc^{Pirc/+}$+control, or $Apc^{Pirc/+}$+OX groups compared to control (see the key for gene differential expression). Statistical significance determined by permutation testing with normalized enrichment score (NES) and Benjamini–Hochberg false discovery rate (FDR) < 0.25. DEG, differentially expressed genes; ROS, reactive oxygen species: ECM, extracellular matrix.

### *Summary*

Taken together, our analyses indicate significant dysregulation of genes and proteins mediating core cellular processes of $Apc^{Pirc/+}$+OX sensory neurons. Our integrated transcriptomics and protein level findings confirmed that cancer and chemotherapy effect common processes (Ahles and Saykin 2007; Reuter, Gupta *et al.* 2010; Argyriou, Bruna *et al.* 2017). Moreover, our findings support our central hypothesis that clinically relevant neuropathy depends on systemic interaction between cancer and chemotherapy by showing for the first time that cancer-chemotherapy codependence exacerbates neuropathy and revealing it operates through distinct mechanistic pathways, unpredicted from cancer or chemotherapy alone.

## Aim 2: Test the hypothesis that cancer-chemotherapy codependent genetic dysregulation is conserved at a protein level.

### *Introduction*

Because inflammatory pathways play multiple roles in regulating neuron function (Vezzani and Viviani 2015), we focused attention on their significant response to codependent neuropathy. We selected the most dysregulated gene in the inflammatory

pathways, *Il6*, for the first molecular validation by assessing gene—protein correspondence.

### *Aim Specific Methods*

*Tissue Collection*

At the conclusion of in vivo experiments, rats were overdosed with isoflurane inhalation (5%) then immediately transcardially perfused with cold vascular rinse (0.01 M PBS pH 7.4) followed by room temperature fixative (2% paraformaldehyde in 0.1 M PBS, pH 7.4). Muscles and dorsal root ganglia were quickly dissected and post-fixed for one hour in the same fixative. After a brief wash in a 0.1 M PBS, tissues were incubated in 0.1 M PBS containing 20% sucrose at 4°C overnight. After DRG removal, colonic tumors from $Apc^{Pirc/+}$ rats were dissected and counted prior to post fixation for immunohistochemical analysis.

*Immunohistochemistry*

Details of our immunohistochemistry procedures have been previously described (Carrasco, Vincent *et al.* 2017). Briefly, 50-µm thick sections of skeletal muscles, DRGs, and tumors were cut using a Cryostat (Leica). Tissues sections from all treatment groups were processed simultaneously. All tissue sections were incubated overnight in primary antibodies diluted in blocking buffer (5% normal goat serum, 0.3% Triton100 in PBS). The primary antibodies used were as follow: rabbit polyclonal anti-NaV1.6 (ASC-009, Alomone Laboratories, 1:200), rabbit polyclonal anti-NaV1.1 (ASC-001, Alomone Laboratories, 1:300), rabbit polyclonal anti-NaV1.7 (ASC 008, Alomone Laboratories,1:100), rabbit polyclonal anti-Kv3.3 (APC-102, Alomone Laboratories, 1:300), mouse monoclonal anti-Kv1.1 (K36/, NeuroMab, University of California Davis, 1:300), guinea pig polyclonal anti-VGLUT1 (135-

104 Synaptic Systems, 1:300), chicken polyclonal anti-neurofilament protein (NF-H, Aves Laboratories, 1:200), mouse monoclonal anti-ASIC2, (E-20, Santa Cruz Biotechnologies,1:200), mouse monoclonal anti-EGRF (SC-120, Santa Cruz Biotechnolgy, 1:100), mouse monoclonal anti-KI67 (SC-23900, Santa Cruz Biotechnology, 1:100), mouse monoclonal anti-IL6 (SC-57315, Santa Cruz Biotechnology, 1:100). After washing with PBS, tissue sections were incubated with appropriate fluorescent-conjugated secondary antibodies (Jackson ImmunoResearch Laboratories) diluted in blocking buffer, for 1 hr. at room temperature. Following washes with PBS, slides were mounted using Vectashield containing DAPI (Vector Laboratories) in order to label cell nuclei.

*3D Digital Reconstructions and Anatomical Quantifications*

Z-axis stacks of images of muscle spindles receptor endings, DRGs and tumors were constructed by sequentially imaging using a confocal microscope (LSM 700A, Zeiss). Muscle spindles terminals z-stacks (1µm steps) were captured with a 40X oil immersion objective (N.A 0.6) at 0.6 digital zoom. DRG and tumors z-stacks (1µm steps) were captured with a 20X objective (N.A 0.4) at 0.6 digital zoom. Stacks of images were processed and analyzed using Amaris (Bitplane) or imageJ (NIH) imaging software. Figures present images as flat maximal projections of the sum of the z-axis optical slices. Analysis of neuron receptor endings (spindles) and soma (DRG) were performed by an investigator blinded to treatment group. Immunoreactivity in nerve terminals and DRG was determined by measuring the mean pixel intensity of on each en-face portions of the terminal (visualized by the VGLUT1 staining) observed on every 1 um single image or on the medium and large size cell somas observed on the flat maximal projections of the z-stacks images respectively.

***Results***

*Dysregulation is conserved at protein level*

Sensory neurons in dorsal root ganglia were immunolabeled with monoclonal antibodies targeting IL6 (Figure 8c). As predicted from the transcriptional profiling (Figure 8d), the IL6 protein was constitutively expressed in $Apc^{WT}$+control rats at lower levels than in $Apc^{Pirc/+}$ control animals or $Apc^{WT}$+OX animals, and at significantly higher levels in $Apc^{Pirc/+}$+OX neurons (Figure 8e), demonstrating that codependent neuropathy was conserved in protein expression (Figure 8e and Figure 11). Previous studies implicate IL6's capacity to mediate hyperexcitability and morphological changes associated with neuron death (Nelson, Ur *et al.* 2002). However, these studies restricted investigation to acute neurotoxicity, which limits generalizability to symptoms that persist long after treatment. Our data present the first evidence that *Il6* (IL6) expression levels remain elevated long after treatment cessation without observable morphological changes. We show that codependent neuropathy significantly increases *Il6* (IL6) when compared to chemotherapy or cancer alone. In light of IL6's capacity to decrease excitability following chronic exposure (Nelson, Ur *et al.* 2002), our data suggest that neuronal dysfunction (see below) as a result of codependent neuropathy may be expressed as hypo-excitability, in contrast with previous work (Sisignano, Baron *et al.* 2014).

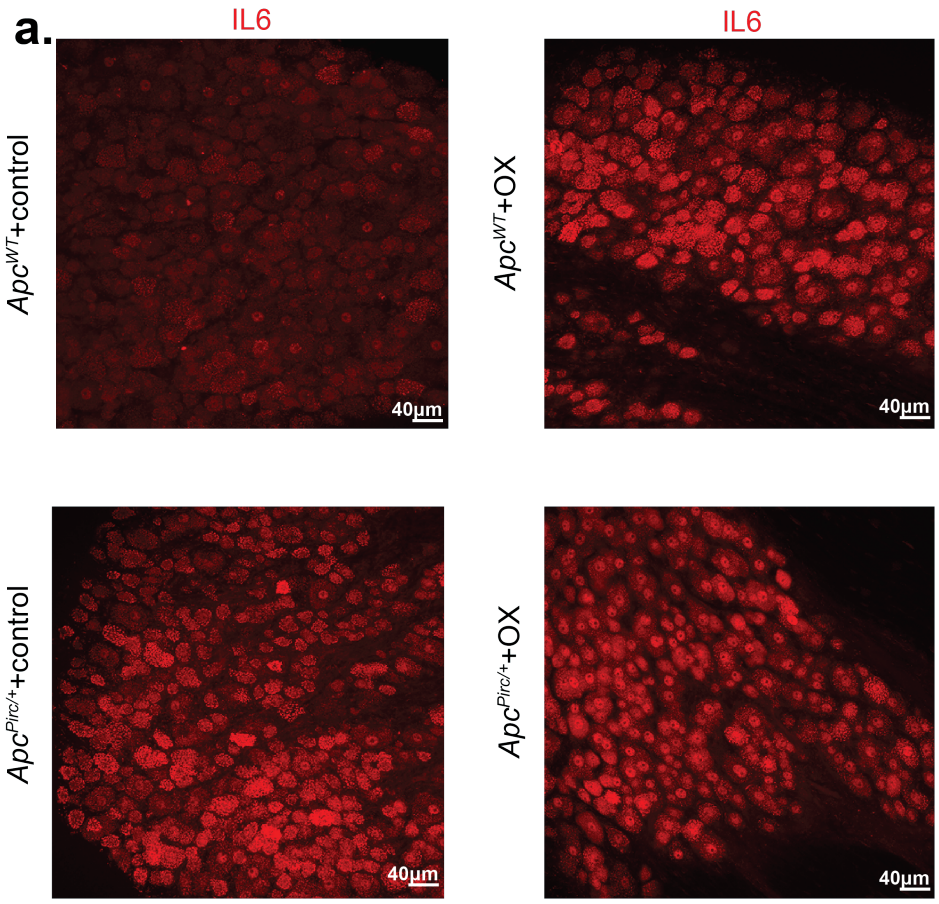


***Figure 11.***

**Immunostaining of sensory neurons in dorsal root ganglia.** Whole-mount staining and confocal axial projections of DRG neurons highlight expression of IL6 (a) in Apc$^{WT}$+control, *Apc$^{WT}$*+OX, *Apc$^{Pirc/+}$*+control, and *Apc$^{Pirc/+}$*+OX rats

*Novel voltage-gated ion channel dysfunction*

Sensory deficits, e.g. somatosensory and hearing loss, are commonly reported by patients long after cessation of chemotherapy, but knowledge of the combined effects of cancer and chemotherapy is missing. Mechanosensory systems, e.g. cochlear hair cells, and various somatosensory neurons in skin and muscle are responsible for encoding this information and exhibit deficits following chemotherapy (Avan, Postma *et al.* 2015).

We therefore next focused on identifying the combined effects of cancer and chemotherapy on a representative member of mechanosensory neurons, called muscle spindles. Muscle spindles share many of the molecular mechanisms (Bewick and Banks 2015) underlying mechanotransduction and encoding found in this broad class of sensory neurons (e.g. hair cells (Chalfie 2009), Merkel (Maksimovic, Nakatani *et al.* 2014)). Further, signaling by these neurons encodes sensory features of muscle mechanics necessary for perceiving (proprioception) and coordinating body position and movement, functions which, when impaired, have the potential to explain persistent disorders in patients (Proske and Gandevia 2009). We performed targeted analyses of our transcriptome database by querying differentially expressed genes identified in $Apc^{Pirc/+}$+OX rats compared to all other groups against genes encoding proteins known to be constitutively expressed in mechanosensory neurons that mediate unique contributions to neuronal signaling (Figure 12) (Bewick and Banks 2015; Woo, Lukacs *et al.* 2015; Carrasco, Vincent *et al.* 2017). We found no evidence for independent nor combinatorial effects of cancer or chemotherapy at the genetic level (Figure 16a and Extended Data) for channels mediating mechanotransduction (e.g. *Asic2*, *Piezo2*, *ENaCs*), signal amplification, and spike encoding (e.g. *Scn1a* (Nav1.1), *Scn8a* (Nav1.6), *Scn9a* (Nav1.7), *Cacna1s,-c,-d, -f (*Cav1.1-4), *Kcnn2* (SK2), *Kcna1* (Kv1.1) which was subsequently confirmed in downstream immunohistochemical analyses (Figure 13, Figure 14, Figure 15).

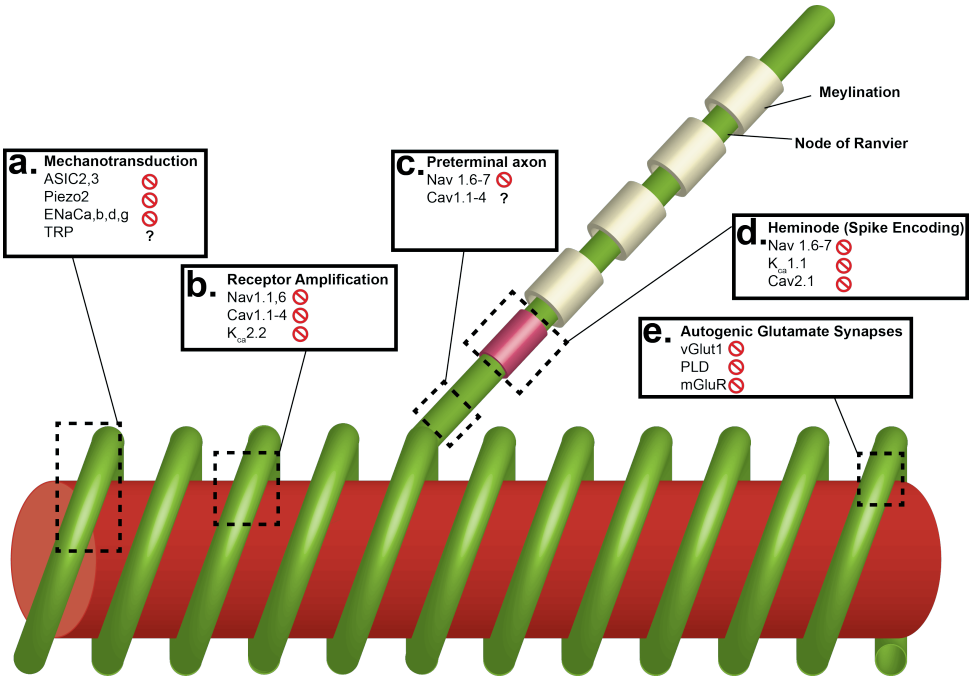


***Figure 12.***

**Model of molecular determinants of neuronal signalling of sensory neurons.** Model of mechanically-, voltage- and ligand-gated ion channels and their distribution in muscle spindle Ia primary ending. The intrafusal muscle fiber (red) is wrapped by an annulospiral ending (green) and a preterminal axon that extends unmyelinated from the terminal to the heminode (pink) followed by a myelinated axon. Dotted-boxes represent specific regional distributions believed to underlie specific functional characteristics of neuronal signaling e.g. mechanotransduction, receptor potential amplification, spike encoding, and autogenic feedback. Red circles with slashes indicate no gene and protein level evidential support for involvement in mediating cancer-chemotherapy codepedent neuronal dysfunction. Bold question marks (?) indicate protein as a possible candidate due to evidential support from transcriptome, yet protein level confirmation is unavailable. a, Deformation of the receptor ending opens mechanotransduction channels that initiate excitatory currents mediated by ASIC2/3 (Simon et al 2010), Piezo2 (Woo et al 2015), ENaCa,b,d,g and to some extend TRP channels (Bewick and Banks 2015). Various Nav (Carrasco et al 2017) and Cav (Bewick and Banks 2015) channels are believed to amplify receptor potentials (b) and assist transmission toward encoding in the preterminal axons (c). d, Recent discovery of specific distribution of Nav channels in the heminodes (Carrasco et al 2017) are believed to underlie encoding of action potential similar to axon initial segments in other systems (Foust et al 2010). e, three components known to regulate auto- genic glutamatergic synapses in proprioceptors critical for signalling.

Next, we performed cell-specific immunohistochemical analyses to test gene–protein correspondence. We found no evidence to suggest dysregulated protein expression nor did evidence emerge to suggest altered protein distributions for most proteins, including those mediating mechanotransduction (ASIC2) (Figure 13), signal amplification (Nav1.1, Nav1.6 shown in Figure 14, and Nav1.7), spike encoding (Kv1.1), and mechanosensory sensitivity (VGLUT1) (Figure 15). These findings demonstrate that many of the molecular mechanisms responsible for mechanotransduction and determining excitability of mechanosensory neurons were preserved in the *Apc*$^{Pirc/+}$+OX rats. These findings narrow the field of candidate mechanisms for which treatment might reasonably restore normal function.

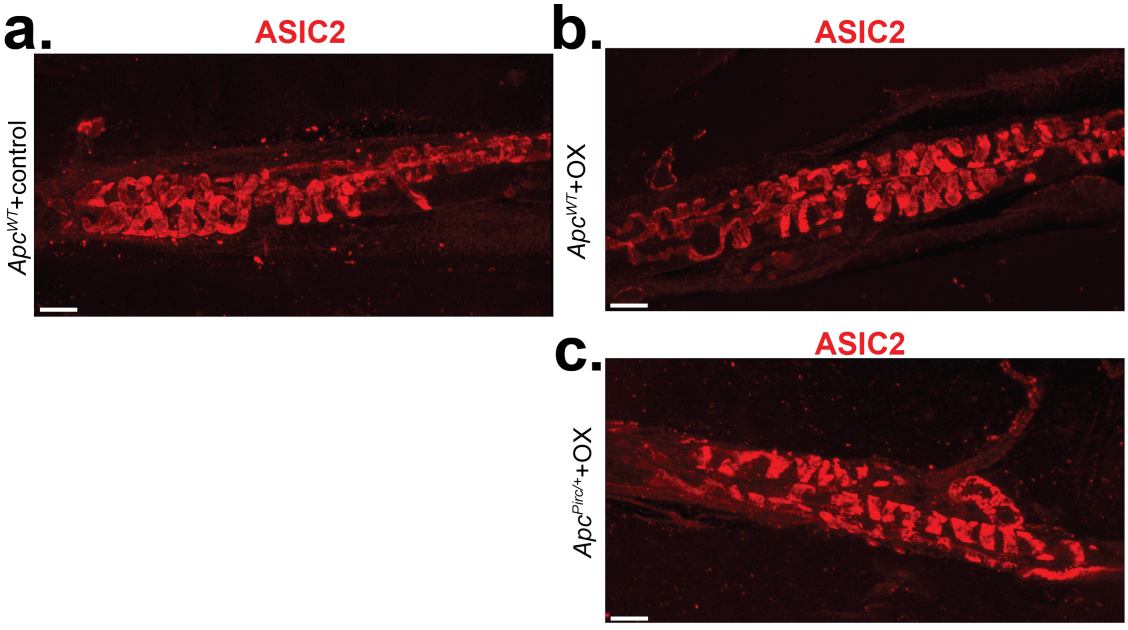


***Figure 13.***

**ASIC2 immunostaining of proprioceptive sensory neurons receptor endings.** Whole-mount staining and confocal axial projection of the preterminal axons and annulospiral receptor endings of proprioceptive sensory neurons showing single channel images of ASIC2 (red) from: a, Apc$^{WT}$ +control rat; b, Apc$^{Pirc/+}$+control; c, Apc$^{WT}$+OX; d, and Apc$^{Pirc/+}$+OX rats.

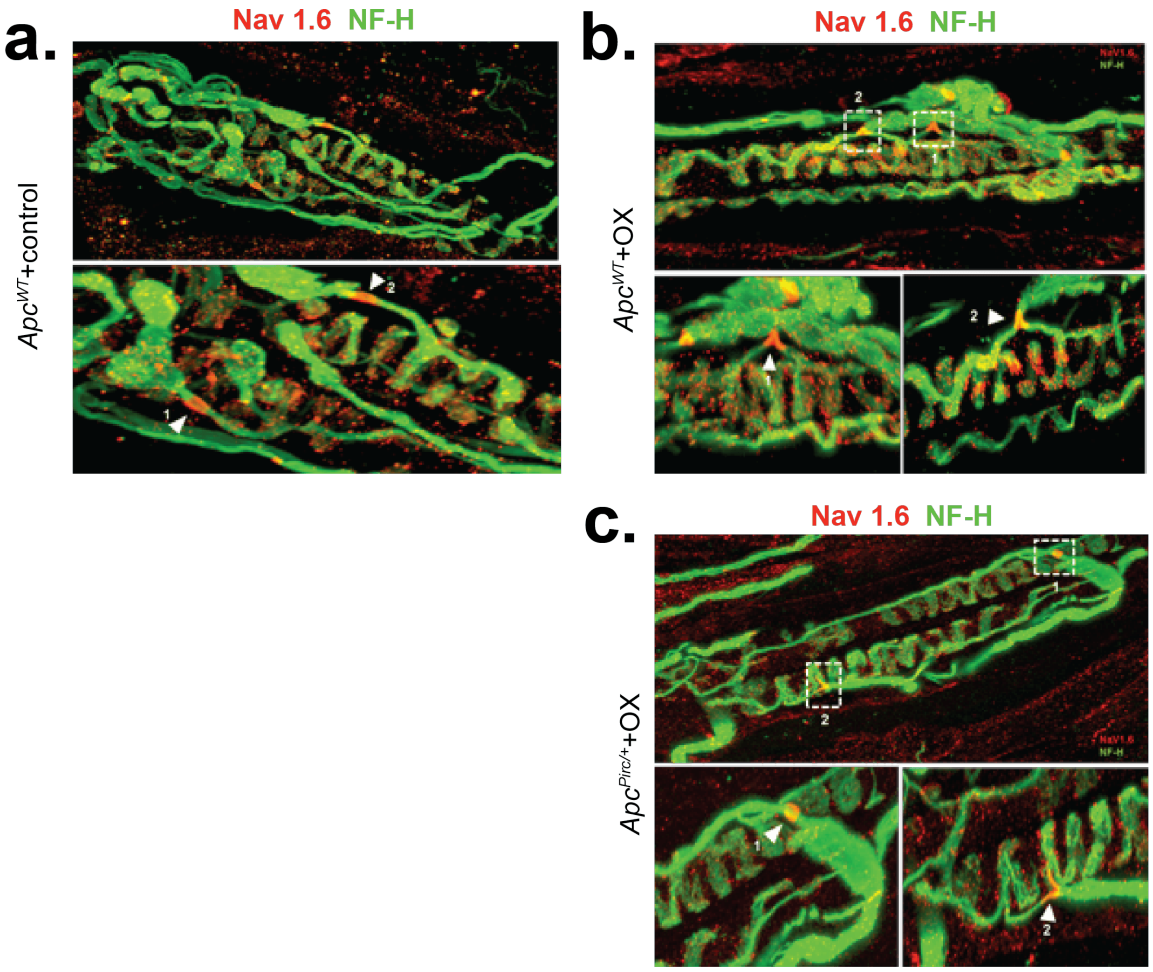


***Figure 14.***

**Nav1.6 immunostaining of proprioceptive sensory neurons receptor endings.** Whole-mount staining and confocal axial projection of the preterminal axons and annulospiral receptor endings of proprioceptive sensory neurons showing single channel images of Nav1.6 (red) and NF-H (green) in top row from: a, $Apc^{WT}$ +control rat; b; c, $Apc^{WT}$+OX; d, and $Apc^{Pirc/+}$+OX rats. Bottom rows show Nav1.6 distribution in heminodes where spike encoding is initiated.

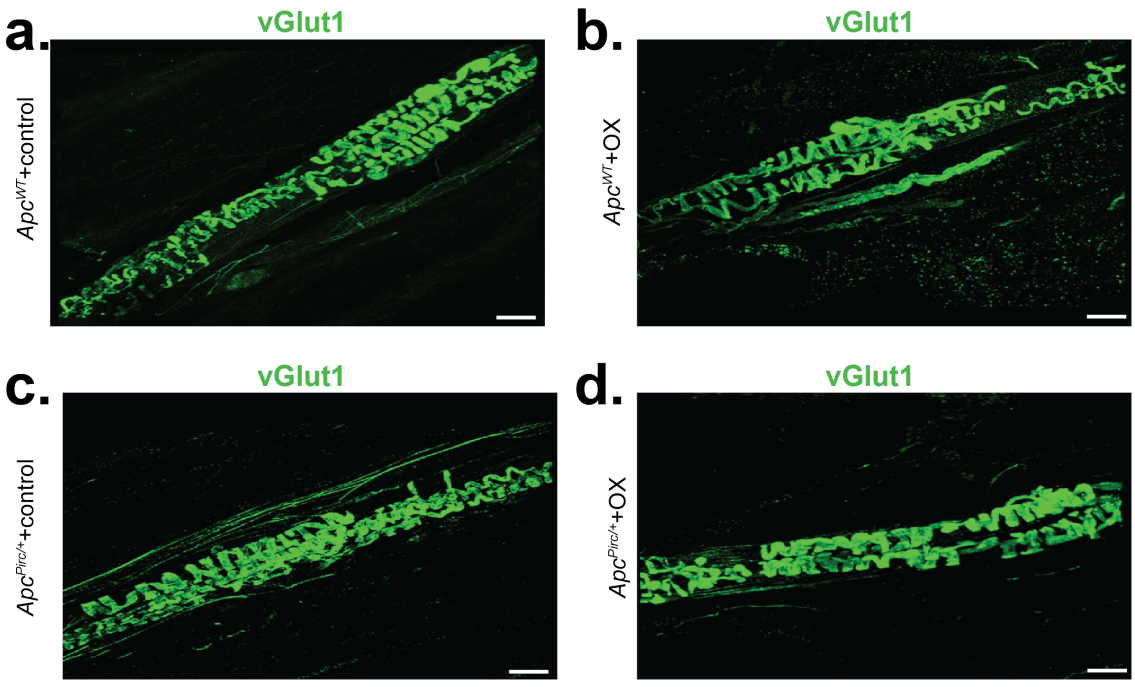


***Figure 15.***

**vGlut1 immunostaining of proprioceptive sensory neurons receptor endings.** Whole-mount staining and confocal axial projection of the preterminal axons and annulospiral receptor endings of proprioceptive sensory neurons showing single channel images of vGlut1 (green) from: a, $Apc^{WT}$ +control rat; b, $Apc^{Pirc/+}$+control; c, $Apc^{WT}$+OX; d, and $Apc^{Pirc/+}$+OX rats.

Having exhausted examination of proteins known to be expressed in mechanosensory neurons, we extended our search to include ion channels yet to be identified, but known to regulate neuronal signaling in other classes of neurons (Rudy, Chow *et al.* 1999; Akemann and Knöpfel 2006; Espinosa, Torres-Vega *et al.* 2008; Waxman and Zamponi 2014). As one of the most dysregulated voltage-gated ion channels, *Kcnc3* (encoding protein Kv3.3) emerged as a novel candidate (Figure 16a, b, Figure 17). Pharmacologic and genetic perturbation of Kv3.3 (*Kcnc3*) impairs neuronal signaling (Akemann and Knöpfel 2006; Espinosa, Torres-Vega *et al.* 2008) and is causally linked to ataxias

(Figueroa, Minassian *et al.* 2010) that are consistent with functional deficits observed in patients with cancer long after cessation of chemotherapy. We then immunolabeled sensory cell bodies in dorsal root ganglia and their receptor endings taken from $Apc^{WT}$+control with monoclonal antibodies targeting Kv3.3, which revealed the first evidence of this ion channel in all large diameter cell bodies in the dorsal root ganglia that supply mechanosensors (Figure 16c and Figure 18) and endings (Figure 16e). Results of comparison across experimental groups indicate that Kv3.3 expression was significantly lower in $Apc^{Pirc/+}$+OX compared with $Apc^{WT}$+control (Figure 16d,), $Apc^{Pirc/+}$+control, or $Apc^{WT}$+OX (Figure 18), demonstrating that codependent dysfunction is conserved in cell-type specific protein expression. Notably, while we discovered correspondence between protein and gene dysregulation, genetic dysregulation appeared larger. This finding may represent the expression of a faulty epigenetic regulatory process that is incompletely compensated at the protein level. Moreover, conserved Kv3.3 expression in neuromuscular junctions suggests that Kv3.3 dysfunction was constrained to sensory neurons (Figure 19).

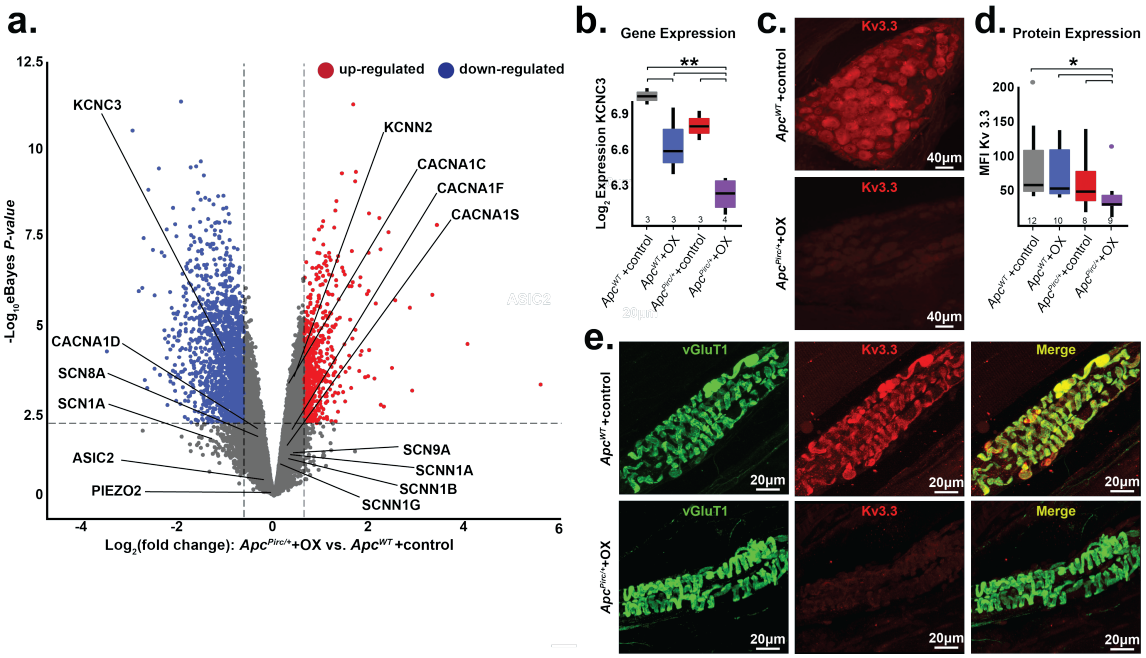


## ***Figure 16.***

**Targeted transcriptional analysis reveals mechanisms for cancer-chemotherapy interaction.** a, Volcano plot comparing up- and downregulated genes in *Apc*$^{Pirc/+}$+OX and *Apc*$^{WT}$+control sensory neuron transcriptomes. Annotation of genes involved in mechanotransduction, signal amplification, action potential generation and maintenance is shown. Significance was determined as Benjamini–Hochberg FDR < 0.01 and log2fold change ≥ 1. b, Gene expression of Kcnc3 encoding Kv3.3, as determined through transcriptional profiling (Kcnc3: 1369133_a_at). c, Confocal images of dorsal root ganglia immunolabeled against Kv3.3 illustrates expression of *Apc*$^{Pirc/+}$+OX relative to *Apc*$^{WT}$+control neurons. d, Quantification of receptor protein expression (mean fluorescence intensity (MFI)) of Kv3.3 determined through averaging over all annulospiral endings (617 from 12 *Apc*$^{WT}$+control neurons, 434 from 10 *Apc*$^{WT}$+OX neurons, 459 from 8 *Apc*$^{Pirc/+}$+control neurons, and 362 from 9 *Apc*$^{Pirc/+}$+OX neurons) for each neuron per experimental group. e, Confocal images of mechanosensory nerve terminals in muscle spindles immunolabeled against VGluT1 (green), Kv3.3 (red), and merged (yellow) illustrates protein expression levels and distribution in *Apc*$^{Pirc/+}$+OX relative to *Apc*$^{WT}$+control. * indicates statistically significant differences between experimental groups as empirically derived from hierarchical Bayesian model (stan_glm). ** indicates $P_{eBayesAdj}$<0.005 and fold-change (FC) >1.5 using a Bayesian moderated linear fixed effects model. Data presented as mean±s.e.m

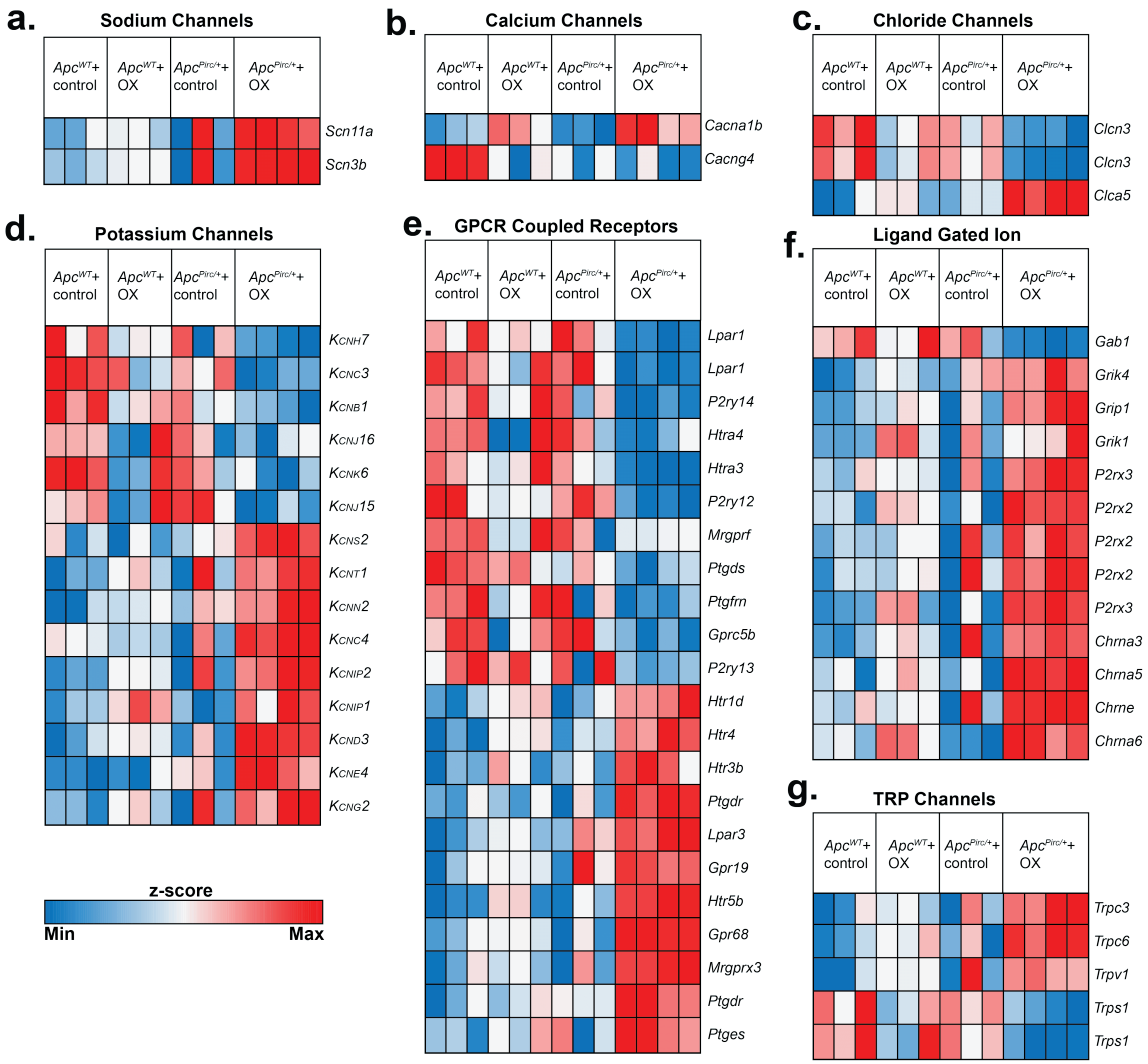


## ***Figure 17.***

**Heat-map distribution of significantly differentially expressed genes specific to neuron neuronal excitability.** Major voltage-gated, mechanically gated, TRP channels and ligand-gated and G-protein coupled receptors across experimental groups. Expression patterns of different sub-types channels and receptors were identified by empirical Bayesian moderated linear fixed effects models (columns are individual samples, heat-maps). (**a**) Sodium channel levels, (**b**) calcium channel levels, (**c**) chloride channel levels (**d**) potassium channel levels, (**e**) G-protein coupled receptors (GPCRs) levels, (**f**) ligand-gated channel levels, and (**g**) transient receptor potential (TRP) channel levels are plotted as heat-maps. Data row standardized (mean centered and s.d. normalized) to specific genes.

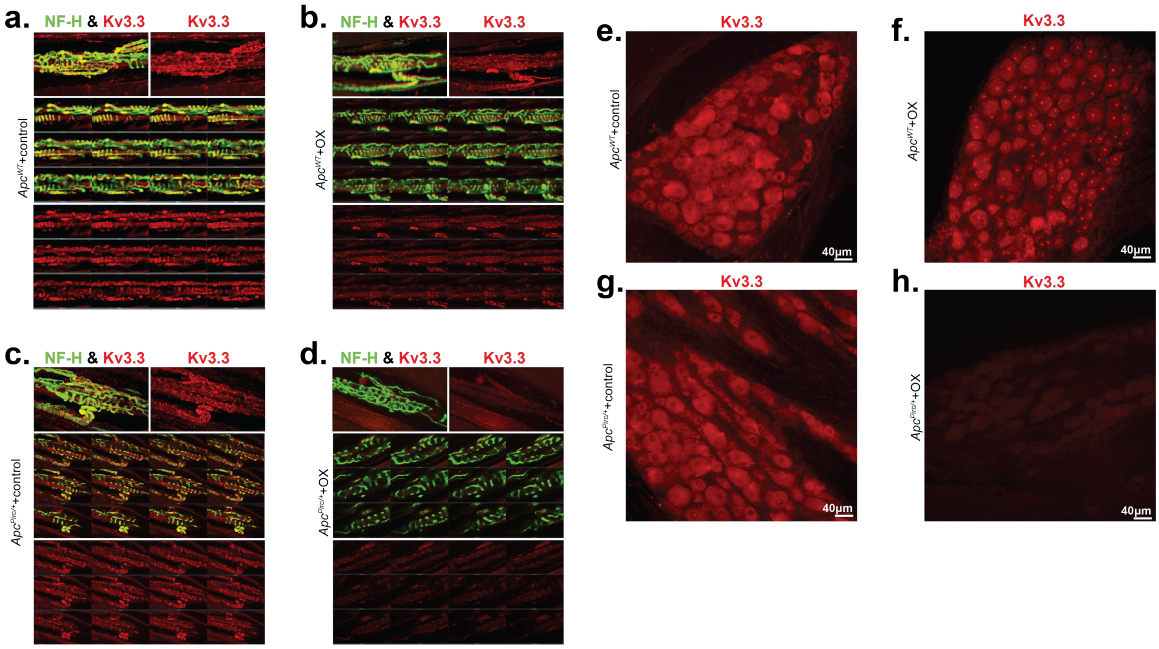


## ***Figure 18.***

**Kv3.3 immunostaining of proprioceptive sensory neurons receptor endings and cell bodies. a-d,** Whole-mount staining and confocal axial projection of the preterminal axons and annulospiral receptor endings of proprioceptive sensory neurons showing merged and single channel images of Kv3.3 (red) and NF-H (green) in top row from: **a,** *Apc*$^{WT}$+control rat; **b**, Apc$^{Pirc/+}$+control; **c,** Apc$^{WT}$+OX; **d**, and *Apc*$^{Pirc/+}$+OX rats. Individual optical planes (from z-stack projection) of axial projection highlight fine three-dimensional structural distribution of merged and single channel images of Kv3.3 (bottom). Whole-mount staining and confocal axial projections of DRG neurons highlight expression of Kv3.3 in **e,** *Apc*$^{WT}$+control rat; **f**, Apc$^{Pirc/+}$+control; **g,** Apc$^{WT}$+OX; **h**, and *Apc*$^{Pirc/+}$+OX rats.

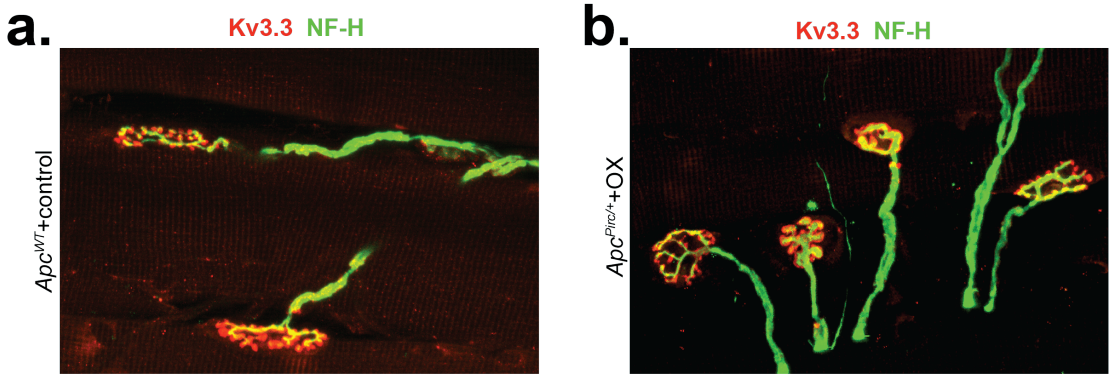


***Figure 19.***

**Kv3.3 Immunostaining of neuromuscular junction.** Whole-mount staining and confocal axial projection of the neuromuscular junction showing merged images of Kv3.3 (red) and NF-H (green) from: **a,** *Apc*$^{WT}$+control and **b**, *Apc*$^{Pirc/+}$+OX rats.

### *Summary*

This is the first evidence implicating Kv3.3 in the development of neuropathy and the first data, to our knowledge, demonstrating a channelopathy that persists long after treatment cessation. The capacity of Kv3.3 to drive fast spiking and to enhance transmitter release – processes that are required for mechanotransduction and spike encoding– suggests that this ion channel might provide both a potential novel mechanism for the dysfunction of mechanosensory neurons and a potential target for therapy.

## Aim 3: Test the hypothesis that neuronal dysfunction depends on cancer-chemotherapy interaction.

### *Introduction*

To test whether interaction we discovered at gene and protein levels was conserved at a functional neuron level in living animals, we tested whether *APC*$^{Pirc/+}$ mutants treated with OX express neuronal signaling dysfunction *in vivo* by examining the capacity of single proprioceptive neurons to respond to physiologically-relevant stimuli (Figure 21).

### *Aim Specific Methods*

*In vivo Intracellular Recording*

Dorsal rootlets positioned in continuity on bipolar recording electrodes were selected for sampling sensory neurons when they produced robust action potential activity in response to stretch of triceps surae muscles. Individual axons penetrated in these rootlets by glass micropipettes (~30 MΩ filled with 2 M K+ acetate) were selected for study when electrical stimulation of triceps surae nerves produced orthodromic action potentials that were readily resolvable and had conduction delay of <2ms. Continuous intracellular recordings from sensory neurons were acquired with Spike2 software (version 8.02). Sensory neurons were classified as Ia by their perfect entrainment to 1-s bouts of high-frequency, small-amplitude vibration (100Hz, 80 μm), pause in firing during rising twitch force response (muscle shortening), and by responding with an initial burst of high-frequency firing (>100 pulses per second (pps)) at the onset of muscle stretch (Vincent, Gabriel *et al.* 2017). Two stretch paradigms were used to characterize the firing responses of afferents to physiologically relevant mechanical stimuli. In both paradigms, triceps surae muscles were stretched by 3 mm from $L_o$ (7% strain). Ramp-hold-release stretches tested afferent encoding of both fast dynamic (20mm/s, 47% strain rate) and

static stimuli; successive triplets of triangular stretch tested slow (4mm/s, 9% strain rate) dynamic and activity-dependent encoding in dynamic stretch known to be influenced by recent signaling history (Vincent, Gabriel *et al.* 2017). Strains and strain-rates fall within values expected for animals engaged in normal activities e.g. locomotion, and have been previously used in our lab (Vincent, Gabriel *et al.* 2017).

*Intracellular Recording Pre-Processing*

Intra-axonal recordings of action potentials together with records of muscle length and force were digitized (20 kHz) and were monitored online and stored on computer for later analysis with Spike2 and custom-written MATLAB scripts. From raw intracellular data of both paradigms, we extracted 31 measured and derived features (Figure 20) that provide a comprehensive quantification of neuronal signaling characteristics. We then categorized features into four broad clusters that represent functional features encoded by these neurons, containing sensitivity (Thr), dynamic (Dyn), static (Stat), and history-dependent (Hx) signaling information. Figure 20 identifies and describes the measured and computed features and functional clustering used for inference.

**a.**

| Sensitivity/Threshold Functional Cluster | | |
|---|---|---|
| 1 | Thr.L3 | Length at which 1st action potential is detected on the 3rd slow ramp (mm) |
| 2 | Thr.L | Length at which 1st action potential is detected on the fast ramp (mm) |
| 3 | Thr.T1 | Time at which 1st action potential is detected on the 1st slow ramp (ms) |
| 4 | Thr.F3 | Muscle tendon force at which 1st action potential is detected on the 3rd slow ramp (dN) |
| 5 | Thr.F1 | Muscle tendon force at which 1st action potential is detected on the 1st slow ramp (dN) |
| 6 | Thr.T | Time at which 1st action potential is detected on the fast ramp (ms) |
| 7 | Thr.F | Muscle tendon force at which 1st action potential is detected on the fast ramp (dN) |
| 8 | Thr.L1 | Length at which 1st action potential is detected on the 1st slow ramp (mm) |
| 9 | Thr.T3 | Time at which 1st action potential is detected on the 3rd slow ramp (ms) |

| Dyamic Signaling Functional Cluster | | |
|---|---|---|
| 10 | Dyn.slp1 | Slope of instantenous firing rate during the 1st slow ramp |
| 11 | Dyn.pfr1 | Peak firing rate achieved during the 1st slow ramp (Hz, pps) |
| 12 | Dyn.spkNum | Number of action potentials (spikes) during the fast ramp (#) |
| 13 | Dyn.DI | Difference between the peak dynamic firing rate and the static firing rate during half hold (Hz) |
| 14 | Dyn.spkNum3 | Number of action potentials (spikes) during the 3rd slow ramp (#) |
| 15 | Dyn.F | |
| 16 | Dyn.slp3 | Slope of instantenous firing rate during the 3rd slow ramp |
| 17 | Dyn.spkNum1 | Number of action potentials (spikes) during the 1st slow ramp (#) |
| 18 | Dyn.IB | Peak instantaneous high-frequency firing rate achieved immediately after stimulus (Hz) |
| 19 | Dyn.slp | Slope of instantenous firing rate during the fast ramp |
| 20 | Dyn.IFRdrop | Drop in instantaneous firing rate after the release on the slow ramps (Hz, pps) |
| 21 | Dyn.pfr3 | Peak firing rate achieved during the 3rd slow ramp (Hz, pps) |
| 22 | Dyn.pfr | Peak firing rate achieved during the fast ramp (Hz, pps) |

| Static Signaling Functional Cluster | | |
|---|---|---|
| 23 | Stat.mSfr | Instantenous firing rate midway through the static hold (Hz, pps) |
| 24 | Stat.afr | Average firing rate during the static hold (Hz, pps) |
| 25 | Stat.HzSTD | The standard deviation of instantaneous firing rate during the static hold |
| 26 | Stat.LSpkF | The muscle force at which the last action potential occurs during the static hold (dN). |
| 27 | Stat.slp | Slope of instantenous firing rate during the static hold. |
| 28 | Stat.LspkT | The time at which the last action potential occurs during the static hold (ms). |
| 29 | Stat.HzEnd | Instantenous firing rate during at the end of the static hold (Hz) |
| 30 | Stat.spkNum | Number of action potentials (spikes) during the static hold (#) |

| History Dependence Functional Cluster | | |
|---|---|---|
| 31 | HxDep.RDR | Difference between the number of action potentials (spikes) in the 1st and 3rd slow ramp |

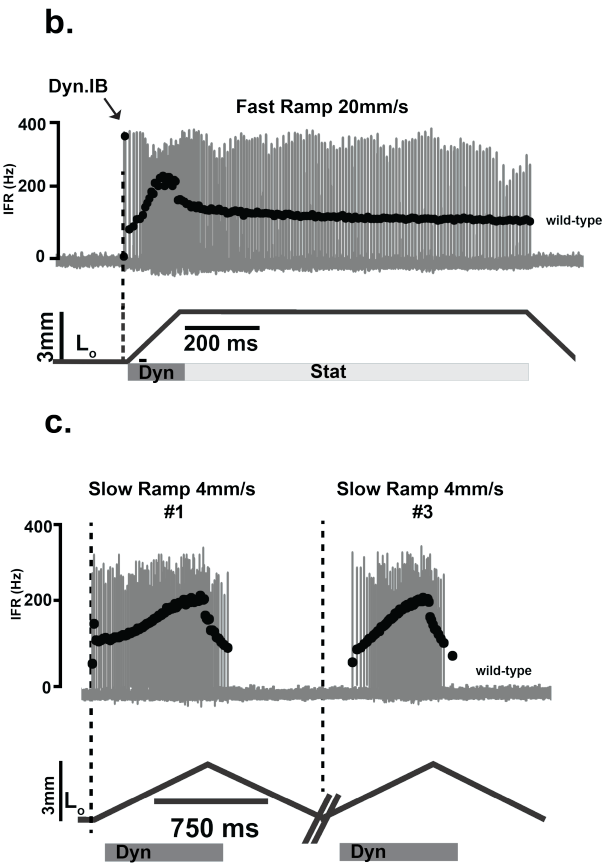


***Figure 20.***

**List of Parameters used for Neurophysiological Analyses,** related to Figures 2, 3 and Extended Data Figure 12. **a,** Measured and derived parameters were computed offline using custom written MATLAB scripts. Letters in the left column indicate the specific parameters included in analyses for each functional feature cluster. Thr: threshold (9 parameters); Dyn: dynamic (11 parameters); Stat: static (8 parameters); HxDep: history-dependent (1 parameter). For detailed experimental recording paradigms see Online Methods. **b**, Representative fast ramp-hold-release (3 mm at 20mm/s) trial from a proprioceptive neuron recorded from dorsal roots in *in vivo* electrophysiological experiments of a wild-type rat. **c**, Representative slow repeated ramp (3 mm at 4mm/s) trial from a proprioceptive neuron recorded from dorsal roots in *in vivo* electrophysiological experiments of a wild-type rat. Corresponding action potential trains and overlaid black circles indicate individual action potentials (spikes) and instantaneous firing rates (IFRs) of the responses. Dashed line marks the point of muscle stretch from background length ($L_o$) and indicates the starting point for threshold/sensitivity measurements. Boxes indicate dynamic (dark grey, 150 ms duration after stretch command onset) and static phases for analysis (light grey, 1 s duration after the dynamic phase)

*Statistical Analysis of Intracellular Recordings*

Linear discriminant analysis (LDA) provided supervised dimensionality reduction for the multiple features of neuron signaling, in an attempt to find a linear combination of features that separated and characterized independent and combinatorial treatment effects. Data were first de-meaned, normalized to unit standard deviation, and tested by Bayesian one-way ANOVA (*stan_glm*) (Gabry and Goodrich 2018). The derived covariance matrix was then normalized by within-group, pooled covariance. The eigenvectors of that modified covariance matrix defined three canonical variables that characterized and separated the four treatment groups identified *a priori* as $Apc^{WT}$+control, $Apc^{WT}$+OX, $Apc^{Pirc/+}$+control, *and* $Apc^{Pirc/+}$+OX. LDA and 10-fold cross validation of model performance (repeated holdout method) was performed with the *MASS* (7.3-51.1) (Venables and Ripley 2002) library in the R environment (3.5.0) (Team 2018). Individual features characterizing the firing responses of neurons sampled from multiple rats were tested for statistically significant differences with Bayesian one-way ANOVA (*stan_glm*). Descriptions of the general approach and detailed model construction and validation is below.

## *Results*

*Neuronal signaling is impaired*

Applying electrophysiological methods to rats in vivo, we recorded spiking activity from single mechanosensory neurons responding to naturalistic mechanical stimuli (Figure 23). From these spiking responses, we collected 31 measured and derived parameters (average of four trials; n = 11 $Apc^{WT}$+control, n=19 $Apc^{WT}$+OX, n=20 $Apc^{Pirc/+}$+control, n = 10 $Apc^{Pirc/+}$+OX; Figure 20) from which we extract four functional features encoded by these neurons, sensitivity, dynamic, static, and history-dependent signaling information (Figure 20). In $Apc^{WT}$+control rats, we found that muscle stretch elicited the spiking

expected from sensory neurons in normal animals (Vincent, Gabriel *et al.* 2017) and humans (Burke, Hagbarth *et al.* 1978), specifically high frequency initial bursting at stimulus onset, increasing dynamic firing during increasing stimulus, sustained static firing with slow accommodation during the hold phase of stretch (Figure 23b), and history-dependent reduction in spike number (Figure 22 and Figure 27h).

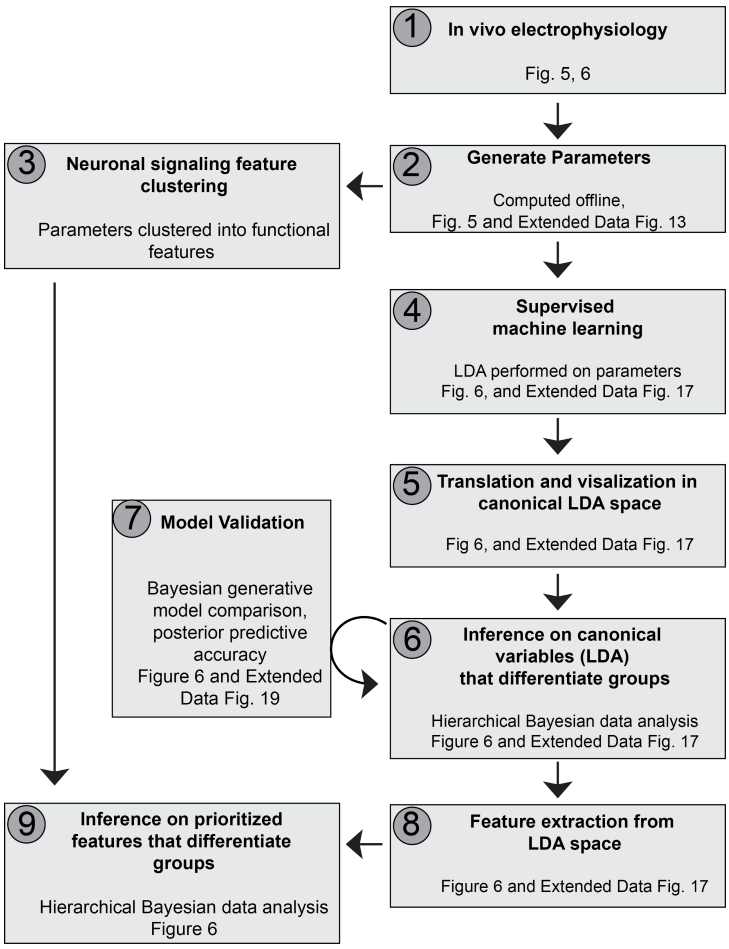


***Figure 21.***

**Steps of In Vivo Electrophysiology Analysis**. Data analysis flowchart depicts the multi-step approach applied for single neuron physiological analyses, inferences and downstream model validation. A detailed description of each step is available in the **Methods Sections.** Linear discriminant analysis, LDA.

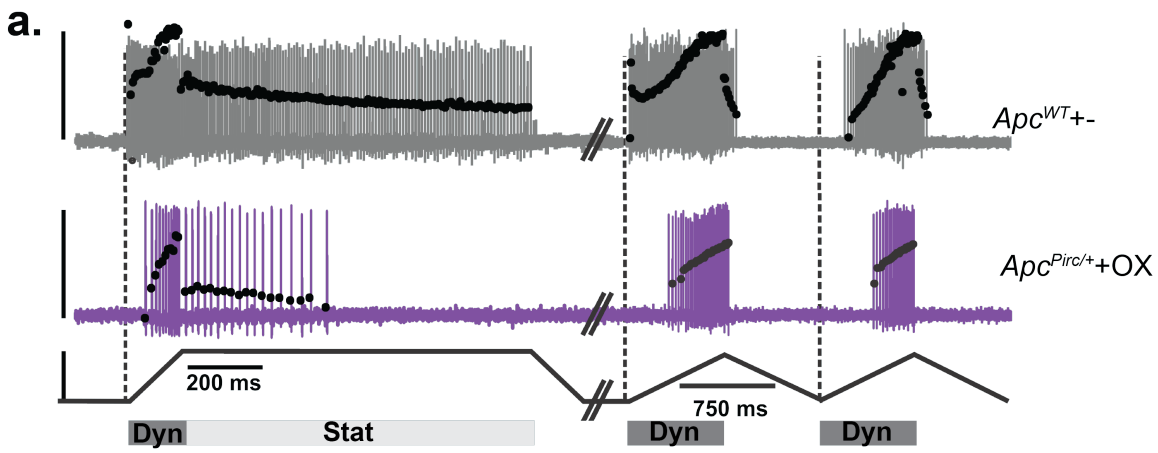


***Figure 22.***

**Neuronal signaling responses to slow and fast naturalistic stimulus.** related to Figures 5, 6. **a,** Representative fast ramp-hold-release (left, 3 mm at 20mm/s) and slow repeated ramp (right, 3 mm at 4mm/s) trial from a proprioceptive neuron recorded from dorsal roots in *in vivo* electrophysiological experiments of an $Apc^{WT}$+control (grey) and $Apc^{Pirc/+}$+OX rat (purple). Corresponding action potential trains and overlaid black circles indicate individual action potentials (spikes) and IFRs (instantaneous firing rates) of the responses. Dashed line marks the point of muscle stretch from background length ($L_o$) and indicates the starting point for threshold/sensitivity measurements. Boxes indicate dynamic (dark grey, 150 ms duration after stretch command onset) and static phases for analysis (light grey, 1 s duration after the dynamic phase).

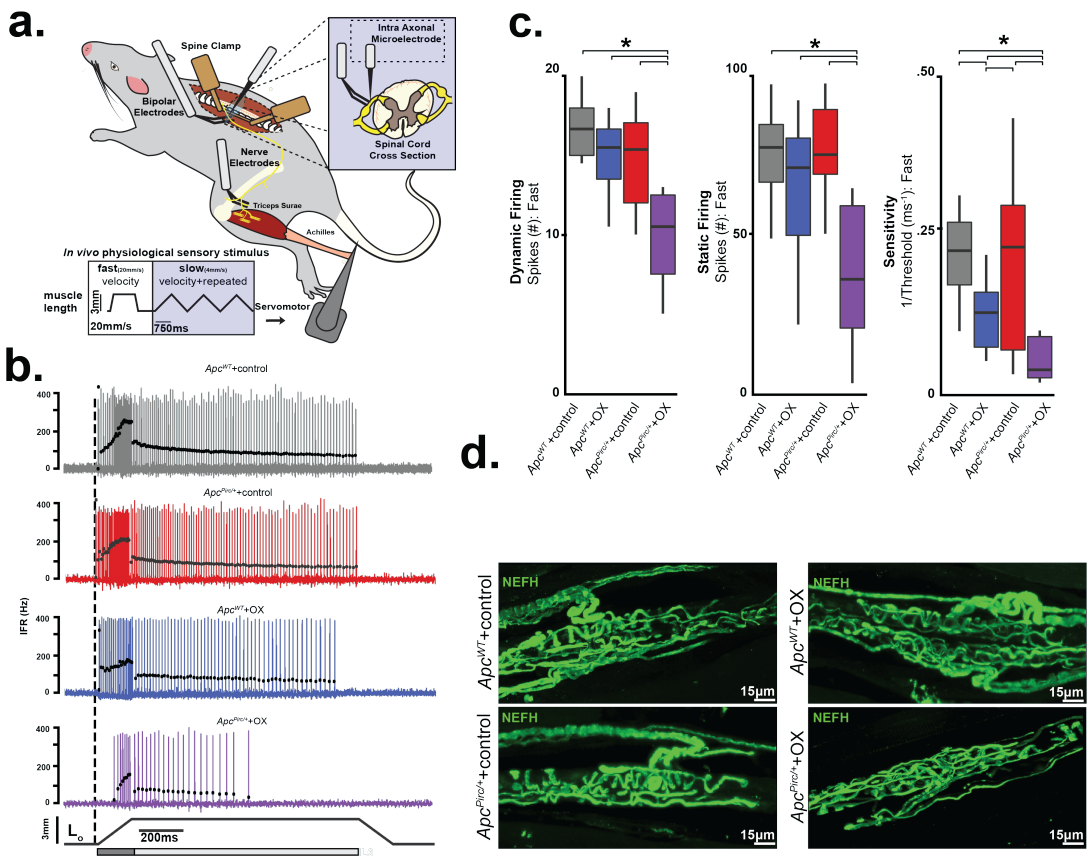


***Figure 23.***

**Mechanosensory signal degradation exacerbated by the cancer–chemotherapy interaction.** a, Schematic of experimental approach for in vivo recordings centrally from intact mechanosensory neurons firing action potentials in response to fast (20mm/s) and slow (4mm/s) naturalistic mechanical stimuli delivered in the periphery. b, Representative cases of spiking activity in *Apc*$^{WT}$+control, *Apc*$^{WT}$+OX, *Apc*$^{Pirc/+}$+control, and *Apc*$^{Pirc/+}$+OX as a measure of sensory encoding. Black circles plot instantaneous firing rates (pps) of corresponding spike (action potential) intervals. Dashed vertical line marks onset of muscle stretch (3mm from resting length (Lo)) shown in bottom trace divided into dynamic and static phases by dark grey (150 ms duration after stretch command onset) and light grey (1 s duration after the dynamic phase) bars. c, Neuronal spiking parameters (n=31 averaged from four trials in each neuron, four shown from fast ramp stimulus) representing different features of sensory stimulus (*Apc*$^{WT}$+control (n = 11), *Apc*$^{WT}$+OX (n = 19), *Apc*$^{Pirc/+}$+control (n = 20) and *Apc*$^{Pirc/+}$+OX (n = 10)): mean initial burst frequency (pps) signaling stretch onset; the number of spikes during dynamic sensory stimulation (shown as a dark grey bar in b); the number of spikes during static sensory stimulation (shown as a light grey bar in b); sensitivity assessed as the inverse of latency to stimulus detection (ms-1), i.e. lower sensitivity corresponds to longer latency and higher

threshold. d, Confocal image of a neurofilament heavy-chain (NEFH, in green) with immunolabeling of the terminal axon and receptor structure in $Apc^{WT}$+control, $Apc^{WT}$+OX, $Apc^{Pirc/+}$+control, and $Apc^{Pirc/+}$+OX rats. Scale bar, 15 μm. * indicates statistically significant differences between experimental groups as empirically derived from hierarchical Bayesian model (stan_glm): 95% highest density intervals do not overlap between groupwise contrasts. Data presented as mean±s.e.m.

We next tested whether $Apc^{Pirc/+}$ or OX treatment alone induce signaling dysfunction. Although we find transcriptional dysregulation in $Apc^{Pirc/+}$+control Figure 6c and Figure 9a), we found a remarkable degree of concordance with signaling in $Apc^{WT}$+control (Figure 23b). $Apc^{Pirc/+}$+control neuronal signaling displayed comparable sensitivity to stimuli and showed similar static behavior across all neurons (n = 20; Figure 23b,c) as the $Apc^{WT}$+control. We then found that OX treatment of $Apc^{WT}$ rats induced mild signaling deficits that were less pronounced, occurred in a small proportion of neurons (5/19), and were primarily restricted to sensitivity functional clusters (Figure 23b,c and Figure 24d), validating our previous findings of restricted deficits (to single signaling parameters) observed in a different strain of healthy rats treated with OX alone (Vincent, Wieczerzak *et al.* 2016).

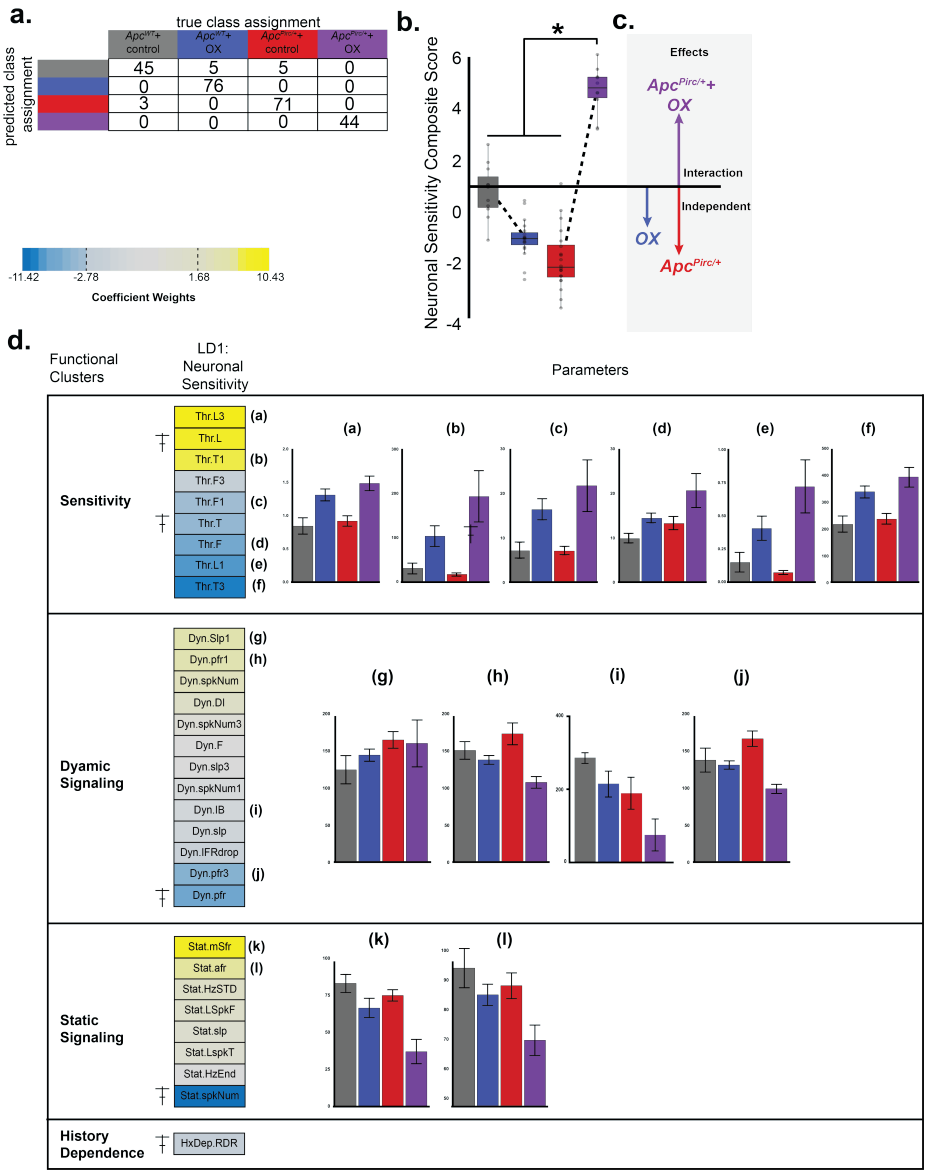


## ***Figure 24.***

**LD1 analysis of all neuronal parameters. a,** Confusion matrix illustrates the results of 10-fold cross validation of LDA model performance (repeated holdout method) that achieved overall 94.7% classification accuracy (posterior prediction check). Table values represent the sum of out-of-sample cross validation predictions (row) against true class assignment (column) **b,** Histogram plot, mean values of LD1 scores (Figure 27) for each group were compared with hierarchical Bayesian ANOVA model. Asterisk indicate statistically significant differences between experimental groups in hierarchical Bayesian ANOVA, (*) indicates 95% highest density intervals (HDI) do not overlap between groupwise contrasts. **c,** Vectors represent the magnitude and direction of the independent and combinatorial effects of cancer and/or chemotherapy. **d,** Parameters (n =31, middle) and respective discriminant coefficients weights with the

interaction-specific LD1, were regrouped into functional feature clusters (left). Histogram plots report mean values for individual parameters (right, a-l) with significant contribution to LD1 loading. Cross symbol indicate parameters are included in Figure 23 and Figure 27. Analyzed from $Apc^{WT}$+control (n = 11), $Apc^{WT}$+OX (n = 19), $Apc^{Pirc/+}$+control (n = 20) and $Apc^{Pirc/+}$+OX (n = 10) neurons.

In contrast to the observations in $Apc^{WT}$+control, $Apc^{WT}$+OX, or $Apc^{Pirc/+}$+control rats, we found drastically impaired neuronal signaling in $Apc^{Pirc/+}$+OX rats (Figure 23b). High frequency initial bursting was attenuated four-fold and sensitivity to stimuli was reduced by three-fold at both high (Figure 24d) and low velocity stretch (Figure 22, Figure 24d). During dynamic stimuli, we found marked reduction in the number of spikes over both stretch conditions (Figure 23c). Neurons in $Apc^{Pirc/+}$+OX rats also failed to sustain firing (Figure 23b). In addition, we observed fewer spikes (Figure 23c) during rapid accommodation immediately preceding signal deletion, despite constant stimulus (Figure 23b). We then simulated naturalistic compensation by subjecting $Apc^{Pirc/+}$+OX neurons to repeated trials at 1, 2, and 3x background stimulus ($L_o$ strain) intensity, which failed to completely rescue signaling back to $Apc^{WT}$+control levels (Figure 25b, c, d). These data are the first to directly demonstrate a damaging functional interaction between the systemic effects of cancer and chemotherapy in sensory neurons in a living animal. While validating our previous findings of signaling deficits in chemotherapy alone (Vincent, Wieczerzak *et al.* 2016), these data indicate that restrictive signaling deficits induced by chemotherapy or cancer alone were insufficient to reproduce the magnitude, direction and number of dysfunctional parameters induced by codependent neuropathy.

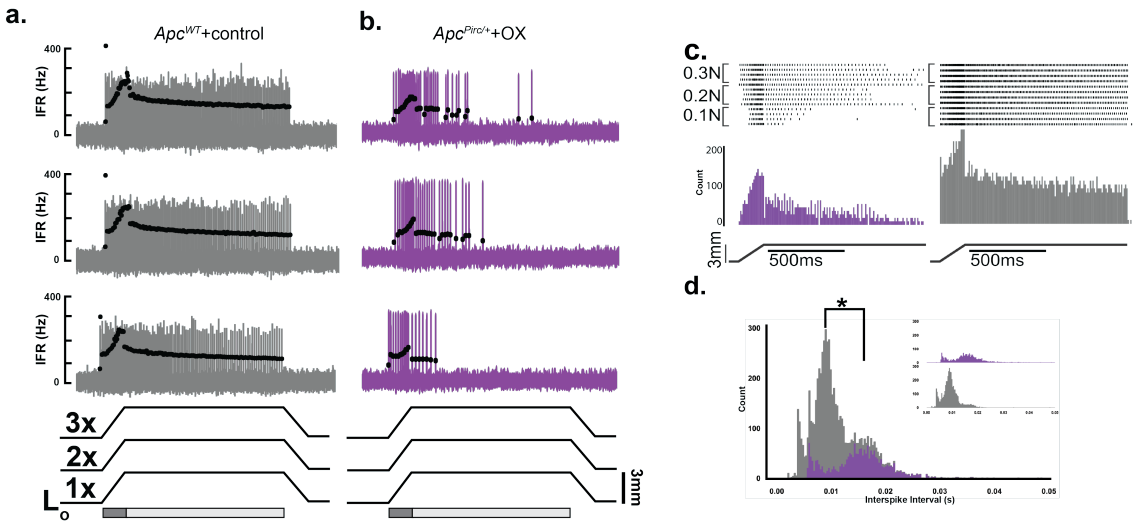


## ***Figure 25.***

**Effects of physiologic compensation. a, b,** Representative fast ramp-hold-release (left, 3 mm at 20mm/s) trial from a proprioceptive neuron recorded from dorsal roots in *in vivo* electrophysiological experiments of a *Apc*$^{WT}$+control (grey **a**) and *Apc*$^{Pirc/+}$+OX rat (purple **b**). Corresponding action potential trains and overlaid black circles indicate individual action potentials (spikes) and IFRs (instantaneous firing rates) of the responses. Dashed line marks the point of muscle stretch from background length ($L_o$) and indicates the starting point for threshold/sensitivity measurements. Boxes indicate dynamic (dark grey, 150 ms duration after stretch command onset) and static phases for analysis (light grey, 1 s duration after the dynamic phase). Stretch evoked (3mm) responses recorded from replicate trials at 1, 2, and 3x $L_o$ for *Apc*$^{WT}$+control (**a**) and *Apc*$^{Pirc/+}$+OX **(b). c,** Raster plots of stretch evoked (3mm) responses from representative neurons in control (right) and *Apc*$^{Pirc/+}$+OX (left) neurons recorded from repeated trials (4 trials) at 1, 2, and 3x background stimulus (Lo strain) intensity. Frequency histograms show cumulative distributions across 4 trials. **d,** Overlaid interval histogram (four trials per neuron at each of three stimulus intensities shows population shift. Inset show non-overlaid interval histograms for clarity. * indicates statistically significant differences between experimental groups as empirically derived from hierarchical Bayesian model (*stan_glm*): 95% highest density intervals do not overlap between groupwsie contrasts.

*Dysfunction does not depend on degeneration*

We next tested whether the impaired neuronal signaling of *Apc*$^{Pirc/+}$+OX neurons might be explained by dying-back degeneration of sensory nerve terminals. While the underlying mechanisms for chemotherapy induced neuropathy are not understood, current opinion identifies 'dying-back' axon degeneration as a major pathology in this disorder (Park, Goldstein *et al.* 2013; Fukuda, Li *et al.* 2017). Blinded reviewers assessed the structural integrity of sensory afferents and receptor endings immunolabeled against neurofilament protein (NEFH) (Carrasco, Vincent *et al.* 2017). We then tested for functional evidence of degeneration by comparing differences in conduction delays, a physical measure of nerve degeneration that is used clinically (Burakgazi, Messersmith *et al.* 2011). Neither histological observation of sensory afferents and receptors (Figure 23d) nor axon conduction tests (Figure 26) revealed evidence of dying-back degeneration of sensory nerve terminals (*Apc*$^{Pirc/+}$+OX: 1.41±0.13ms, n=10. *Apc*$^{WT}$+control: 1.52±0.14ms, n=11, Figure 26). Our findings demonstrate that transcriptional changes we observed for some markers of nerve degeneration (Figure 10) were insufficient to yield nerve degeneration. While our results indicate selective resistance of mechanosensory neurons in *Apc*$^{Pirc/+}$+OX rats, they are in line with the inconsistency of physical evidence for nerve degeneration reported in clinical studies (Burakgazi, Messersmith *et al.* 2011). Furthermore, the ability of muscle vibration to entrain firing of these neurons in all treatment groups as they do in *Apc*$^{WT}$+control rats further refutes the existence of degeneration's necessity in signaling disorders (Figure 26). Overall, our findings suggest that the structure and core ability of mechanosensory neurons to produce action potentials remain unimpaired by codependent neuropathy and does not depend on dying-back degeneration.

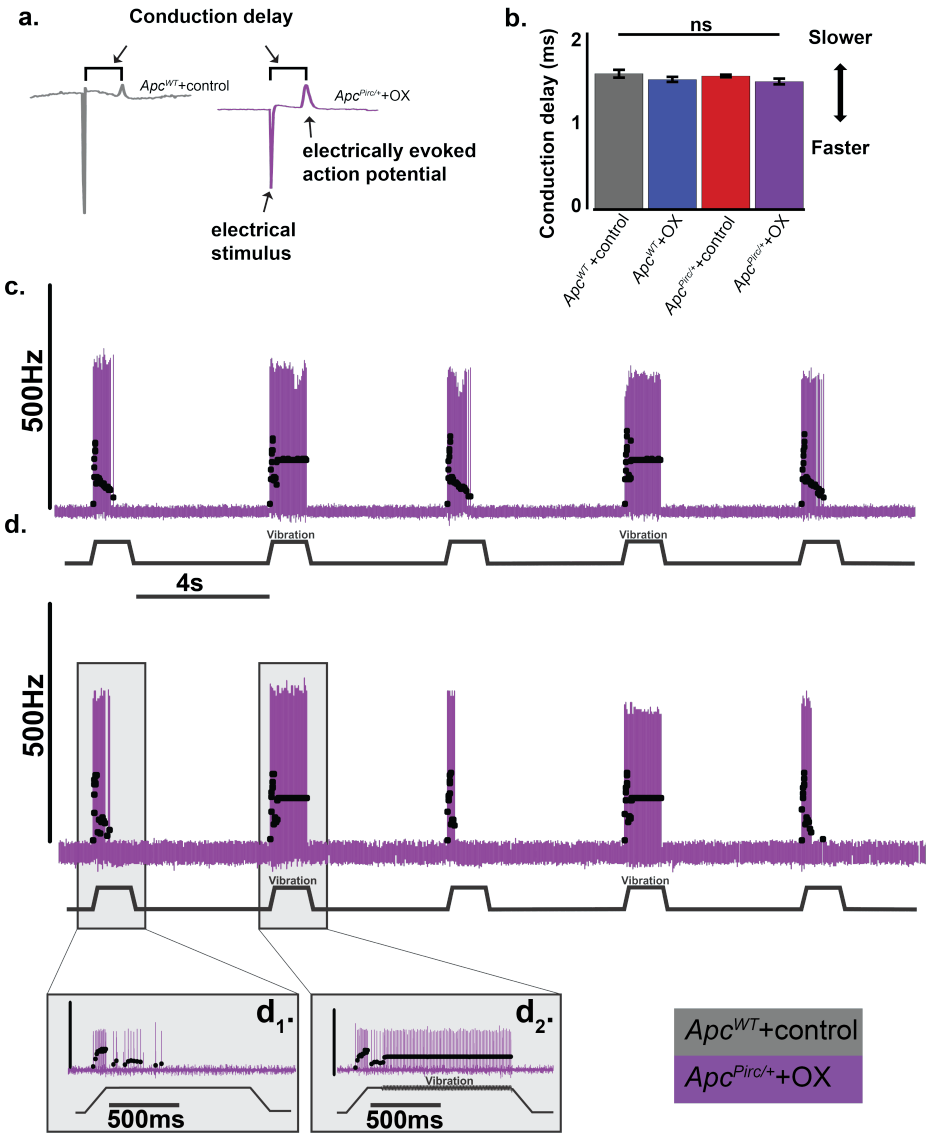


***Figure 26.***

**Cancer and chemotherapy interaction does not lead to electrophysiological evidence of degeneration. a,** raw intracellular record from control and *Apc*$^{Pirc/+}$+OX neurons shows derivation of conduction delay (ms). Conduction delay is calculated by subtracting the time from electrical stimulus to electrically evoked action potential. **b,** Mean conduction delay (ms) computed for all neurons as a measure of axonal demyelination were analyzed from *Apc*$^{WT}$+control (n = 11), *Apc*$^{WT}$+OX (n = 19), *Apc*$^{Pirc/+}$+control (n = 20) and *Apc*$^{Pirc/+}$+OX (n = 10) neurons with hierarchical Bayesian ANOVA model. ns, no significant difference. **c & d,** Two representative stretch evoked responses of two sensory neurons (*Apc*$^{Pirc/+}$+OX) recorded from dorsal roots in *in vivo* electrophysiological experiments with corresponding action potential trains. Overlaid black circles are IFRs of the responses. Insets show expanded view from **(d)** in a trial without (**d**$_1$) and with (**d**$_2$) superimposed vibration stimulus.

*Neuronal dysfunction depends on cancer-chemotherapy interaction*

Data presented in Figure 23 suggests damaging cancer-chemotherapy interactions are conserved *in vivo* and have consequences in sensory function. In order to assess the extent of interaction quantitatively, we took an unbiased statistical approach by subjecting all neurons (n=60, 240 total trials) from all experimental groups to a machine learning algorithm (linear discriminant (LD) analysis). Our approach reduced complex feature space into canonical variables giving us a high-level understanding of where interaction emerges, without biased feature selection *a priori*. Our analysis yielded three canonical variables (Figure 27a) that achieved overall 94.7% classification accuracy (Figure 24a). We then visualized neuronal signaling in the new 3D composite space created by LD1-3 (Figure 27a). By projecting high dimensional parameter and feature data onto a simplified 3D canonical space, statistically significant non-linear interaction between cancer and chemotherapy clearly emerged in the first dimension (LD1; 54.23% proportion of variance; Figure 27a and Figure 24b). Notably, dysfunction in LD1 induced by the cancer—chemotherapy interaction occurred in the opposite direction to that predicted by independent effects, and its magnitude was amplified greater than their sum (Figure 27a and Figure 24b, c). To test the statistical significance of the cancer—chemotherapy interaction, we conducted Bayesian model comparison with full factorial and all restricted models using leave-one-out cross validation. We then quantified and validated each model's predictive performance by computing the expected log predictive densities (ELPD;  measure of a model's out-of-sample predictive accuracy in Figure 27b-e) (Vehtari, Gelman *et al.* 2017).  We found decisive evidence in favor of a model including a cancer–chemotherapy interaction predictor (ELPD diff ≥ 48 SE <8.1; Figure 27e). Moreover, our data and generative modeling conclude that codependent

interaction (Figure 27b-d) is necessary to accurately and reliability reproduce clinically relevant neuronal signaling deficits observed in *Apc*$^{Pirc/+}$+OX rats (Figure 27e).

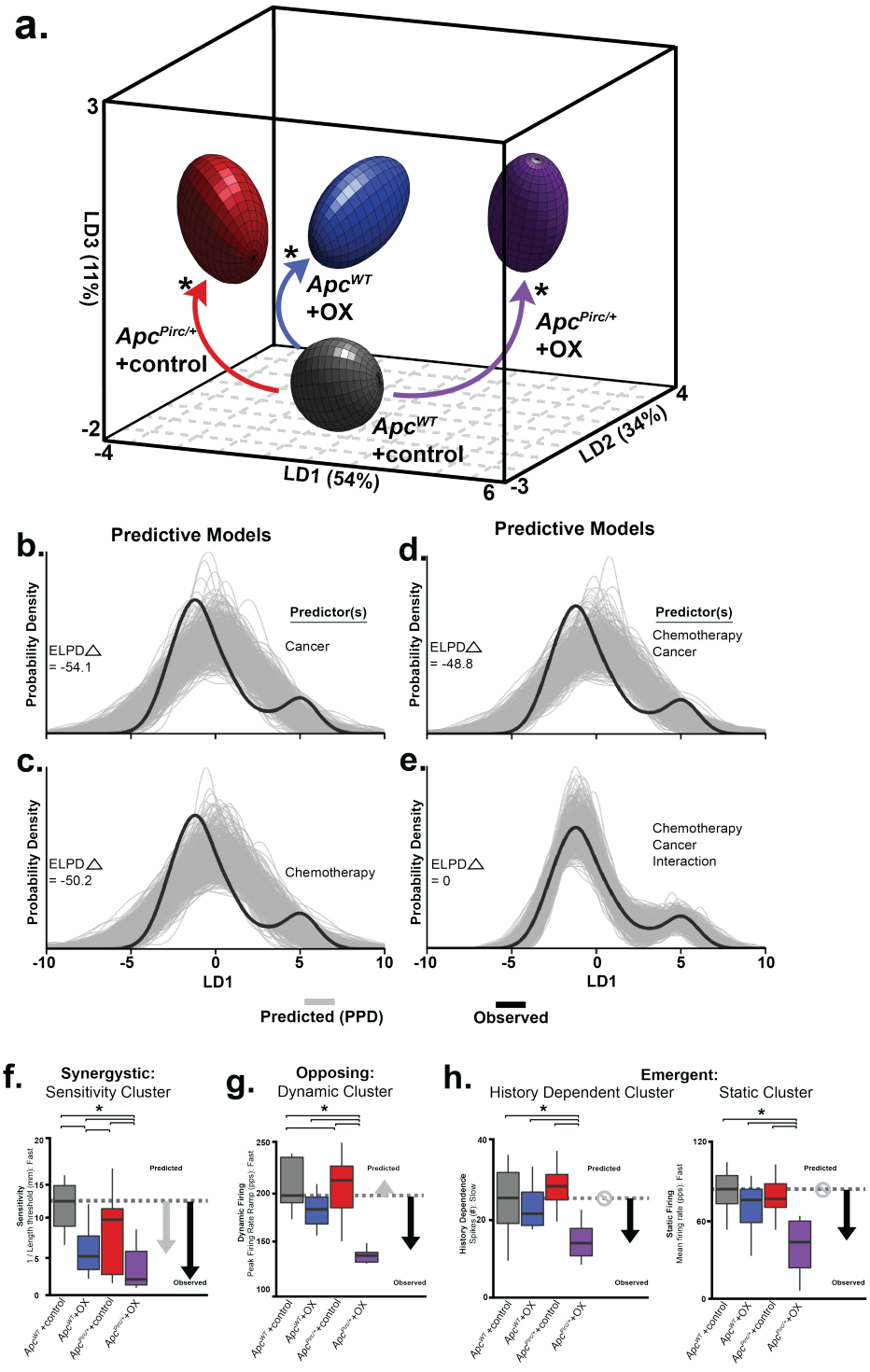

## ***Figure 27.***

**Cancer-chemotherapy codependence exacerbates sensory dysfunction beyond that predicted by cancer or chemotherapy alone**. a, Neuronal spiking parameters (n=31, averaged from four trials, from each neuron (n=60)) representing different features of sensory stimuli were subjected to linear discriminant (LD) analysis. Neuronal signaling was visualized in the new 3D composite space created by LD1-3. 3D ellipsoids enclosing 68% of data were computed with least-squares elliptical fitting to emphasize differences between control and $Apc^{Pirc/+}$+OX neurons. Effects of independent (OX or $Apc^{Pirc/+}$) and combinatorial ($Apc^{Pirc/+}$+OX) treatment are indicated by curved arrows. b-e, The hierarchical Bayesian model used to test for significant group differences in LD1 scores reconfigured to operate in a predictive fashion. Predictors included in each model are listed to the right of each plot. Generative models in (b-d) utilizing one (b,c) or both independent (d) predictor(s), i.e. cancer ($Apc^{Pirc/+}$) or chemotherapy (OX) for posterior prediction . The generative model in (e) utilizes both independent predictors and an interaction term for posterior prediction. Grey lines in b-e represent 500 novel (generative) samples drawn from the posterior distributions. Black lines illustrate experimentally observed mean LD1 score. Predictive accuracy was measured by calculating expected log predictive density (ELPD) for each model and benchmarked off of the highest performing model. Delta ELPD (triangular symbol) indicates difference from optimal model. Negative models represent worse predictive performance. f, Sensitivity assessed as the inverse of latency to stimulus detection (mm-1), i.e. lower sensitivity corresponds to longer latency and higher threshold. g, Peak firing rate (pps) achieved during the dynamic sensory stimulus (shown as dark grey bar in Figure 23b). h, change in dynamic spike number in successive, slow stretch dynamic sensory stimulus (see Methods and Figure 20) and mean firing rate (pps) achieved during the static sensory stimulus (shown as light grey bar in Figure 23b). Recordings were analyzed from $Apc^{WT}$+control (n = 11), $Apc^{WT}$+OX (n = 19), $Apc^{Pirc/+}$+control (n = 20) and $Apc^{Pirc/+}$+OX (n = 10) in b-g, * indicates statistically significant differences between experimental groups as empirically derived from hierarchical Bayesian model (stan_glm). Grey arrows in f-h indicate direction and significant differences from $Apc^{WT}$+control predicted from the linear sum of the independent effects of $Apc^{WT}$+OX and $Apc^{Pirc/+}$+control groups. Black arrows indicate experimentally observed effects of their combination. Circles with slashes indicated no difference predicted for $Apc^{WT}$+OX group and $Apc^{Pirc/+}$+control groups. Data presented as mean ± s.e.m.

Having determined the significance of an interactive effect, we then asked which functional clusters are highly enriched in LD1. By examining the discriminant function

coefficients, we found that static signaling and sensitivity functional clusters represent a large portion of the explained variance in LD1. These findings suggest the sensitivity and static signaling clusters are most susceptible to codependent neuropathy (Figure 24d).

While dynamic signaling provided relatively modest contributions to LD1 (lower coefficient weights in Figure 24d), examining the parameter level data allowed us to discover the expression of distinct classes of interactions. Independently, OX and $Apc^{Pirc/+}$ induce highly conserved (87.5%) opposing effects exclusively within the dynamic functional cluster. We consistently found that $Apc^{Pirc/+}$ mutation increased and OX treatment decreased dynamic firing (Figure 27g). This led us to predict that their combination would nullify dysfunction and approximate $Apc^{WT}$+control signaling. Instead, we observed opposing interactions that resulted in drastic reduction in dynamic firing properties. By contrast, for history-dependent functional clusters, we found that cancer–chemotherapy interaction emerged exclusively in $Apc^{Pirc/+}$+OX neurons, since neither $Apc^{WT}$+OX nor $Apc^{Pirc/+}$+control neurons were disrupted (Figure 27h).

***Summary***

Taken together, we found that 58% of the neuronal signaling parameters in $Apc^{Pirc/+}$+OX rats showed high-confidence interaction effects, in that those deficits were greater than those observed in either $Apc^{WT}$+OX nor $Apc^{Pirc/+}$+control rats. Our findings demonstrate that complex systemic perturbations of chemotherapy and cancer result in synergistic interactions for sensitivity signaling characteristics, i.e. where cancer and chemotherapy impart influence in the same direction. (Figure 27f), opposing interactions for peak firing rate during dynamic signaling, i.e. where cancer and chemotherapy impart influence in the opposite directions. (Figure 27g), and emergent interactions for history dependent and static signaling characteristics, i.e. where cancer and chemotherapy independently impart no influence but their combination has effects (Figure 27h). In summary,

*Apc*$^{Pirc/+}$+OX rats express widespread neuronal signaling dysfunction that targets all functional clusters, was independent of structural or physiologically detected degeneration and were not fully accounted for by a global decrease in sensitivity.

## Aim 4: Test the hypothesis that down regulated Kv3.3 expression is sufficient to reproduce neuronal dysfunction observed following chronic chemotherapy treatment of cancer.

### *Introduction*

To test the sufficiency of down-regulated Kv3.3 receptor (annulospinal) currents to reproduce *Apc*$^{Pirc/+}$+OX neuronal dysfunction, we developed a novel biophysical model of rat muscle-spindle based on the known region-specific channel composition of rat muscle spindles (Bewick and Banks 2015; Woo, Lukacs *et al.* 2015; Carrasco, Vincent *et al.* 2017) and newly discovered Kv3.3 channel.

### *Aim Specific Methods*

*Biophysical modeling of muscle spindle firing*

In the NEURON 7.6 simulation environment, we developed a novel biophysical model of rat muscle-spindle based on the known region-specific channel composition of rat muscle spindles (Bewick and Banks 2015; Woo, Lukacs *et al.* 2015; Carrasco, Vincent *et al.* 2017) and newly discovered Kv3.3 channel. The model was designed to simulate the behavior of muscle spindles from *Apc*$^{WT}$+control animals as they respond to identical stimulations to those presented *in vivo*.

We modeled a single branch of the Ia fiber system with terminal, preterminal axon, heminode (first node), and subsequent four myelin and node segments. Figure 28 shows channels distributions for different compartments based on available information. When

channels are found in more than one location, their densities are higher on the nodes and paranodes than elsewhere. We also included an activating Ca channel that is built into the modeled SK channels. The mechano-sensitive channel is activated by tension in the receptor area and also has a slow tension-dependent inactivation.

We modelled mechanotransduction by dividing the spindle into a polar (intrafusal muscle) and non-polar region (sensory terminal). The non-polar region is purely elastic whereas the tension developed in the polar regions shows a non-linear relation between tension and muscle length and velocity analogous to extrafusal muscle as described by (Hasan 1983). We derived the following equation relating sensory terminal length (m) two muscle length (x) and velocity as described by Hasan 1983 with the exception of not directly translating this function into spindle firing rate as originally described. Instead we model the transformation of stretch-evoked mechanical stimuli to conductance depending on the length of the sensory region, e.g. proportional to m and $\frac{dm}{dt}$:

$$\frac{dm}{dt} = \frac{dx}{dt}\, a \left( \frac{\mathrm{bm} - \mathrm{x} - \mathrm{c}}{\mathrm{x} - \mathrm{c} - \mathrm{m}} \right)^3$$

where a (0.0003 (mm/ms)), b (250) and c (-15 (mm)) are constants. Constant a is inversely related to the strength of the velocity effect, b reflects the relative compliance of the two regions and c represents the slack length of the polar regions (Hasan 1983). Additionally, we model the max conductance (gbar) of the mechanotransduction region (gbar=0.01 ($M\Omega t/cm^2$)), the slope of Boltzman equation specifying sensory length (Lslp) to conductance (Lslp = 0.05 (mm)), half activation point (Lhalf = 0.1 (mm)), and membrane time constant (taum = 5 (ms)). Along with the modeled mechanotransduction process we modeled gbar for each channel in each specific region as documented in the following table.

*Table 1.*

**Conductances Parameters for Biophysical Modeling.** Breakdown of maximum conductances for each of the four modelled regions for both Apc$^{WT}$+control and *Apc$^{Pirc/+}$*+OX animals. Parameters labelled in red indicate experimentally altered values in *Apc$^{Pirc/+}$*+OX.

| Terminal | *Apc$^{WT}$*+control | *Apc$^{Pirc/+}$*+OX |
|---|---|---|
| | gbar | gbar |
| Na1.6 | 200pS/μm$^2$ | 200pS/μm$^2$ |
| Nav1.7 | 200pS/μm$^2$ | 200pS/μm$^2$ |
| Nav1.8 | 0.001MΩt/cm$^2$ | 0.001MΩt/cm$^2$ |
| Na1.1 | 200pS/μm$^2$ | 200pS/μm$^2$ |
| KCNQ | 0.004MΩt/cm$^2$ | 0.006MΩt/cm$^2$ |
| Kv3.3 | 0.008S/cm$^2$ | 0.000S/cm$^2$ |
| Kv1.1 | 0.008S/cm$^2$ | 0.008S/cm$^2$ |
| SK(mAHP) | 0.0005 S/cm$^2$ | 0.0005 S/cm$^2$ |
| Ca2+lowThr | 5e-5 S/cm$^2$ | 5e-5 S/cm$^2$ |

| Paranode | *Apc$^{WT}$*+control | *Apc$^{Pirc/+}$*+OX |
|---|---|---|
| | gbar | gbar |
| Nav1.8 | 0.001MΩt/cm$^2$ | 0.001MΩt/cm$^2$ |
| Kv3.3 | 0.008S/cm$^2$ | 0.000S/cm$^2$ |
| Kv1.1 | 0.008S/cm$^2$ | 0.008S/cm$^2$ |

| Pre-Terminal | *Apc$^{WT}$*+control | *Apc$^{Pirc/+}$*+OX |
|---|---|---|
| | gbar | gbar |
| Na1.6 | 200pS/μm$^2$ | 200pS/μm$^2$ |
| Nav1.7 | 200pS/μm$^2$ | 200pS/μm$^2$ |
| Na1.1 | 200pS/μm$^2$ | 200pS/μm$^2$ |
| KCNQ | 0.004MΩt/cm$^2$ | 0.006MΩt/cm$^2$ |
| Kv1.1 | 0.008S/cm$^2$ | 0.008S/cm$^2$ |
| SK(mAHP) | 0.0005 S/cm$^2$ | 0.0005 S/cm$^2$ |
| Ca2+lowThr | 5e-5 S/cm$^2$ | 5e-5 S/cm$^2$ |

| Nodes | *Apc$^{WT}$*+control | *Apc$^{Pirc/+}$*+OX |
|---|---|---|
| | gbar | gbar |
| Na1.6 | 200pS/μm$^2$ | 200pS/μm$^2$ |
| Nav1.7 | 200pS/μm$^2$ | 200pS/μm$^2$ |
| KCNQ | 0.004MΩt/cm$^2$ | 0.006MΩt/cm$^2$ |

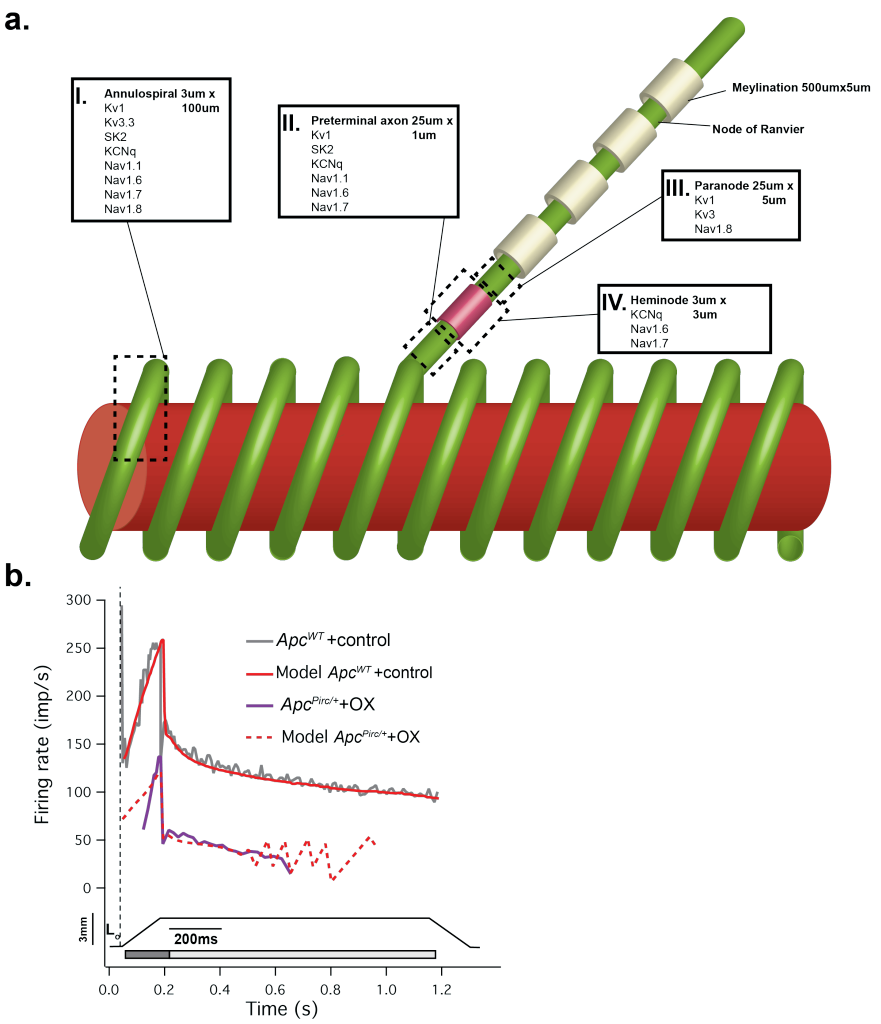


## ***Figure 28.***

**Anatomical distribution of ion channel constituents of biophysical computational model of muscle spindle**. a, Model of one branch of the Ia fiber system with terminal, preterminal axon, first node (heminode), and subsequent node-myelin pairs. Model of identifies the spatial distribution of ion channels in muscle spindle Ia primary ending. The intrafusal muscle fiber (red) is wrapped by an annulospiral ending (green) and a preterminal axon that extends unmyelinated from the terminal to the heminode (pink) followed by a myelinated axon. Dotted-boxes represent specific regional distributions believed to underlie specific functional characteristics of neuronal signaling e.g. mechanotransduction, signal amplification, encoding, and autogenic feedback. b, Example of $Apc^{WT}$+control and $Apc^{Pirc/+}$+OX response from the biophysical spindle model (red) overlaying experimental $Apc^{WT}$+control and $Apc^{Pirc/+}$+OX data. Figure shows the mean instantaneous firing rates. Dashed vertical line marks onset of muscle stretch (3mm) from resting length ($L_o$). Dynamic and static phases of naturalistic stimuli indicated by dark grey (150ms duration after stretch command onset) and light grey (1s duration after the dynamic phase) bars.

### *Results*

*Biophysical model of muscle spindle reproduces canonical firing behavior*

The model was developed and implemented in NEURON 7.6 to simulate the behavior of muscle spindles from $Apc^{WT}$+control animals and those treated with $Apc^{Pirc/+}$+OX as they respond to identical stimulations to those presented *in vivo* (Methods). The $Apc^{WT}$+control simulation (Figure 28b) reproduced experimental firing behaviors over dynamic and static simulated length change stimuli i.e., linearly increasing firing rates as length changes over constant velocity and slow firing rate accommodate (decay) as length stimuli is help at a constant length.

*Down regulating Kv3.3 is sufficient to explain key features of firing dysfunction*

We then modelled $Apc^{Pirc/+}$+OX muscle spindles by systematically eliminating Kv3.3 expression on the receptor as was seen the above immunohistochemical analyses (section *1.3.2.2*). $Apc^{Pirc/+}$+OX simulation (Figure 28b) reproduced certain features of *in vivo* data and not others. Notably, through this targeted ionic perturbation we eliminated static firing throughout the hold phase and blunted the dynamic firing rates whereas no change in threshold was observed.

### *Summary*

Collectively, the results of computer simulations indicate that a reduction in Kv3.3 expression, as observed experimentally, is sufficient to reproduce many of the firing defects in mechanosensory neurons and suggest this as one candidate biophysical mechanism that may be directly or indirectly targeted by the cancer-chemotherapy interaction. Moreover, the failure of simulated Kv3.3 down-regulation to reproduce defects in threshold provides strong evidence that additional biophysical mechanisms are present. For example, up-regulated gene KCNN2 that encodes SK2 (Figure 17) recently discovery in mammalian muscle spindle receptors may provide the additional

$Ca^{2+}$ gated $K^+$ current to increase threshold. Alternatively, and increased Kv1.1 or KCNQ could lead to a comparable change in threshold. Because both Kv1.1 and KNCQ channels have low voltage thresholds, small increases in expression, that could be masked by our bulk transcriptional profiling, of either channel could increase spindle threshold.

## Aim 5: Test the hypothesis that cancer exacerbates sensorimotor dysfunction after chronic chemotherapy treatment in an awake behaving animal.

### *Introduction*

To test the behavioral consequences of the cancer-chemotherapy interaction, we evaluated *Apc*$^{Pirc/+}$+ OX rats' performance in horizontal random rung ladder walking. This precise walking task overbalances performance on proprioceptive function (Metz and Whishaw 2002; Metz and Whishaw 2009) since rats move forward with vision directed forward. Under these experimental conditions, success relies on proprioceptive function that assists with foot placement on rungs that pass out of sight.

### *Aim Specific Methods*

*Behavioral analysis*

We used the ladder rung walking task as a validated outcome to detect and describe sensorimotor deficits (Metz and Whishaw 2002; Metz and Whishaw 2009). The ladder rung apparatus was built as previously described (Metz and Whishaw 2002). Secure hind foot placement was assessed using the seven-category scale scoring system introduced by (Metz and Whishaw 2002; Metz and Whishaw 2009) with modifications as to not distinguish whether or not an error was associated with a deep fall. The total

number of errors in forelimb (e.g. Figure 29d) and hindlimb (e.g. Figure 29e) placement was calculated and the mean error/step ratio was calculated per animal and represented as percent of error where an increase in the number of errors/steps corresponds to a decrease in secure foot placement of the hind and/or fore foot.

### *Results*

*Behavioral dysfunction exacerbated by cancer-chemotherapy interaction*

*Apc*$^{WT}$+control and *Apc*$^{Pirc/+}$+control rats achieved a high incidence of rear and fore foot placement, when walking on the rungs of a uneven horizontal ladder, with a foot-drop error rate of only 2.4% (±2.7% SD, 6 animals; Figure 29a and Movie S1) and 2.5% respectively (±2.9% SD, 4 animals; Figure 29a and Movie S1). In contrast, *Apc*$^{Pirc/+}$+ OX exhibited a 19.2% foot-drop error rate (±5.6% SD, 7 animals; hierarchical Bayesian model (stan_glm) vs. *Apc*$^{WT}$+control and *Apc*$^{Pirc/+}$+control; Figure 29a and Movie S2). *Apc*$^{Pirc/+}$+ OX error rates significantly exceeded our previous findings following OX treatment alone (*Wistar*+OX) of 8.4% (±3.1% SD, 7 animals; hierarchical Bayesian model (stan_glm) vs *Apc*$^{Pirc/+}$+ OX; Figure 29). Independent analysis of fore- (Figure 29b) and hind-foot (Figure 29c) error rates revealed that skilled motor behavior degradation was significantly exacerbated by the emergence of fore-limb errors (10.4%±3.9SD) not present in *Apc*$^{WT}$+control (0%), *Apc*$^{Pirc/+}$+control (2.3%±2.8SD), or *Wistar*+OX (0%; hierarchical Bayesian model (stan_glm)).

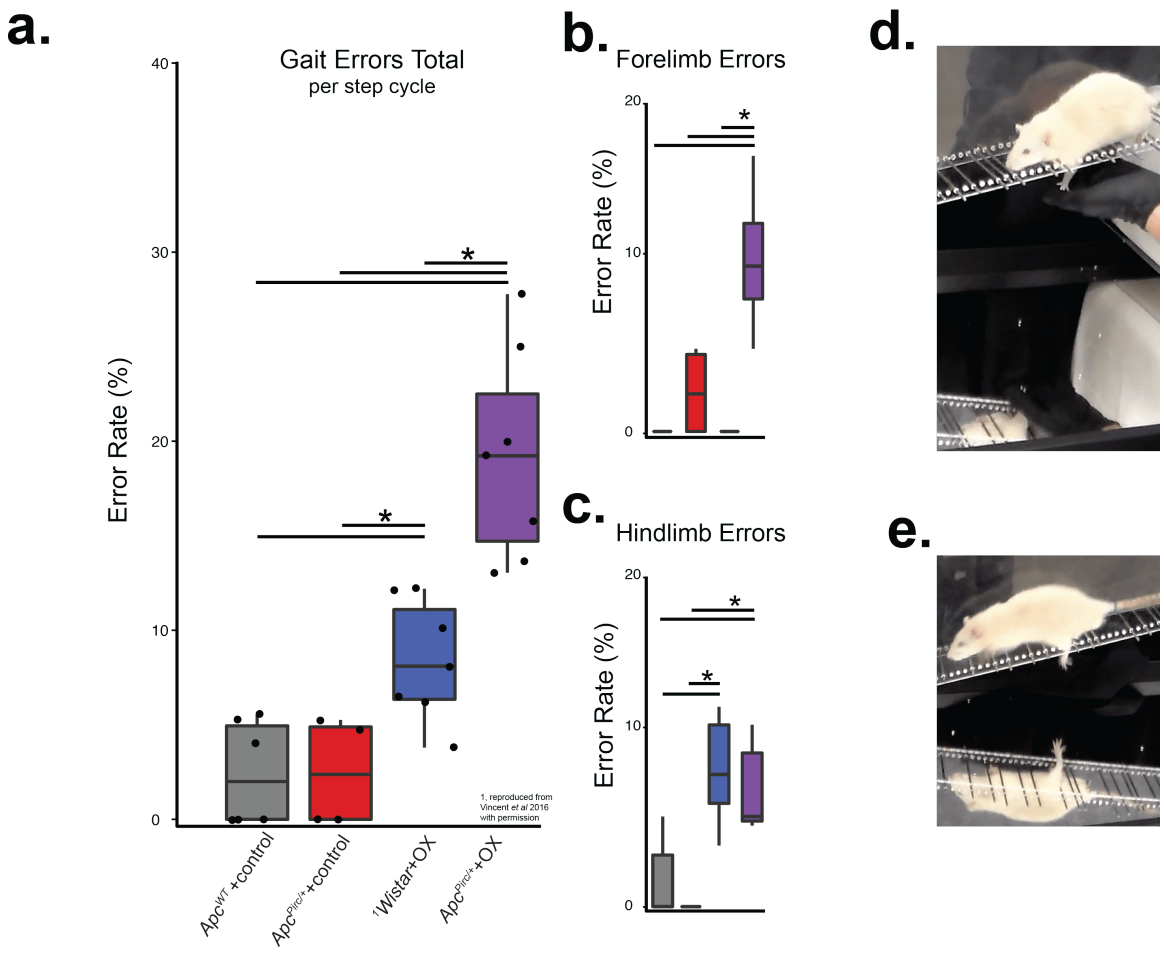


***Figure 29.***

**Behavioral dysfunction exacerbated by cancer-chemotherapy interaction**. a, Total gait errors as measured by secure fore- and hindfoot placement was scored by errors/step cycle during ladder rung walking. Recordings were analyzed from *Apc*$^{WT}$+control (n = 6), Wistar+OX (n = 7), *Apc*$^{Pirc/+}$+control (n = 4) and *Apc*$^{Pirc/+}$+OX (n = 7) animals. b-c, indicate the contributions of fore- (b) and hindlimb (c) errors to total error rates. d, Photograph shows left forelimb slip in double image (simultaneous side and underneath views) of *Apc*$^{Pirc/+}$+OX rat walking on ladder rungs. e, Photograph shows left hind limb slip in double image (simultaneous side and underneath views) of *Apc*$^{Pirc/+}$+OX rat walking on ladder rungs (representative cases of entire ladder rung walking trials can be viewed at Movie S1 and Movie S2 for *Apc*$^{WT}$+control and *Apc*$^{Pirc/+}$+OX rats respectively). * indicates statistically significant differences between experimental groups as empirically derived from hierarchical Bayesian model (stan_glm): 95% highest density intervals do not overlap between group contrasts. [1]Wistar+OX data reproduced from Vincent et al 2016 with permission.

***Summary***

Our data reveal that proprioceptive sensory input from muscle spindles ensures limb placement accuracy in a skilled motor behavioral task. Moreover, discovering that cancer-chemotherapy interaction results in the emergence of novel forelimb deficits (Figure 29b, d) typically not observed in this challenge to hindlimb capacities (Figure 29c, e) provides further evidence that exacerbation effects are unpredicted from studying chemotherapy alone.

## Project 1: Discussion

Here we present original evidence that cancer transforms the nature and magnitude of neuropathy induced by chemotherapy alone. Our preclinical study of rats is the first to compare the neuropathic effects of chemotherapy and cancer, both independently and in combination, currently impractical in human study. These comparisons for global transcriptional analysis of sensory neurons in dorsal root ganglia revealed dysregulation of genes uniquely induced, amplified or suppressed by the combination of cancer and chemotherapy. Codependence was conserved as impaired spike encoding of mechanosensory stimuli and novel ion channelopathy.

Our transcription analyses expose two potential targets for treating sensorimotor disorders among the debilitating patient symptoms that persist following treatment of various cancers with platinum-based compounds and other antineoplastic agents, e.g. taxanes. Patients display deficits in the spatiotemporal parameters (speed and stride) of walking gait, in control of posture, and in balance relying on proprioception (Marshall, Zipp *et al.* 2017; Monfort, Pan *et al.* 2019). Acknowledging that these disabilities may

arise from a variety of lesions in the nervous system, the deficits we observe here at the receptor origin of detection and encoding of muscle mechanics would necessarily impair movements and postures and cannot be fully compensated by other senses, e.g. vision. Furthermore, signaling by mechanosensory neurons in rats closely resembles that in human (Burke, Hagbarth *et al.* 1978). For these reasons, we assign special attention to depressed signaling by muscle spindles and to the associated decrease in expression of the voltage-gated ion channel Kv3.3 and its gene *Kcnc3*. Kv3 channels play important role in attaining and maintaining high neuronal firing rates. Unique biophysical properties, e.g. high activation threshold, rapid activation, and deactivation kinetics, allow neurons that express Kv3 channels to quickly repolarize without compromising the inward current or Nav channels reactivation (Rudy and McBain 2001; Kaczmarek and Zhang 2017; Gu, Servello *et al.* 2018). Reports that *Kcnc3* gene knock out impairs firing responses of neurons (Akemann and Knöpfel 2006; Espinosa, Torres-Vega *et al.* 2008) and results in ataxia (Figueroa, Minassian *et al.* 2010) promote this gene and its ion channel as potential contributors to signaling deficits observed in the present study.

While our biophysical modelling provides evidence that Kv3.3 is sufficient to explain certain neuronal signaling deficit, we are uncertain about the necessity of Kv3.3 channelopathy to explain the full suite of deficient mechanosensory signaling in cancer treated by chemotherapy. Uncertainty arises in part, because comprehensive understanding of the molecular mechanisms underlying the function of these sensory neurons is lacking, although advanced by our discovery of Kv3.3 in mechanoreceptors of healthy animals. Another candidate target for treating sensorimotor disorders is the inflammatory signaling molecule IL6, shown here to express large increases in both gene and protein expression. As a result of its effect in suppressing neuronal firing behavior (Nelson, Ur *et al.* 2002) IL6 has the potential to explain decreased signaling by

mechanosensory neurons. We identify both Kv3.3 and IL6, therefore, as targets worthy of testing for their potential value in treating movement disorders. Additional points of interaction likely exist, which remain either undiscussed (e.g. FosB) or potentially masked due to transcriptional profiling of DRG's that may result in variable differential expression across heterogenous cell types.

Muscle proprioceptors (Group Ia) provide invaluable sensory feedback to control movement (Prochazka and Ellaway 2012; Proske and Gandevia 2012), make rapid adjustments to unexpected perturbations (Nichols, Cope *et al.* 1999; Shemmell, Krutky *et al.* 2010), and preserve an internal representation of the body's interaction with the environment (Ivanenko, Dominici *et al.* 2011). It seems to reason then that disruption in sensory encoding is a plausible model to explain the severely compromised ability to carry out precision ladder walking (Abelew, Miller *et al.* 2000; Sghirlanzoni, Pareyson *et al.* 2005). We observed abnormal sensorimotor behavior characterized as difficulty with achieving proper limb placement in $Apc^{Pirc/+}$+OX rats. Deficits were significantly greater than those previously observed in our lab from animals treated with OX alone. This observation further supports a link to altered proprioceptor signaling while also suggesting that the magnitude of signaling deficits might contribute to the magnitude of sensorimotor deficits, as evidenced by the emergence of forelimb errors that coincide with additional exacerbated signaling deficits. Data obtained in $Apc^{Pirc/+}$+ OX rats were in agreement with previous results observed in animals without functional spindles (Egr3 mutants) (Akay, Tourtellotte *et al.* 2014), indicating that the loss of sensory feedback from muscle spindles following cancer treatment may be sufficient to explain sensorimotor deficits experienced by cancer survivors.

The emergence of forelimb errors might be explained by greater signaling impairment, i.e. lost sensitivity to stimuli and reduced dynamic response, in addition to the previously

described impaired static responsiveness. This necessarily results in larger information loss that may not be able to be compensated by vision or the CNS learning a new representation of the corrupt information. Stated another way, while the forelimbs are in the line of site for this task (ladder rung walking), the extent of sensory information loss may result in such decompensated (e.g. fragile) motor performance that even tasks that can rely on another feedback source, e.g. vision, can suffer. In addition, shifting dependence of feedback away from proprioceptive signals, that can operate on the scale of 10s of milliseconds, onto visual systems that operate on the scale of 100s of milliseconds imparts addition feedback delay that can accentuate errors that occur during the rapid movements required to complete the ladder rung walking task.

Another contributor to the emergence of forelimb errors when cancer and chemotherapy interact might be differences in spinal circuitry and their interaction with corrupt sensory feedback. It is well documented that forelimbs and hindlimbs are controlled by functionally and anatomically distinct spinal circuits (Ballion, Morin *et al.* 2001; Juvin, Simmers *et al.* 2005; Frigon 2017). Various experimental preparations showing the forelimbs and hindlimbs can be physically and/or functionally uncoupled suggests that their responses to perturbations, e.g. chemotherapy alone or cancer and chemotherapy, might also be uncoupled(Ballion, Morin *et al.* 2001; Juvin, Simmers *et al.* 2005). This latter suggestion highlights the possibility that the signaling deficits identified in our previous reports (Vincent, Wieczerzak *et al.* 2016) could have been restricted to the hindlimb alone and it is not until the extent of the systemic perturbation was large enough, e.g. due to the addition of cancer that forelimb sensorimotor control faltered.

Our study, being restricted to a single time point following chemotherapy, does not assess the stability of potential treatment targets that emerge from codependent neuropathy. It is reasonable to expect, however, that the codependence undergoes

dynamic change. Cancer, presumably also its associated systemic effects, undergoes complex progression as subpopulations of cancer cells differentially resist, adapt, or succumb to chemotherapy. Moreover, biological systems themselves initiate dynamic responses to perturbations. In the nervous system, homeostatic regulation initiates compensatory mechanisms to offset perturbations in neuronal excitability (Waxman and Zamponi 2014). It is thought provoking in this regard to consider the possibility that the chronic hypoexcitability which follows the acute hyperexcitability (Cavaletti and Marmiroli 2010; Park, Goldstein *et al.* 2013) that develops during chemotherapy reflects the actions of a dysregulated compensatory mechanism. Understanding these non-linear interactions processes and their effects on potential treatment are both challenging and necessary for developing effective cancer treatment.

# CHAPTER 4. PROJECT 2

Project 2 is based on a single manuscript:

1. Housley, S. N., Nardelli, P, and Cope, T. C. (2019). Mechanosensory encoding and neural decoding of musculoskeletal dynamics impaired following cancer treatment. (in preparation)

## Introduction

Chemotherapy induced neuropathy (CIN) comprises a constellation of debilitating neurological disorders including sensorimotor impairments severe enough to persist long into disease free survival (Quasthoff and Hartung 2002; Cavaletti and Marmiroli 2010; Alcindor and Beauger 2011; Seretny, Currie *et al.* 2014; Sisignano, Baron *et al.* 2014; Stone and DeAngelis 2016). CIN reduces quality of life for many patients and can limit antineoplastic treatment, complicating its utility (Cavaletti and Marmiroli 2010; Alcindor and Beauger 2011; Stone and DeAngelis 2016). Despite intense pursuit, clinical trials founded on preclinical studies in animals without cancer (Currie, Angel-Scott *et al.* 2018), have largely failed to deliver effective treatment for and/or prevention of CIN (Hershman, Lacchetti *et al.* 2014).

This fundamental gap in understanding of CIN pathophysiology led us to test, in **Project 1,** whether clinically relevant CIN depends on codependence between cancer and chemotherapy (Housley, Nardelli *et al.* 2019). Through multiscale study of a class of sensory neurons in animals with cancer treated by chemotherapy, we discovered the first evidence that CIN cannot be explained by the effects of chemotherapy alone but depend instead on complex interactions with cancer-related processes. Among the observed changes across genetic, protein and whole cell neurologic function, neurons

failed to encode natural movement stimuli in their spiking activity with dysfunction depending on both cancer and chemotherapy.

A key question that remains relates to whether the cancer—chemotherapy codependence that causes dysfunction in neuronal encoding is conserved across diverse classes of mechanosensory neurons. Mechanosensory neurons are necessary for generating the information content (population code) needed for proprioception. For example, Golgi tendon organs (Ib) and group Ia and II muscle spindle afferents encode unique static and time-varying information, e.g. length, velocity, and inertial loads of body position as movements result in physical interactions with the environment. If deficits are conserved across the population, conflicting sensory signals or deletions of critical pieces of information would prove detrimental for a unified representation of body position under static and dynamic conditions, e.g. proprioception. Deficits in this population code may explain the lasting perceptual and functional deficits documented in patients treated with chemotherapy. Alternatively, the central nervous system (CNS) may compensate for the loss of information by learning a new representation of the population code to partially or fully compensate for information loss, thus preserving proprioception performance. Therefore, developing a detailed understanding of dysfunction across the population is necessary for developing mechanistic understanding, for predicting functional deficits or for understanding how the CNS may compensate for profound information loss.

The present study was designed to test the hypothesis that cancer's exacerbation of chemotherapy induced neuronal signaling deficits is conserved across the population of mechanosensory neurons in muscle. We recorded intracellular spiking activity from four classes of physiologically identified mechanosensory neurons responding to naturalistic mechanical stimuli *in vivo*. Results support our hypothesis in finding significant deficits in spike encoding across multiple measures used to

parameterize responses to naturalistic stimuli in all neuron classes. Analyses reveal co-suppression of specific signaling parameters across all neuronal classes, suggesting the existence of a global co-regulatory process that governs the balance of information content from multiples neuron classes flowing to the central nervous system. To understand the consequences of corrupt population spiking activity, we employed deep-learning algorithms to test how decoding of spatiotemporal features of movement are altered after chemotherapy treatment of cancer. Results indicate that spiking activity from the population of neurons in animals with cancer, treated by chemotherapy contain significantly less information about key features of movement including: timing, magnitudes, and velocity. We then modeled the CNS's capacity to compensate for this information loss by retraining the networks on corrupt population codes which revealed the CNS would not be able to fully compensate (learn) a new representation that restores predictive abilities. Intracellular recordings of synaptic potentials in a CNS neuron provided biological validation of modeling results confirming upstream neurons ability to accurately predict stimuli remain impaired. Collectively, our results show global deficiency in the population code of mechanosensory neuron population and resulting corrupt spatiotemporal decoding of movement features necessarily results in upstream neurons or networks to unpredictable inferences about the bodies interaction with the external environment and may contribute to lasting behavioral deficits documented in patients treated with chemotherapy.

## Aim 6: Test the hypothesis that cancer's exacerbation of chemotherapy induced neuronal signaling deficits is conserved across the population of mechanosensory neurons in muscle.

### *Aim Specific Methods*

*Neuronal Classification*

Dorsal rootlets positioned in continuity on bipolar recording electrodes were selected for sampling sensory neurons when they produced robust population activity (extracellular responses from many sensory neurons) in response to both electrical stimulation of triceps surae nerves and stretch of triceps surae muscles. Individual axons penetrated in these rootlets by glass micropipettes (~30 MΩ filled with 2 M $K^+$ acetate) were selected for study when electrical stimulation of triceps surae nerves produced orthodromic action potentials that were readily resolvable and had conduction delay of <3 ms. We classified muscle afferents on the basis of their responses to specific stimuli, e.g., muscle twitch contraction and vibration on basis of binary scoring of three criteria (Vincent, Gabriel *et al.* 2017). Afferents that fired during the rising phase of isometric twitch force (evoked by nerve stimulation with electrical pulses 0.04-ms duration at 1 pps) were designated group Ib tendon organ afferents, while those that did not were labeled muscle spindle afferents. Muscle spindle afferents designated Ia were distinguished from group II by firing with virtually perfect entrainment to 1-s bouts of high-frequency, small-amplitude vibration (100 –333 Hz, 80 $\mu$m) and by responding with an initial burst of high-frequency firing (>100 pulses per second (pps)) at the onset of muscle stretch. These same criteria distinguish analogous afferent groups in the cat (Matthews 1972).

*Population code construction*

Intracellular recordings from physiologically identified sensory neurons of all four classes were used to construct population codes (ensembles of neuronal firing). Since identical natural stimulation patterns were used for all neuronal recordings, the stimulation profiles were used to precisely time synchronized independently recorded neurons. This allowed us to model population codes of physiologically identified neurons of precisely known locations from $Apc^{WT}$+control and $Apc^{Pirc/+}$+ OX animals, not possible in previous studies (Stein, Weber *et al.* 2004; Weber, Stein *et al.* 2007).

## *Results*

*Encoding deficits conserved across diverse classes of mechanosensory neurons*

Applying electrophysiological methods to rats in vivo, we recorded spiking activity from single mechanosensory neurons responding to naturalistic mechanical stimuli (Figure 30). We sampled group Ia, unclassified spindle, group Ib, and group II totaling 225 neurons from $Apc^{WT}$+control, $Apc^{WT}$+OX, $Apc^{Pirc/+}$+control, and $Apc^{Pirc/+}$+OX experimental groups (Figure 30 and see Table 2 for complete description). For simplicity raw data and canonical analyses of group Ia neurons are not reproduced from **Project 1**.

*Table 2.*

**Distribution of decoding data.** Breakdown of data from 225 neurons acquired from 20 animals. Neuronal classes in top row and experimental group left most column.

| | **Ia** (n=60) | **Unclassified** (n=57) | **II** (n=57) | **Ib** (n=51) |
|---|---|---|---|---|
| ***Apc*$^{WT}$+control** (n=6) | 11 | 19 | 17 | 14 |
| ***Apc*$^{WT}$+OX** (n=3) | 19 | 14 | 9 | 5 |
| ***Apc*$^{Pirc/+}$+control** (n=4) | 20 | 19 | 17 | 18 |
| ***Apc*$^{Pirc/+}$+OX** (n=7) | 10 | 5 | 14 | 14 |

From these spiking responses, we collected 31 measured and derived parameters (average of four trials: (Figure 20 and Table 3). In $Apc^{WT}$+control rats, we found that muscle stretch elicited the expected spike encoding behavior from multiple classes of sensory neurons in normal animals (Vincent, Gabriel *et al.* 2017) and humans (Burke, Hagbarth *et al.* 1978) (grey traces Figure 30). We next asked whether $Apc^{Pirc/+}$ or OX treatment alone induce signaling dysfunction. In agreement analyses of group Ia neurons presented in Aim 3, we found a remarkable degree of concordance with signaling in $Apc^{WT}$+control (Figure 30). $Apc^{Pirc/+}$+control neuronal signaling displayed comparable sensitivity to stimuli and showed similar static behavior across all neuronal classes (red traces in Figure 30) as the $Apc^{WT}$+control with the exception of group II neurons that spiked longer $Apc^{WT}$+control. As was true for group Ia neurons, OX treatment of $Apc^{WT}$ rats induced mild signaling deficits. Deficits were primarily restricted to sustained firing (blue traces in Figure 30), validating our previous findings of restricted deficits observed in a different strain of healthy rats treated with OX alone (Vincent, Wieczerzak *et al.* 2016).

*Table 3.*

**Summary Statistics of Neuronal Signaling.** Breakdown of summary statistics of each neuronal class and their respective signaling parameters.

| **Group II** | **$Apc^{WT}$+control** | **N=17** | **$Apc^{WT}$+OX** | **N=9** | **$Apc^{Pirc/+}$+control** | **N=17** | **$Apc^{Pirc/+}$+OX** | **N=14** |
|---|---|---|---|---|---|---|---|---|
| **Variables** | **Mean** | **SEM** | **Mean** | **SEM** | **Mean** | **SEM** | **Mean** | **SEM** |
| **Dyn.DI** | 61.28 | 4.68 | 48.33 | 5.74 | 60.96 | 8.22 | 38.34 | 5.73 |
| **Dyn.F** | 156.71 | 18.43 | 172.44 | 25.23 | 188.05 | 25.04 | 186.48 | 16.02 |
| **Dyn.IFRdrop** | 29.61 | 6.3 | 18.86 | 4.35 | 30.88 | 8.7 | 51.41 | 19.87 |
| **Dyn.pfr** | 127.93 | 5.35 | 103.8 | 15.02 | 118.42 | 11.73 | 72.08 | 9.81 |
| **Dyn.pfr1** | 102.29 | 8.13 | 89.95 | 17.29 | 94.2 | 8.75 | 64.59 | 6.45 |
| **Dyn.pfr3** | 96 | 8.93 | 80.27 | 15.38 | 87.38 | 8.27 | 54.44 | 7.25 |

Table 3 continued

| | | | | | | | | |
|---|---|---|---|---|---|---|---|---|
| **Dyn.RDR** | 17.47 | 1.7 | 12.33 | 2.39 | 12.76 | 1.44 | 5.79 | 1.71 |
| **Dyn.slp** | 700.22 | 71.12 | 628.37 | 62.21 | 1114.62 | 154.25 | 777.86 | 140.92 |
| **Dyn.slp1** | 87.3 | 8.96 | 111.97 | 18.06 | 131.08 | 14.4 | 139.41 | 27.93 |
| **Dyn.slp3** | 147.04 | 18.81 | 138.17 | 21.61 | 181.14 | 22.34 | 135.78 | 27.54 |
| **Dyn.spkNum** | 11.54 | 0.54 | 10.19 | 1.31 | 8.65 | 0.88 | 5.23 | 0.74 |
| **Dyn.spkNum1** | 48.18 | 4.07 | 38.11 | 8.31 | 37.06 | 3.93 | 17.43 | 3.05 |
| **Dyn.spkNum3** | 30.94 | 3 | 25.78 | 6.26 | 24.29 | 2.78 | 11.64 | 1.73 |
| **Stat.afr** | 73.19 | 4.76 | 64.44 | 10.39 | 66.15 | 6.37 | 38.54 | 5.7 |
| **Stat.HzEnd** | 56.87 | 5.22 | 52.77 | 8.73 | 50.02 | 5.45 | 23.44 | 5.45 |
| **Stat.HzSTD** | 19.03 | 1.37 | 26.19 | 9.28 | 21.35 | 3.42 | 14.78 | 2.07 |
| **Stat.LSpkF** | 110.75 | 9.87 | 107.43 | 4.92 | 112.21 | 10.11 | 105.39 | 4.79 |
| **Stat.LSpkT** | 994.73 | 1.18 | 964.82 | 27.9 | 991.11 | 2.05 | 906.6 | 68.3 |
| **Stat.mSfr** | 66.65 | 4.84 | 55.91 | 10.3 | 57.46 | 5.71 | 32.91 | 5.59 |
| **Stat.slp** | -44.31 | 2.51 | -38.18 | 5.19 | -45.92 | 5.5 | -31.41 | 3.66 |
| **Stat.spkNum** | 67.99 | 5 | 57.82 | 10.33 | 59.56 | 6.52 | 33.39 | 5.63 |
| **Thr.F** | 11.03 | 0.84 | 13.64 | 1.1 | 22.9 | 4.01 | 31.6 | 8.04 |
| **Thr.F1** | 8.15 | 1.37 | 24.85 | 8.71 | 20.84 | 4.33 | 41.64 | 10.85 |
| **Thr.F3** | 17.65 | 2.99 | 35.48 | 10.46 | 31.58 | 5.28 | 47.45 | 10 |
| **Thr.L** | 0.16 | 0.03 | 0.2 | 0.03 | 0.55 | 0.11 | 0.89 | 0.22 |
| **Thr.L1** | 0.18 | 0.06 | 0.57 | 0.23 | 0.55 | 0.14 | 1.08 | 0.22 |
| **Thr.L3** | 0.76 | 0.1 | 1.07 | 0.24 | 1.16 | 0.12 | 1.44 | 0.15 |
| **Thr.T** | 8.84 | 1.35 | 9.52 | 1.63 | 26.77 | 5.36 | 45.32 | 10.69 |
| **Thr.T1** | 43.64 | 14.28 | 145.93 | 58.69 | 136.98 | 33.67 | 267.06 | 55.02 |
| **Thr.T3** | 200.45 | 24.32 | 272.67 | 61.1 | 295.37 | 29.82 | 367.2 | 38.11 |

Table 3 continued

| Group Ib | $Apc^{WT}$+control | N=14 | $Apc^{WT}$+OX | N=5 | $Apc^{Pirc/+}$+control | N=18 | $Apc^{Pirc/+}$+OX | N=14 |
|---|---|---|---|---|---|---|---|---|
| variable | Mean | SEM | Mean | SEM | Mean | SEM | Mean | SEM |
| Dyn.DI | 68.41 | 7.14 | 72.24 | 6.36 | 41.95 | 5.34 | 26.99 | 8.49 |
| Dyn.F | 286.55 | 13.76 | 214.62 | 35.18 | 226.12 | 24.98 | 265.07 | 24.01 |
| Dyn.IFRdrop | 23.91 | 4.38 | 35.98 | 15.08 | 22.46 | 5.68 | 60 | 16.89 |
| Dyn.pfr | 145.78 | 13.51 | 102.36 | 4.3 | 95.11 | 8.41 | 40.78 | 11.74 |
| Dyn.pfr1 | 149.61 | 11.69 | 98.32 | 7.22 | 101.84 | 11.1 | 53.72 | 9.36 |
| Dyn.pfr3 | 136.6 | 11.08 | 92.55 | 6.99 | 93.02 | 10.82 | 41.59 | 9.97 |
| Dyn.RDR | 7.64 | 0.89 | 8.2 | 3.34 | 10.94 | 1.22 | 2.5 | 0.57 |
| Dyn.slp | 2144.72 | 323.56 | 1708.74 | 735.8 | 1146.52 | 260.42 | 336.44 | 137.58 |
| Dyn.slp1 | 259.76 | 54.67 | 297.86 | 91.14 | 160.45 | 22.37 | 267.74 | 61.51 |
| Dyn.slp3 | 377.86 | 31.98 | 381.65 | 81.26 | 189.87 | 32.28 | 202.51 | 49.17 |
| Dyn.spkNum | 7.98 | 0.84 | 7 | 1.7 | 6.35 | 0.68 | 2 | 0.46 |
| Dyn.spkNum1 | 33.93 | 4.02 | 23.4 | 5.21 | 32.39 | 3.62 | 7.21 | 1.86 |
| Dyn.spkNum3 | 26.29 | 3.66 | 15.2 | 2.63 | 21.44 | 2.94 | 4.79 | 1.38 |
| Stat.afr | 87.79 | 8.26 | 58.71 | 3.88 | 57.98 | 4.52 | 42.3 | 8.81 |
| Stat.HzEnd | 62.88 | 9.55 | 6.56 | 6.34 | 44.42 | 4.72 | 9.96 | 5.56 |
| Stat.HzSTD | 26.67 | 2.44 | 20.11 | 2.15 | 14.29 | 1.32 | 14.28 | 3.7 |
| Stat.LSpkF | 166.04 | 15.23 | 121.93 | 16.86 | 121.61 | 13.73 | 149.08 | 11.96 |
| Stat.LSpkT | 990.38 | 4.08 | 752.28 | 63.25 | 990.31 | 2.55 | 316.84 | 113.42 |
| Stat.mSfr | 75.54 | 8.42 | 39.67 | 4.67 | 52.33 | 4.27 | 13.06 | 6.54 |
| Stat.slp | -61.81 | 5.23 | -90.77 | 16.72 | -36.71 | 3.25 | -51.03 | 24.47 |
| Stat.spkNum | 79.95 | 8.56 | 28.75 | 5.14 | 53.57 | 4.44 | 14.13 | 6.7 |
| Thr.F | 47.86 | 10.39 | 47.16 | 22.01 | 37.04 | 10.22 | 96.39 | 19.51 |
| Thr.F1 | 66.42 | 9.93 | 82.25 | 30.21 | 37.61 | 10.41 | 121.7 | 20.69 |
| Thr.F3 | 83.46 | 9.32 | 102.23 | 26.18 | 55.65 | 10.5 | 126.48 | 24.76 |
| Thr.L | 1.01 | 0.18 | 0.86 | 0.44 | 0.78 | 0.17 | 1.86 | 0.28 |
| Thr.L1 | 1.37 | 0.17 | 1.42 | 0.47 | 0.77 | 0.17 | 2.2 | 0.2 |

Table 3 continued

| | | | | | | | | |
|---|---|---|---|---|---|---|---|---|
| **Thr.L3** | 1.78 | 0.1 | 1.99 | 0.25 | 1.55 | 0.12 | 2.13 | 0.26 |
| **Thr.T** | 50.71 | 9.18 | 53.76 | 24.54 | 37.47 | 8.4 | 96.96 | 14.29 |
| **Thr.T1** | 324.18 | 49.42 | 360.65 | 119.97 | 177.2 | 42.28 | 562.46 | 35.74 |
| **Thr.T3** | 457.52 | 24.25 | 512.72 | 64.6 | 388.79 | 28.7 | 605.41 | 37.43 |

| **Group unclassified** | ***Apc*$^{WT}$+control** | **N=19** | ***Apc*$^{WT}$+OX** | **N=14** | ***Apc*$^{Pirc/+}$+control** | **N=19** | ***Apc*$^{Pirc/+}$+OX** | **N=5** |
|---|---|---|---|---|---|---|---|---|
| **variable** | **Mean** | **SEM** | **Mean** | **SEM** | **Mean** | **SEM** | **Mean** | **SEM** |
| **Dyn.DI** | 106.72 | 7.95 | 120.52 | 11.13 | 129.67 | 7.12 | 84.38 | 13.96 |
| **Dyn.F** | 248.81 | 21.74 | 159.98 | 12.59 | 233.98 | 24.84 | 143.33 | 11.79 |
| **Dyn.IFRdrop** | 72.86 | 8.77 | 92.57 | 9.06 | 114.26 | 8.42 | 65.1 | 15.26 |
| **Dyn.pfr** | 173.79 | 7.42 | 168.61 | 11.11 | 185.4 | 8.79 | 103.32 | 13.77 |
| **Dyn.pfr1** | 131.93 | 4.55 | 112.07 | 8.44 | 134.35 | 8.23 | 73.43 | 13.06 |
| **Dyn.pfr3** | 134.16 | 6.99 | 104.16 | 8.3 | 132.48 | 8.46 | 61.9 | 18.76 |
| **Dyn.RDR** | 20.68 | 1.02 | 13.43 | 2.18 | 19.11 | 1.64 | 7 | 0.63 |
| **Dyn.slp** | 1459.37 | 140.71 | 2001.68 | 220.49 | 1677.63 | 93.59 | 1641.3 | 358.14 |
| **Dyn.slp1** | 142.08 | 7.59 | 168.86 | 10.62 | 175.21 | 11.23 | 189.73 | 33.6 |
| **Dyn.slp3** | 213.73 | 12.52 | 246.02 | 19.92 | 274.11 | 19.28 | 225.45 | 69.6 |
| **Dyn.spkNum** | 13.12 | 0.6 | 10.32 | 0.8 | 11.87 | 0.75 | 4.65 | 0.52 |
| **Dyn.spkNum1** | 60.63 | 2.99 | 38.64 | 4.26 | 52.37 | 4.15 | 15.6 | 2.8 |
| **Dyn.spkNum3** | 39.42 | 2.65 | 25.21 | 2.67 | 33.26 | 3.51 | 8.6 | 2.93 |
| **Stat.afr** | 73.84 | 3.97 | 68.92 | 4.23 | 68.11 | 3.65 | 46.48 | 6.27 |
| **Stat.HzEnd** | 49.15 | 5.95 | 40.71 | 5.13 | 44.91 | 3.78 | 12.3 | 7.56 |
| **Stat.HzSTD** | 27.23 | 2.22 | 35.2 | 4.22 | 35.11 | 2 | 31.25 | 5.71 |
| **Stat.LSpkF** | 116.26 | 8.71 | 109.91 | 7.57 | 121.45 | 9.06 | 110.13 | 9.71 |
| **Stat.LSpkT** | 985.25 | 5.95 | 899.9 | 45.2 | 992.09 | 1.45 | 497.85 | 128.72 |
| **Stat.mSfr** | 65.26 | 5.23 | 53.62 | 3.84 | 55.73 | 3.83 | 19.93 | 7.92 |

Table 3 continued

| | | | | | | | | |
|---|---|---|---|---|---|---|---|---|
| **Stat.slp** | -58.45 | 5.52 | -69.11 | 6.88 | -71.93 | 4.44 | -195.39 | 34.99 |
| **Stat.spkNum** | 64.39 | 4.49 | 50.84 | 4.53 | 56.68 | 3.76 | 16.53 | 6.52 |
| **Thr.F** | 17.59 | 1.59 | 31.18 | 3.61 | 22.34 | 3.57 | 41.44 | 10.09 |
| **Thr.F1** | 11.96 | 2.24 | 29.91 | 4.19 | 15.81 | 2.13 | 49.01 | 6.85 |
| **Thr.F3** | 31.06 | 2.7 | 46.32 | 6.19 | 39.18 | 3.97 | 78.01 | 18.59 |
| **Thr.L** | 0.51 | 0.08 | 0.89 | 0.12 | 0.54 | 0.08 | 1.38 | 0.33 |
| **Thr.L1** | 0.21 | 0.05 | 0.75 | 0.12 | 0.37 | 0.07 | 1.69 | 0.16 |
| **Thr.L3** | 1.01 | 0.09 | 1.4 | 0.14 | 1.29 | 0.07 | 2.33 | 0.19 |
| **Thr.T** | 25.02 | 3.87 | 45.12 | 6.23 | 25.56 | 4 | 112.06 | 50.34 |
| **Thr.T1** | 53.35 | 14.85 | 214.73 | 41.31 | 91.38 | 16.68 | 419.77 | 39.16 |
| **Thr.T3** | 271.17 | 18.46 | 371.08 | 38.44 | 328.78 | 16.81 | 585.55 | 47.13 |

| **Group Ia** | ***Apc*$^{WT}$+control** | **N=11** | ***Apc*$^{WT}$+OX** | **N=19** | ***Apc*$^{Pirc/+}$+control** | **N=20** | ***Apc*$^{Pirc/+}$+OX** | **N=10** |
|---|---|---|---|---|---|---|---|---|
| **variable** | **Mean** | **SEM** | **Mean** | **SEM** | **Mean** | **SEM** | **Mean** | **SEM** |
| **Dyn.DI** | 120.23 | 12.93 | 116.75 | 6.16 | 149.53 | 7.78 | 108.85 | 11.9 |
| **Dyn.F** | 185.55 | 25.91 | 160.02 | 12.99 | 251.45 | 28.39 | 150.63 | 7.95 |
| **Dyn.IB** | 282.63 | 14.33 | 205.66 | 36.76 | 175.31 | 48.52 | 76.12 | 51.18 |
| **Dyn.IFRdrop** | 86.41 | 10.38 | 111.06 | 6.46 | 87.5 | 8.93 | 82.52 | 8.41 |
| **Dyn.pfr** | 203.16 | 15.79 | 186.39 | 5.71 | 224.28 | 10.06 | 134.27 | 4.21 |
| **Dyn.pfr1** | 150.52 | 11.87 | 137.87 | 5.8 | 172.9 | 14.55 | 107.62 | 7.79 |
| **Dyn.pfr3** | 137.51 | 16.15 | 130.91 | 5.5 | 166.29 | 10.42 | 99.15 | 6.12 |
| **Dyn.RDR** | 24.64 | 2.63 | 23.05 | 1.29 | 28 | 1.8 | 14.1 | 1.47 |
| **Dyn.slp** | 929.94 | 137.19 | 1103.86 | 110.65 | 1243.56 | 104.05 | 1373.12 | 177.08 |
| **Dyn.slp1** | 124.51 | 18.98 | 144.3 | 7.99 | 164.65 | 11.12 | 160.04 | 31.58 |
| **Dyn.slp3** | 206.58 | 31.49 | 226.11 | 9.04 | 271.66 | 17.3 | 250.56 | 34.01 |
| **Dyn.spkNum** | 18.77 | 1.41 | 16.04 | 0.82 | 17 | 1.27 | 9.9 | 0.9 |

Table 3 continued

| | | | | | | | | |
|---|---|---|---|---|---|---|---|---|
| **Dyn.spkNum1** | 72.73 | 7.75 | 61.53 | 4.31 | 79 | 6.09 | 35.6 | 3.77 |
| **Dyn.spkNum3** | 48.09 | 5.45 | 38.47 | 3.81 | 51 | 4.5 | 21.5 | 2.5 |
| **Stat.afr** | 93.98 | 6.64 | 84.97 | 3.61 | 88.05 | 4.34 | 67.6 | 4.88 |
| **Stat.HzEnd** | 73.47 | 6.47 | 50.72 | 7.09 | 62.75 | 4 | 24.02 | 8.41 |
| **Stat.HzSTD** | 29.85 | 3.15 | 29.26 | 2.1 | 37.23 | 2.21 | 35.69 | 3.71 |
| **Stat.LSpkF** | 122.5 | 11.3 | 113.24 | 10.12 | 115.67 | 8.63 | 120.71 | 7.15 |
| **Stat.LSpkT** | 991.44 | 6.28 | 877.94 | 52.03 | 994.86 | 1.85 | 723.29 | 115.62 |
| **Stat.mSfr** | 82.93 | 6.28 | 66.23 | 6.58 | 74.75 | 3.8 | 34.78 | 7.4 |
| **Stat.slp** | -59.42 | 7.87 | -153.24 | 73.55 | -75.47 | 4.55 | -289.61 | 145.17 |
| **Stat.spkNum** | 85.64 | 6.57 | 66.88 | 6.27 | 76.8 | 4.25 | 36.8 | 7.36 |
| **Thr.F** | 9.86 | 1.07 | 14.41 | 1.09 | 13.25 | 1.47 | 20.62 | 3.84 |
| **Thr.F1** | 7.14 | 1.8 | 16.37 | 2.37 | 7.08 | 0.92 | 21.71 | 5.84 |
| **Thr.F3** | 19.44 | 3.3 | 36.32 | 3.36 | 29.64 | 3.46 | 37.72 | 4.66 |
| **Thr.L** | 0.09 | 0.01 | 0.24 | 0.03 | 0.2 | 0.05 | 0.65 | 0.16 |
| **Thr.L1** | 0.15 | 0.07 | 0.4 | 0.09 | 0.07 | 0.01 | 0.72 | 0.2 |
| **Thr.L3** | 0.84 | 0.12 | 1.31 | 0.09 | 0.91 | 0.08 | 1.48 | 0.11 |
| **Thr.T** | 6.18 | 1.36 | 13.09 | 2.01 | 9.68 | 2.3 | 33.01 | 7.74 |
| **Thr.T1** | 29.89 | 12.06 | 102.97 | 23.37 | 16.16 | 3.61 | 192.75 | 58.1 |
| **Thr.T3** | 217.57 | 30.48 | 338.68 | 22.71 | 236.96 | 19.58 | 393.54 | 36.69 |

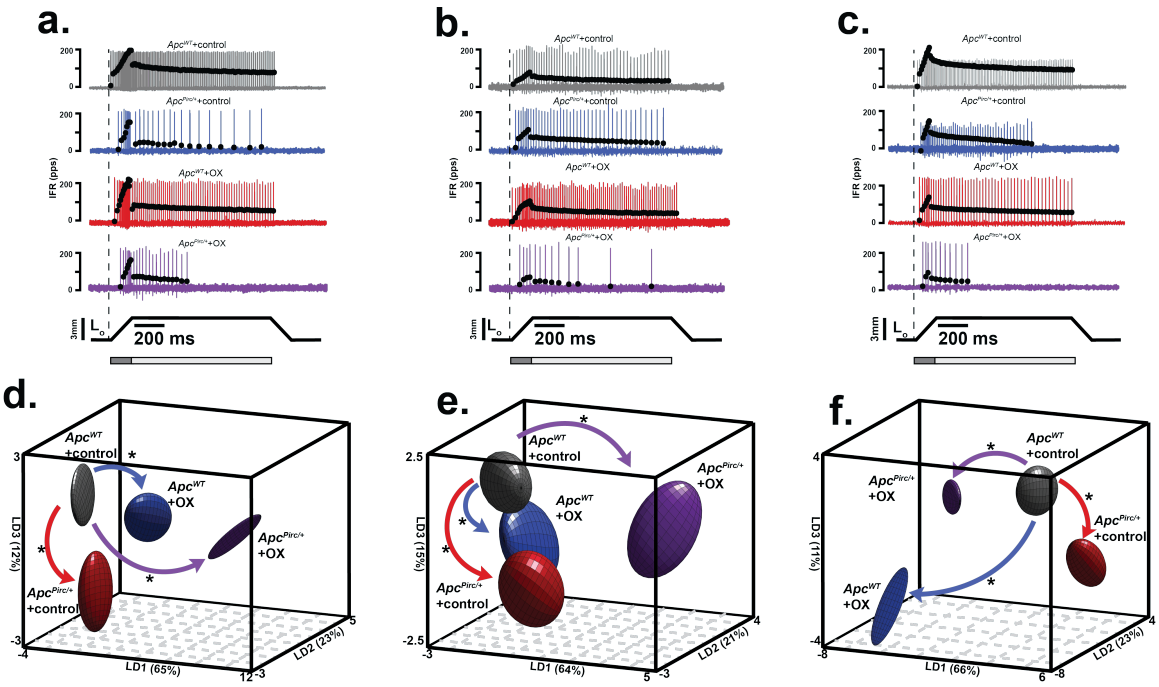


***Figure 30.***

**Impaired Mechanosensory Neuron Population Code After Cancer Treatment.** a-c. Representative cases of spiking activity in *Apc*$^{WT}$+control (grey), *Apc*$^{WT}$+OX (blue), *Apc*$^{Pirc/+}$+control (red) and *Apc*$^{Pirc/+}$+ OX (purple) as a measure of sensory encoding in unclassified spindle (a), group II (b), and group Ib (c). Black circles plot instantaneous firing rates (pps) of corresponding spike (action potential) intervals. Dashed vertical line marks onset of muscle stretch (3mm from resting length ($L_o$)) shown in bottom trace divided into dynamic and static phases by dark grey (150ms duration after stretch command onset) and light grey (1s duration after the dynamic phase) bars. d-f. Neuronal spiking parameters (n=31, averaged from four trials, from each neuron in each of the neuronal classes, unclassified spindle (d), group Ib (e), and group II (f). Features represent different features of sensory stimuli and were subjected to linear discriminant (LD) analysis. Neuronal signaling was visualized in the new 3D composite space created by LD1-3. 3D ellipsoids enclosing 68% of data were computed with least-squares elliptical fitting. Effects of independent (OX or *Apc*$^{Pirc/+}$) and combinatorial (*Apc*$^{Pirc/+}$+OX) treatment are indicated by colored curved arrows.

Purple traces in Figure 30 illustrate representative firing profiles for each neuron class in *Apc*$^{Pirc/+}$+OX rats. We found drastically impaired neuronal signaling across all classes.

Sensitivity to stimuli was reduced at both high and low velocity stretch (data not shown). During dynamic stimuli, we found marked reduction in the number of spikes over both stretch conditions. Neurons also failed to sustain firing. In addition, we observed fewer spikes during rapid accommodation immediately preceding signal deletion, despite constant stimulus. These data confirm that a damaging functional interaction between the systemic effects of cancer and chemotherapy is conserved across multiple classes of sensory neurons in living animals.

To quantify inferences drawn from raw data, we took an unbiased statistical approach by subjecting all signaling parameters from all neurons, classes and experimental groups to a LD analysis. This reduced complex feature space into canonical variables giving us a high-level understanding of where interaction emerges, without biased parameter selection *a priori*. Our analysis yielded three canonical variables (Figure 30d-f) that achieved overall 98.7% classification accuracy. We then visualized neuronal signaling in the new 3D composite space created by LD1-3 (Figure 30d-f) revealing a first dimension (LD1) that accounted for a large fraction of the explained variance for each class of neurons, ranging from 64-66% (Figure 30 d-f). Coincidentally, LD1 also represented the non-linear interaction between cancer and chemotherapy, that can be visualized by the 3D separation of the purple spheroid in LD1 (as was the case for group Ia).

By examining the discriminant function coefficients, we found that fast and slow threshold levels, static firing average (and number of spikes), and dynamic firing rates represent the dominant portion of the explained variance in LD1. This suggests that these parameters are most susceptible to codependent interaction and justify further quantification and validation. Line graphs in (Figure 31) show the hierarchal Bayesian modeling results for the selected parameters as well as the experimentally measured data used to power the generative models. Across all parameters and neurons classes

the codependent interaction significantly exacerbated signaling deficits. Interestingly, the balance of parameter values between neuronal classes, e.g. the relative thresholds between group Ia and Ib, appear to be conserved, which suggest a global co-regulatory process may be present. In other words, a process that governs the balance of information content from multiples neuron classes flowing to the central nervous system. Collectively, our data indicate that all muscle proprioceptors are vulnerable to neurotoxic hypo-excitability induced by chronic cancer treatment.

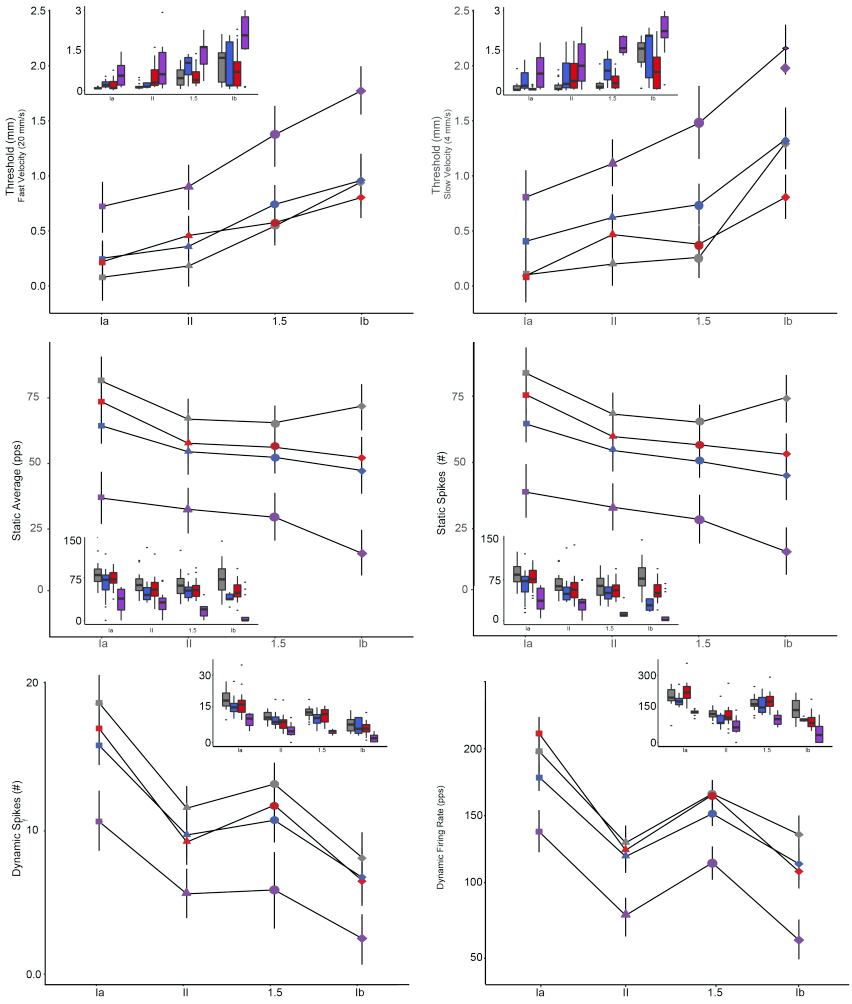


***Figure 31.***

**Co-Suppression of Key Mechanosensory Features.** Hierarchal Bayesian modeling results used to test for significant group differences of neuronal spiking parameters (six shown). Colored and shape coded points represented the empirically derived mean posterior predictive density and 95% highest density intervals (vertical lines). Statistically significance is determined when vertical lines do not overlap between parameters, i.e. 95% highest density intervals are exclusive. Insets in each model output display boxplots of experimentally measured data used in hierarchal models.

## *Latent Mechanosensory Features Similarly Impaired*

We leveraged an unsupervised analytical approach, principal component analysis (PCA), to validate the supervised analyses performed above. PCA was simultaneously

applied to 31 parameters of mechanosensory encoding measured in response to natural stimuli for all classes and experimental groups. PCA confirmed fast and slow threshold levels, static firing average and number of spikes, and dynamic firing rates represent the parameters most indicative of groupwise separation (vectors in (Figure 32a). Neurons were then visualized in the new latent feature space created by PC1–3 where individual points represent individual neurons. Failure to adequately separate groups by either class (Figure 32b, unclassified spindle: green, group Ib: blue, group II: purple, and group Ia: yellow) or treatment group (Figure 32c, $Apc^{WT}$+control: grey, $Apc^{WT}$+OX: blue, $Apc^{Pirc/+}$+control: red and $Apc^{Pirc/+}$+ OX: purple) indicates substantial class by treatment interaction. To overcome this, neurons were co-labeled based on class and treatment. Mean centroids were calculated and visualized in 2D projections (Figure 32d and expanded view of dotted box in Figure 32d) created from PC1-2. Vectors were calculated to show the magnitude and direction of independent (OX or $Apc^{Pirc/+}$) and combinatorial ($Apc^{Pirc/+}$+OX) treatment effects across each class in the latent feature space. $Apc^{Pirc/+}$ consistently influenced PC2, whereas OX effects consistently acted on PC1. While $Apc^{Pirc/+}$+OX similarly acted on PC1, the magnitude was significantly greater than that observed from OX. Interestingly, linear summation of OX and $Apc^{Pirc/+}$ effects does not accurately predict the location of $Apc^{Pirc/+}$+OX. Collectively, our results confirm that using cancer or chemotherapy as independent predictor fails to accurately predict their combination. Further, our analyses indicate that despite unique encoding properties and firing profiles, the combinatorial effects of cancer and chemotherapy influence neuronal firing in a similar manner. This becomes evident when high dimensional parameter spaces, that accurately described neuronal firing, are simplified to low-dimensional latent variables.

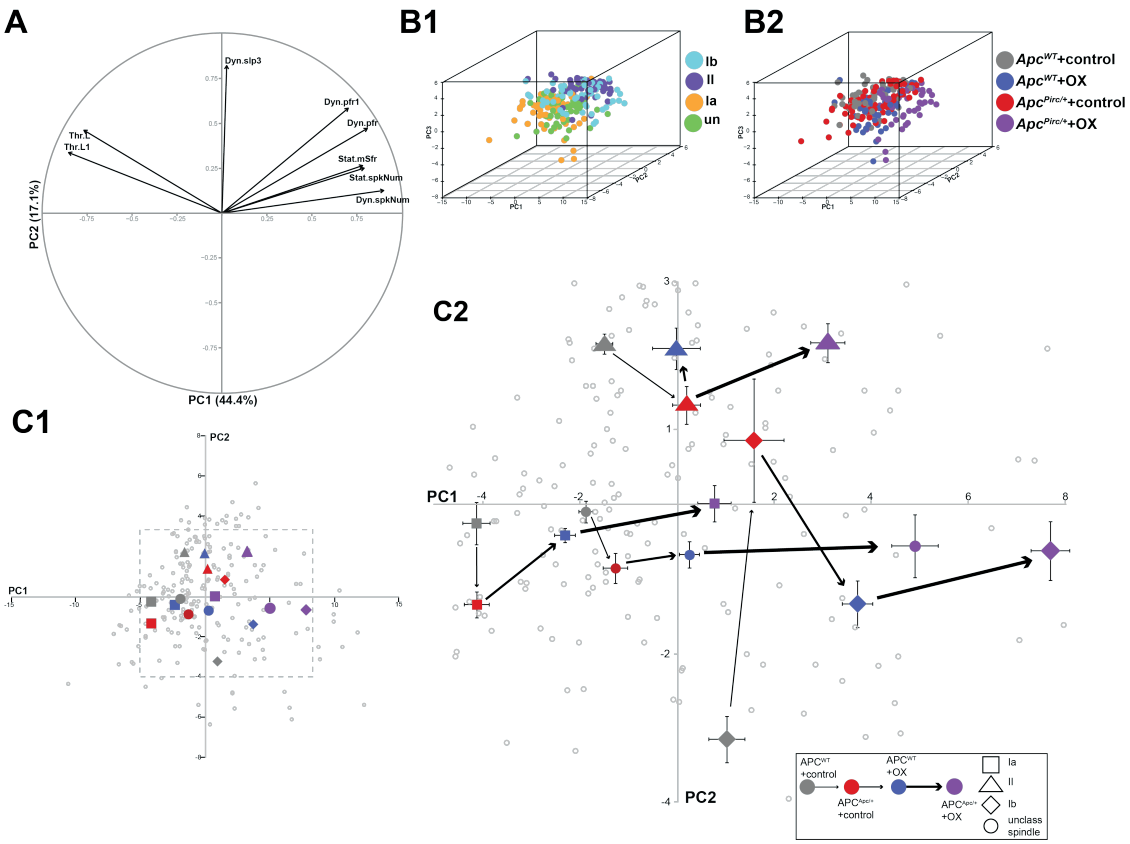


## *Figure 32.*

**Latent Mechanosensory Features Similarly Impaired Across Diverse Mechanosensory Neuron Classes.** Principal component (PC) analysis was applied to 31 parameters of mechanosensory encoding measured in response to natural stimuli. a, vectors represent the magnitude and direction of correlation between individual parameters and the two latent features capturing the most variance (PC1-2). b-c, Neurons visualized in the new latent feature space created by PC1–3. Points represent individual neurons highlighted by specific mechanosensory class (b, unclassified spindle: green, group Ib: blue, group II: purple, and group Ia: yellow) or treatment group (c, *Apc*$^{WT}$+control: grey, *Apc*$^{WT}$+OX: blue, *Apc*$^{Pirc/+}$+control: red and *Apc*$^{Pirc/+}$+ OX: purple). Neurons were co-labeled based on class and treatment and mean centroids were calculated and visualized in the 2D projections (d) created from PC1-2. e, expanded view of dotted box in d. Magnitude and direction of arrows demonstrates the independent (OX or *Apc*$^{Pirc/+}$) and combinatorial (*Apc*$^{Pirc/+}$+OX) treatment effects across the latent feature space.

*Population level deficits do not reflect hypoexcitable scaling*

Having established codependent interactions are conserved across multiple sensory neuron classes, we aimed to understand the consequences of those deficits when the information is convolved in a population code as it is at a sensorium level. Intracellular recordings from physiologically identified sensory neurons of all four classes were used to construct population codes (ensembles of neuronal firing). We precisely time synchronized independently recorded neurons by aligning identical stimulation patterns. This allowed us to model population codes of physiologically identified neurons of precisely known locations from $Apc^{WT}$+control and $Apc^{Pirc/+}$+ OX animals, not possible in previous studies (Stein, Weber *et al.* 2004; Weber, Stein *et al.* 2007). Figure 33 presents the population code of 40 neurons recorded each from both $Apc^{WT}$+control rats (grey) and $Apc^{Pirc/+}$+ OX rats (purple). Visual inspection of the $Apc^{WT}$+control population reveals that while variable firing responses exist (top panel), likely reflecting the diverse encoding properties of multiple neuron classes, the average firing rate (bottom panel) closely mirrored the stimuli (bottom traces), both in onset and shape. By contrast, the sparse $Apc^{Pirc/+}$+ OX population (top panel) displayed delayed onset and reduced correlation to stimuli.

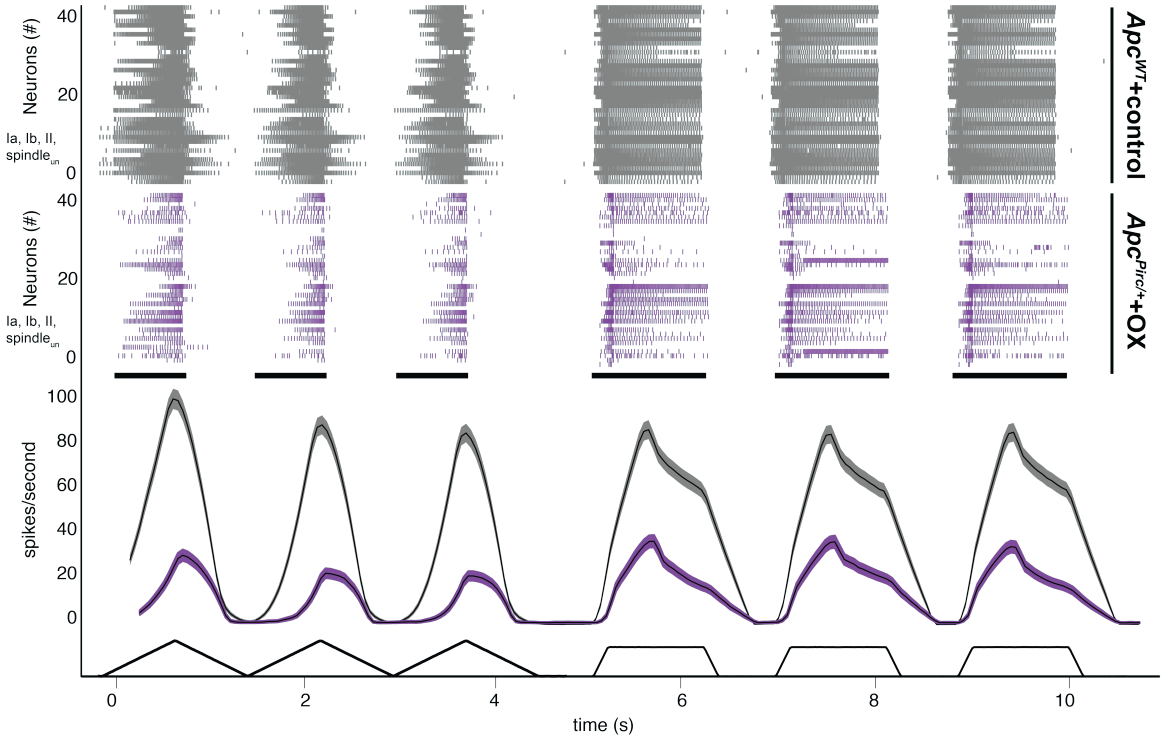


## ***Figure 33.***

**Blunted Population Code.** Population code of 40 neurons recorded each from both *Apc*$^{WT}$+control rats (grey) and *Apc*$^{Pirc/+}$+ OX rats (purple). Vertical lines in raster plot (top panel) indicate the presence of individual spiking events during a representative 10s recording as three slow (4mm/s) ramp-release followed by three, fast (20mm/s) ramp-hold-release mechanical stimuli initiate neuronal activity. Bottom panel illustrates the average firing rate (black line) and standard error (shaded region) computed from the same recording epoch as above. Both population codes were constructed from the same distribution of neuronal classes, 10 group Ia, 5 unclassified spindle, 14 group Ib, and 11 group II.

### *Summary*

Collectively, results confirm the expected blunted population code while also providing the first evidence that the codependent interactions does not result in a simple hypoexcitable scaling, as evidence by substantial temporal dispersion.

## Aim 7: Test the hypothesis that decoding of spatiotemporal features of movement from a population code of mechanosensory neurons is attenuated after chemotherapy treatment of cancer.

### *Aim Specific Methods*

*General deep learning methods*

We leverage deep, recurrent artificial neural networks to discover structure in high dimensional inputs (binned ensemble neuronal firing rates). These methods are inspired by biologically plausible models of neural circuits, particularly the spinal sensory-motor circuits studied here, that learn a hierarchical representation or transformation of the input data that make prediction easier (Rumelhart, Hinton *et al.* 1988; Goodfellow, Bengio *et al.* 2016). The deep neural network utilized here, consists of a layer of computational units called neurons or nodes. The deepness refers to the number of layers between the input and output. We selected a single hidden layer that represents the LV/VI interneuronal populations that is fully connected to the output layer. Biologically these interneuronal populations receive a vast synaptic connections from the mechanosensory neurons (input data) studied here (Vincent, Gabriel *et al.* 2017) and reside directly upstream of the motor pools (analogous to our output layer). By tuning the connection weights, the network can learn to approximate a function used for prediction, i.e. how a motor pool receiving this synaptic input could draw inferences about its previous activity. In this work we are interested in training a deep neural network to decode (extract) relevant musculoskeletal features of the rat hindlimb from activity recorded from ensembles of healthy mechanosensory neurons activity and how that ensemble of neuronal activity is altered following cancer treatment (Figure 33). This

approach allows predictions to be made of specific sensory-motor deficits not possible from analyzing spike trains alone. Because both the full structural and functional connectivity remain unknown throughout the segmental spinal circuits we chose a fully connected schema throughout as a rational starting point.

*Model architecture.*

The model architecture was constructed using the Keras library for Python (Chollet 2018), using TensorFlow backend (Abadi, Agarwal *et al.* 2016). The architecture relates the multidimensional input (binned neuronal firing rates) to output (musculoskeletal parameter) space, as described in Figure 34. The model considered not only the current time bin but the six-time bins that preceded and followed it to better inform its decisions about the musculoskeletal parameters. The network comprised a single layer of long-short-term memory units (LSTMs), a modification on the basic recurrent structure that minimized the impact of numerical instability during back-propagation and further improve the capture of long-term dependencies (Hochreiter and Schmidhuber 1997). The LSTM units were fully connected to an output layer with three units (length, force, stiffness) using RMSprop (Tieleman and Hinton 2012) as the optimization routine. Models were run with GPU parallelization using NVIDIA's cuDNN package (v 7.6). To combat the tendency to overfit unconstrained predictors, particularly on smaller data sets, we utilized an effective method to curb overfitting. We used a technique called dropout to prevent complex co-adaptations, or paired relationships between units in the network by allowing connections between individual units to be removed with some specified probability, range from 0-1, during training (Srivastava, Hinton *et al.* 2014; Gal and Ghahramani 2016). The specific dropout probability was set as a hyperparameter prior to training during each fold. This and other hyperparameters, e.g number LSTM units, is discussed below.

*Preprocessing*

Input data (neuronal activity) was z-score normalized. Output data (musculoskeletal parameter) was zero-centered. Data for training/validation/testing were preprocessed using identical approaches.

*Predictive Performance*

Predictive performance of models was measured as the fraction of variance accounted defined as $R^2 = 1 - (\frac{\sum_i (y_i - \hat{y}_i)^2}{\sum_i (y_i - \bar{y}_i)^2})$ where $\hat{y}_i$ are the predicted values, $y_i$ are the true values, and $\bar{y}_i$ is the mean value. $R^2$ values are reported for each musculoskeletal parameter: length, force, and stiffness. $R^2$ values in the range [0, 1] are interpreted in the same way as the Coefficient of Determination. Negative $R^2$ values are interpreted as the model injecting more variance into the process than there exists in the data set.

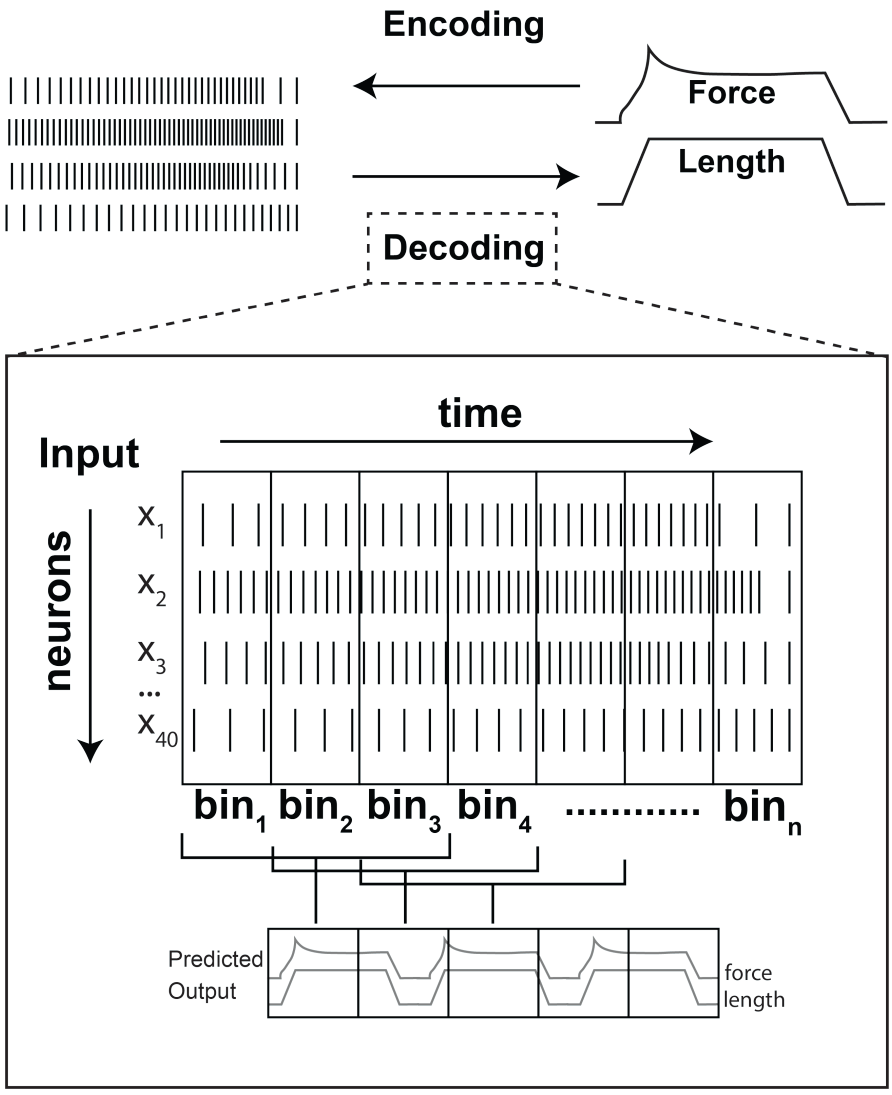


***Figure 34.***

**Conceptual schematic of encoding and decoding processes.** Encoding is the process by which static and dynamic musculoskeletal parameters (top right) is translated into ensembles of spiking neurons. Decoding is the process by which information, e.g. about the musculoskeletal parameters, is extracted from spiking activity. Bottom inset illustrates the decoding methodology via artificial neural network. To decode (predict or extract information from spikes) the output in a given time bin, the firing rates of all neurons (N=40) in time bins (bins=3), In this schematic, one bin preceding the output, one concurrent bin, and one following bin). Here, we show two outputs being predicted for simplicity but we report three outputs; muscle length, force, and stiffness.

*Cross-validation*

Models were assessed using a 10-fold cross-validation approach by splitting the data into a training, validation and testing sets (Stone 1974; Browne 2000). For each fold, a separate model was constructed, leaving that fold out for use as test data and using eight of the remaining folds as training data. The test data fold was used to compare the performance across different model forms. The one remaining fold was used as a validation data set: model performance with respect to this data set was used to select some independently optimize hyperparameters (described below) before evaluating the model for comparison with other model forms using the test data thereby eliminating any bias introduced by selecting hyperparameters on the basis of the test performance (Bishop 1996). For each fold, models were trained to minimize the mean squared error between the predicted and true musculoskeletal parameter of the training data.

*Hyperparameter optimization*

In addition to parameters that link the neural activity to the output variables, e.g. weights on connections in network, the model also has hyperparameters, which relate to the design of the network itself that needs to be identified prior to training. Unbiased hyperparameters (number of hidden units in the layers, amount of dropout (Srivastava, Hinton *et al.* 2014), and number of training epochs) selection was performed on each cross-validation fold. Optimization was directed to identify hyperparameters that led to the highest $R^2$ on the validation set using Bayesian optimization (hyperopt Python package) (Bergstra, Yamins *et al.* 2013). This algorithm uses a Bayesian-based optimization algorithm called the Tree-structured Parzen Estimator to explore a hyperparameter space across multiple epochs. Briefly, this optimization approach samples hyperparameter values from pre-defined prior distributions, uses a loss function to evaluate the current hyperparameters, and then repeats these steps using knowledge

gained from the evaluations it has already performed. After a desired number of epochs, the hyperparameter set associated with the minimal loss value across all epochs is chosen as the optimal hyperparameter set. Those hyperparameters were used to calculate the $R^2$ value on the testing set.

*In Vivo Validation of Decoding Deficits*

Biological validation of decoding results was obtained by recording synaptic potentials in triceps surae motoneurons in response mechanical stretch of the triceps surae muscles. The triceps surae muscles were stretched by 3mm at a constant velocity (20 mm/s) over 150ms rise during ramp-hold-release stretch, the muscles were held at that length for 1s, and then released to resting length at constant velocity over 150ms. Stretches were repeated for 15-20 trials at 4-s intervals then averaged.

***Results***

*High fidelity feature extraction by healthy nervous system*

Since the $Apc^{Pirc/+}$+ OX population code was not a downscaled $Apc^{WT}$+control sensorium, the potential for information loss encouraged us to test the consequences of the $Apc^{Pirc/+}$+ OX population. We employed a deep-learning algorithm (long-short-term memory network: LSTM) to test how decoding of spatiotemporal features of movement are altered after chemotherapy treatment of cancer. The process of decoding allows neurons and networks of neurons upstream of the sensorium to extract features of the spiking activity in order to draw inferences on that information, e.g. current body position or inertial loads on limbs as movements result in physical interactions with the environment. First, we aimed to understand LSTM performance when decoding the $Apc^{WT}$+control sensorium. Figure 35 (left) summarizes average decoding performance quantified across all 10-fold cross validation runs for LSTM trained on $Apc^{WT+}$+control data. Results indicate highly accurate decoding of all parameters but muscle force was

consistently decoded more significantly more accurate than length or stiffness. Figure 35 (right) shows representative raw traces of three ground truths and three model predictions generated after training.

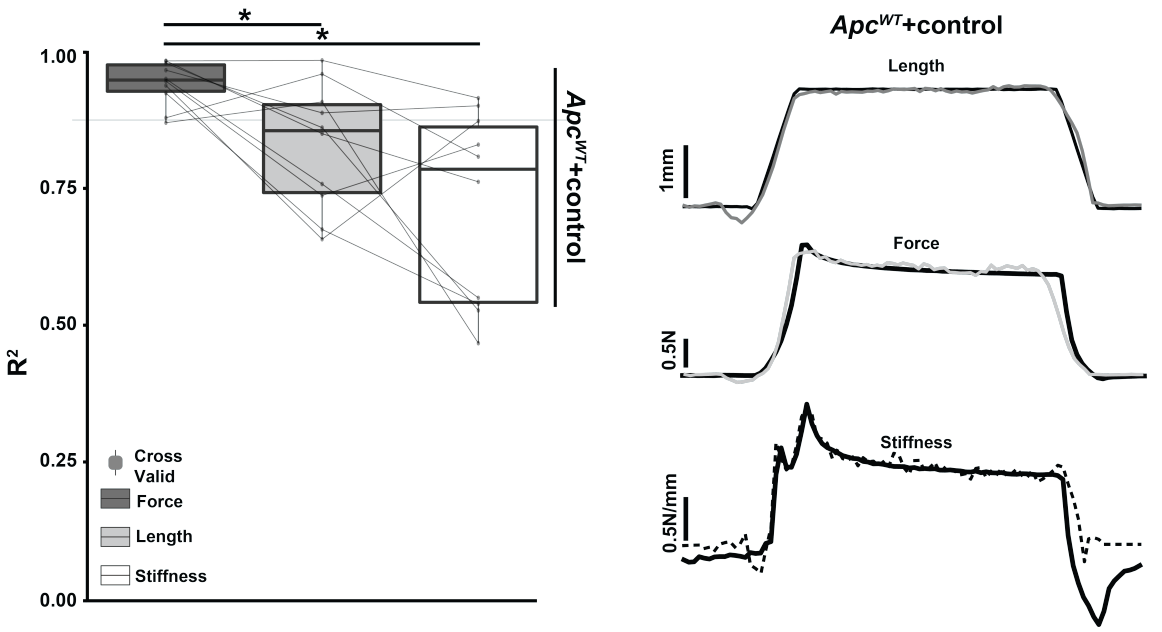


***Figure 35.***

**High fidelity feature extraction by healthy nervous system. a,** Average decoding performance across all 10-fold cross validation runs for model trained on $Apc^{WT+}$+control data. Boxes represent the three outputs (mechanical stimuli) being predicted by model force, length, stiffness. **b,** Raw traces of three ground truths (black lines) and three model predictions generated after training (color coded after a). Model contained ~$7.5x10^5$ parameters. * indicates statistically significant differences as empirically derived from hierarchical Bayesian model (stan_glm): 95% highest density intervals do not overlap.

*Cancer treatment degrades accurate decoding*

We then computed the LSTM model performance when tested on the $Apc^{Pirc/+}$+ OX population. Figure 36 illustrates the three musculoskeletal parameters with superimposed LSTM predictions for two types of stimuli, fast ramp-hold-release (a) and slow ramp-release (b). Figure 36c summarizes average decoding performance

quantified across all 10-fold cross validation runs when compared to $Apc^{WT}$+control model performance. Significant degradation in predictive accuracy was observed with muscle force experiencing the greatest reduction in accuracy ($R^2$=-0.03%) while length and stiffness conserved the greatest accuracy ($R^2$ =20% and 30.2%).

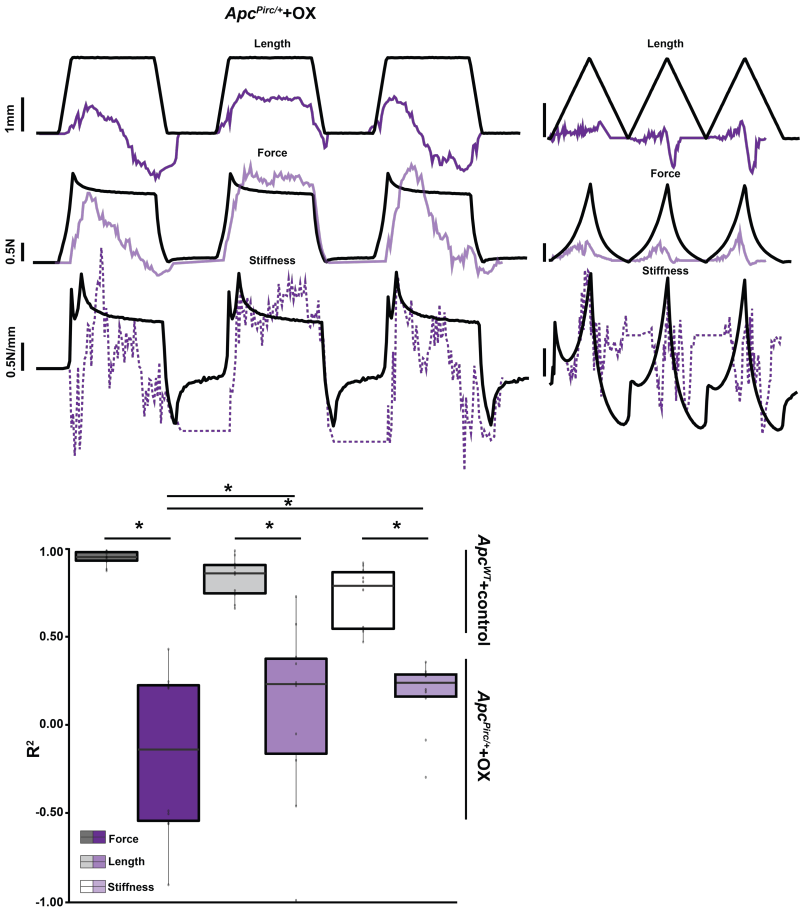


***Figure 36.***

**Cancer treatment degrades accurate decoding.** a-b, Long-short-term memory (LSTM) model predictions of mechanical stimuli for *$Apc^{Pirc/+}$*+ OX neuronal population (Purple) and ground truth (Black) for each of the three outputs. Model trained on *$Apc^{WT}$*+control data and tested on same number and proportion (classes) of *$Apc^{Pirc/+}$*+ OX neurons for various stimuli, e.g. fast ramp- hold-release (a) and slow velocity ramp-release stretches (b). b. Average decoding performance across all 10-fold cross validation runs for *$Apc^{Pirc/+}$*+ OX neurons when compared to *$Apc^{WT}$*+control performance. * indicates statistically significant differences as empirically derived from hierarchical Bayesian model (stan_glm): 95% highest density intervals do not overlap.

*Functional consequences*

We then focused on specific features of the LSTM predictions to gain insight into where functional consequences may manifest during animal (human included) movement. Analyses quantified the features as defined in Figure 37a. We find significant errors were made for the background force and stiffness whereas background lengths were largely conserved (Figure 37b), significant lag in discriminating the onset of stimuli (Figure 37c), significantly impaired detection of sustained lengths, forces, and stiffnesses, as well as inconsistent predictions of peak forces and length changes.

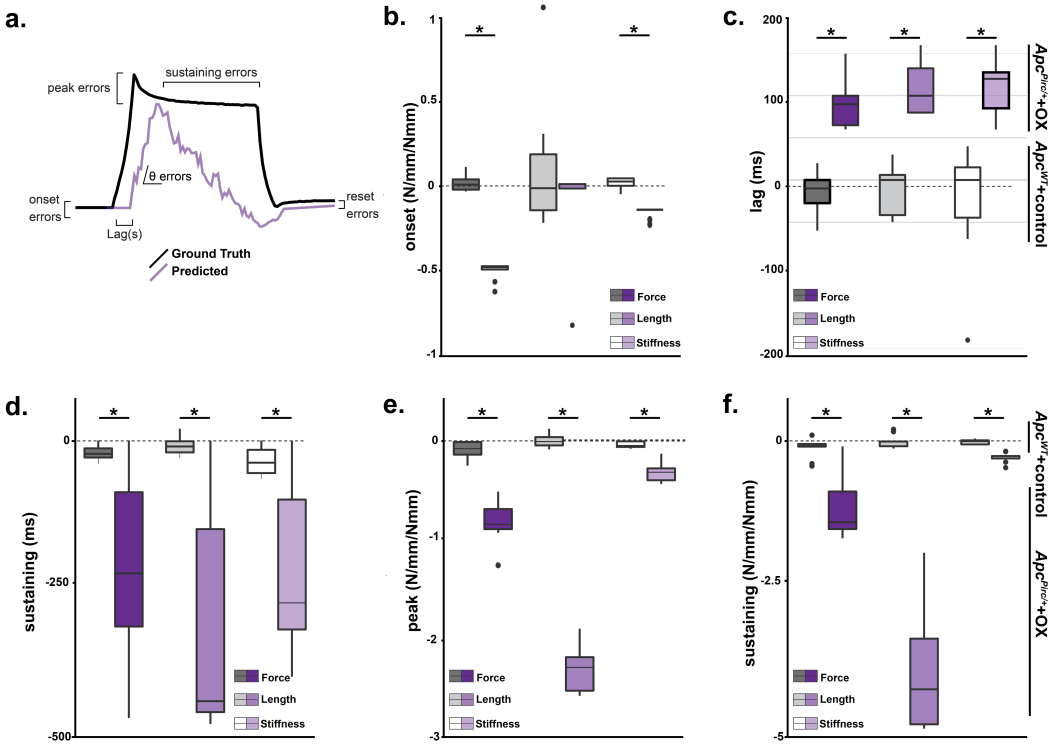


***Figure 37.***

**Functional consequences. a**. Analytic schematic for measuring functional errors. **b-f**. Average errors for various parameters across the three outputs (length, force, stiffness) predicted by both *Apc*$^{WT}$+control and *Apc*$^{Pirc/+}$+ OX neuronal models. Boxes indicate average errors from ground truth, e.g. 0 is perfect prediction. * indicates statistically significant differences as empirically derived from hierarchical Bayesian model (stan_glm): 95% highest density intervals do not overlap.

## Aim 8: Test the hypothesis that learning can compensate for a corrupt population code after chemotherapy treatment of cancer.

### *Aim Specific Methods*

*Reparametrizing Decoding Model*

To model how the CNS may compensate for a corrupt sensory population, restore predictive power and improve the accuracy of feature extraction, we trained a LSTM network, *de novo*, on the $Apc^{Pirc/+}$+OX population hereafter designated $LSTM_{OX}$. During training, this affords the $LSTM_{OX}$ access to ground truth. This affords iterative updating of the relationship between input data and predictive outputs and is a biologically plausible process by which the representations and transformations of neuronal input could update a unified representation of body position under static and dynamic conditions, e.g. learning or compensating. The $LSTM_{OX}$ was trained, tested and validated, under identical conditions as described above for the LSTM.

### *Results*

*CNS cannot fully compensate*

Figure 38 illustrates the three musculoskeletal parameters with superimposed $LSTM_{OX}$ predictions. $LSTM_{OX}$ performance was substantially improved as compared to the predictions (Figure 36a, b), yet fell significantly short of $Apc^{WT}$+control model performance (Figure 35). This suggested that the CNS would not be able to fully compensate for and learn a new representation of the corrupt population code that restores predictive abilities.

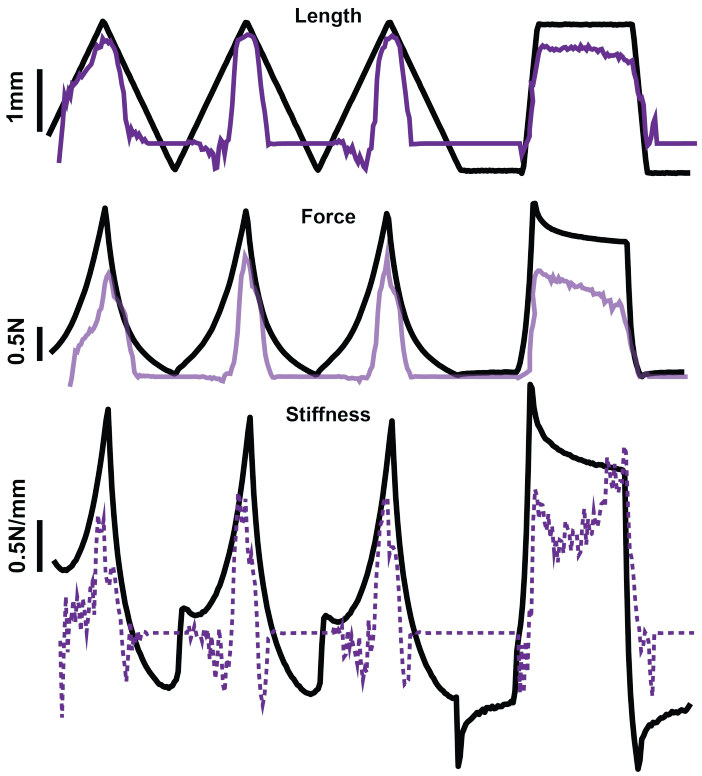


***Figure 38.***

**CNS cannot fully compensate**. Long-short-term memory ($LSTM_{ox}$) model predictions of mechanical stimuli for *Apc*$^{Pirc/+}$ + OX neuronal population (purple) and ground truth (black) for each of the three outputs. Model trained, tested and validated *Apc*$^{Pirc/+}$ + OX data for various stimuli, e.g. fast ramp- hold-release (right) and slow velocity ramp-release stretches (left).

## Project 2: Discussion

Here we present original evidence that encoding deficits induced by chemotherapy, exacerbated by cancer are conserved across diverse classes of mechanosensory neurons. Our results show global deficiency in the population code of mechanosensory neuron population and resulting corrupt spatiotemporal decoding of movement features. Since these neurons are responsible for encoding the foundational spiking activity to generate a unified representation of body position under static and dynamic conditions,

their impairment necessarily results in upstream neurons or networks to unpredictable inferences about the bodies interaction with the external environment. By modeling the compensatory or learning processes, our results further suggest that the CNS would not have the capacity to fully compensated through learning. This inability may help to explain the lasting behavioral deficits documented in patients treated with chemotherapy.

Redundancy as a Compensatory Mechanism

Multiple classes of mechanosensory neurons combine their signals in a population code that is decoded by the CNS to regulate and perceive body movements and postures. A large portion of that population code is uniquely provided by the neurons studied here, namely Golgi tendon organs (Ib) and group Ia and II muscle spindle afferents. Mechanosensory neurons are classically understood to encode unique time varying features of muscle mechanics. Dynamic muscle parameters are thought to be represented by group Ia afferents, static muscle parameters by group II afferents, and higher stretch threshold by group Ib afferents. Despite these unique capabilities, we have previously documented that this diverse population of neurons encode parameters that are distributed in a continuum with substantial overlap, e.g. robust Ib response to passive muscle stretch in the physiological range (Vincent, Gabriel *et al.* 2017). From this, we infer that the mechanosensory population code, is to some degree, redundant. While other have suggested that redundant codes may be unnecessary to decode information about movement (Stein, Weber *et al.* 2004), redundancy reduction can be problematic since codes maybe sensitive to noise and require careful processing when attempting to encoded and extract information (Schneidman, Bialek *et al.* 2003). In fact, the existence of redundancy may actually indicate the prevalence of a stimulus, a critical factor in developing representation and performing analysis via probabilistic computations (Barlow 2001). Outside of probabilistic encoding or decoding processes,

specific behavioral success has been attributed to sensory feedback that emerges from both distinct and redundant mechanosensory sources (Akay, Tourtellotte *et al.* 2014). Sensory feedback from muscle spindles appears to selectively influence the pattern of flexor muscles activations during locomotion, whereas the joint responses of muscle spindles and Ib afferents determine the pattern of extensor muscle firing (Akay, Tourtellotte *et al.* 2014). Taken together, redundant mechanosensory population code may protect or compensate for losses in specific classes of neurons or encoded parameters in $Apc^{Pirc/+}$+ OX rats or cancer survivors that have undergone chemotherapy treatment. Alternatively, dysfunctional encoding might overwhelm redundancies resulting in decompensated sensorimotor performance. Dysfunction might similarly arise during certain behaviors or phases of movement that depend on selective mechanosensory information. Population statistics, canonical analyses, and computational modeling provided rigorous tests of these hypotheses. In all cases, we find that the redundancy in the mechanosensory population code is insufficient to compensate for distributed information loss across each neuron class. This finding strengthens the evidential support that mechanosensory deficits play a prominent role in behavioral deficits observed in clinical cancer settings. These findings may also explain why $Apc^{Pirc/+}$+ OX rat task performance is worse than our previous observations in animals treated with OX alone, in that selective dysfunction of muscle spindles static responsiveness was compensated, by redundant signals from Ib and II neurons.

Clinical and Functional Significance

While we have yet to establish a causal relationship, impaired sensory feedback has real potential to contribute to decompensated sensorimotor performance observed in our precision behavioral tasks in awake behaving animals (Aim 5) and is likely involved in instability and ataxia's seen in cancer survivors (Burakgazi, Messersmith *et al.* 2011;

Tofthagen, Overcash *et al.* 2012; Kneis, Wehrle *et al.* 2016; Marshall, Zipp *et al.* 2017; Taleb, Bouzobra *et al.* 2017). This is due to the fact that these neurons provide the CNS with its only means of detecting mechanical perturbation in the muscular system.

As we have previously documented, reasonable predictions about the consequences of corrupt signaling can be drawn from evaluating spike trains (neuronal signaling). However, the extent to which you can draw direct comparisons between neuronal signaling and their behavioral consequences is less certain given the precise nature and features of the transformation from external stimuli to action potentials remains unknown. This makes understanding objective consequences and making real-world predictions of compromised neuronal signals challenging.

We took the first steps to overcome this limitation by using a deep-learning neuronal decoding algorithm in a novel way. Neural decoding typically uses population level data recorded from the nervous system to make predictions about variables in the outside world, e.g. arm position, that can be used to control devices (e.g., robotic limbs). In this way, neuronal decoding algorithms model the processes by which information is extracted by the CNS. We extended this analytic method to understand and quantify prediction errors that could be made when exposed to compromised neuronal signals. This allowed us to, for the first time, make quantifiable measures about what movement limitations would emerge from neuronal signaling deficit. Our analyses revealed several unexpected predictions including: both over and underestimation of applied forces, severe delays in detection of applied perturbation (in some cases adding 100s of milliseconds of delay, e.g. Figure 38), and drift in perceived length changes despite constant stimuli. These unique insights should inform the focus of future clinical evaluations and direct resources toward specific rehabilitative interventions.

CNS Implications

The CNS has a vast capacity to reorganize or develop a new representation following insult (Chen, Cohen *et al.* 2002; Anderson, Spencer-Smith *et al.* 2011; Ionta, Villiger *et al.* 2016). To investigate this role, we also took the first steps toward understanding the CNS's capacity to compensate for signaling loses by modeling the maximum decoding potential when our deep-learning neural decoding was given access to ground truth during optimization. This advantage improved the accuracy of decoding external states yet revealed that substantial errors persist. Moreover, these data further support our hypothesis that sensory encoding deficits contribute to functional limitations and that despite the impressive capacity for reorganization, the CNS would not be able to fully compensate.

It remains to be seen how deficits in primary afferent signaling propagate to higher network level dysfunction, e.g. perception, body schema despite is suspected dominant role in on-line representations (Shenton, Schwoebel *et al.* 2004). Our modeling was limited by the fact that we estimated errors that the CNS may make if it were only exposed to mechanosensory neuron populations. In this way, our modeling approximate spinal neurons populations, e.g. motoneurons, pre-motoneurons, dorsal spinocerebellar tract (DSCT) neurons, etc. best. These neuron populations have limited access to other forms of sensory information that may augment losses. While no compensation can be made for absent/corrupt primary afferent information, its precise contribution to errors in global phenomena, e.g. body schema remains to be determined since they likely emerge from the convergence of primary afferent information with a vast array of other sensory information, e.g. vestibular or visual (Driver and Spence 1998; Shimojo and Shams 2001; Stein 2012).

# CHAPTER 5. CONCLUSIONS

Our overall objective was designed to correct the limitations of previous preclinical studies to gain understanding of clinically relevant *chronic* CIPN. Our unbiased integrative genomics and protein level studies revealed that clinically relevant chemotherapy induced neurotoxicity is codependent and exacerbated by cancer itself. Further, we confirm codependence is conserved in the living adult nervous system and is expressed as profound neuronal signaling dysfunction. Corrupted signaling necessarily impairs the central nervous system of information about body position, sensorimotor coordination, and error detection that likely contributes to significant errors we discovered in validated measures of sensorimotor behavior in awake behaving animals similar to those described by patients. Further, *in silico* biophysical modeling of sensory encoding deficits helped test the sufficiency of our newly identified molecular mechanisms of codependent interaction that may act as a novel clinical treatment strategy, while deep-learning decoding algorithms afforded the first insights into the extent to which sensory encoding errors might compromise information processes by the central nervous system. Collectively, our results confirm cancer as a critical feature in understanding mechanisms that contribute to neuronal dysfunction caused by chemotherapy and have the potential to explain the abject failure of current treatments for neuronal dysfunction in cancer treatment.

While the present report is limited to rats, extensive conservation of core molecular and cellular processes across mammalian species (Breschi, Gingeras *et al.* 2017) leads reasonable expectation that cancer-chemotherapy codependency, whether different in detail, extends to humans. All considered, we conclude that inattention to co-dependencies necessarily prevents the development of mechanism-based treatments

for sensory neuropathy, which remains unexplained and unabated in patients receiving chemotherapy for cancer.

*Role of the Mechanical Environment in Sensory Encoding Deficits*

While this work focused on developing a deeper understanding and testing specific hypotheses surrounding the role of cancer in chronic chemotherapy-induced sensory neuropathy, the sensory nervous system's (and more specifically the mechanosensory system studied in this work) inextricable link to the mechanical environment their housed in, i.e. muscular system, necessitates discussion of its potential role in our findings. Mechanosensory function depends on the transduction of mechanical stimuli, e.g. kinetics or kinematics, by receptor endings into trains of action potentials (encoding). Any alteration to active or passive properties of muscular system or motor physiology has the potential to contribute to encoding deficits. This possibility is plausible since both chemotherapy (Sakai, Sagara *et al.* 2014; Sorensen, Petersen *et al.* 2017) and cancer (Dodson, Baracos *et al.* 2011; Aoyagi, Terracina *et al.* 2015; VanderVeen, Hardee *et al.* 2017; Schmidt, Rohm *et al.* 2018) are known to influence muscle homeostasis.

Cachexia is a well-documented adverse effect of cancer that primarily targets skeletal muscle, as opposed to anorexia or starvation which typically affects adipose tissue (Porporato 2016). It is associated with severe muscle wasting, reduced physical function, reduced tolerance to anticancer therapy, and reduced survival in a variety of clinical populations (Tisdale 2002; Fearon, Strasser *et al.* 2011). Preclinical studies have begun to identified specific mechanisms not entirely explained by the muscle atrophy (Roberts, Frye *et al.* 2013) such as: decreased tetanic force, and specific tension, along with slowed contraction rates and increases in muscle fatigability (VanderVeen, Hardee *et al.* 2017); Roberts, Frye et al. 2013). These findings are consistent with observations of *ex vivo* muscle preparations extracted from cancer patients, e.g. decreases in

stiffness (relative stiffness–pCa$^{2+}$ relationship) and maximal force production per cross-sectional area, and a right-shift in Ca$^{2+}$ activation sensitivity across both MyHC type I and IIa (Ochala and Larsson 2008). While we did not observe overt alteration in peak muscle contraction force or rate of rise during electrically evoked twitch contractions or changes to the force-length relationships during physiologic stimuli, all of the above have the potential to contribute to alterations in mechanotransduction that we may not be able to detect from our whole muscle measures.

Chemotherapy also has the potential to influence certain aspects of muscle homeostasis (Sakai, Sagara *et al.* 2014; Sorensen, Petersen *et al.* 2017). Following oxaliplatin treatment histological analysis of pretibial flexors revealed significant leftward shift in the fiber size distribution, i.e. smaller cross-sectional area, whereas whole quadriceps muscle atrophy could be detected in as little as 5 days of cisplatin treatment (Sakai, Sagara *et al.* 2014). In addition, chemotherapy induces changes consistent with myopathy including accumulation of both Ca$^{2+}$ and lipids along with higher levels of collagen deposition present another challenge to canonical muscular architecture that could contribute to altered mechanotransduction.

While the previous discussion, centers on the independent effects of cancer and chemotherapy, the present work underscores the potential for combinatorial effects on different systems including motor physiology. This becomes credible since some effects of chemotherapy overlap those seen in cancer cachexia (Sakai, Sagara *et al.* 2014; Sorensen, Petersen *et al.* 2017). As an example, recent gene expression data suggest that changes in skeletal muscle induced by oxaliplatin may activate similar pathways to those activated during cancer cachexia (Feather, Lees *et al.* 2018). Recent preclinical data suggest even more explicit evidence of suspected interaction at a muscular systems level (Damrauer, Stadler *et al.* 2018) which is in agreement with our gross level

measure of muscle homeostasis (body weight as an analogue of muscle mass in Figure 39) that may help clarify some unexplained problems in clinical populations (Vichaya, Chiu *et al.* 2015; Vardy, Dhillon *et al.* 2016) and paucity of treatment approaches. Collectively, these results suggest that both cancer and chemotherapy treatment induced pathological changes to the muscular system may contribute to corrupt sensory encoding. Notably changes to the mechanical environment may help explain the as yet unknown cause of decreases in sensitivity (increases in threshold) for all mechanosensitive neurons studied (Aims 3, 4, and 6).

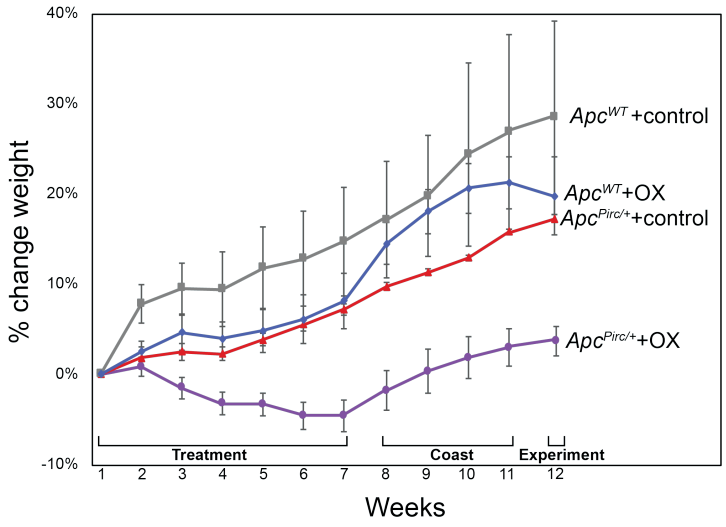


***Figure 39.***

**Longitudinal change in animal weight.** Longitudinal study of animal weights reveals systemic non-linear interaction of cancer and chemotherapy. a, Weekly weight measures tracking systemic effects of cancer and/or chemotherapy. Rats included were used for transcriptional, protein, and physiologic studies. Data are mean±s.d. from 15 $Apc^{WT}$+control, 10 $Apc^{WT}$+OX, 6 $Apc^{Pirc/+}$+control, and 8 $Apc^{Pirc/+}$+OX rats.

*Role of the Motoneurons in Decompensated Task Performance*

Despite having strong reason to suspect sensory encoding defects (Aim 3) are prominent players in preclinical (Aim 5) and clinical measures of decompensated task

performance and patient complaints (see Introduction), we have not established a causal link. This leaves the possibility of additional contributors. One prominent candidate is the motoneuron, the efferent component of sensorimotor behaviors. We recently identified the first evidence that chemotherapy chronically impairs firing behavior of spinal motoneurons (Housley, Nardelli *et al.* 2020 in revision). Data indicate that unstainable and unpredictable repetitive firing originates in the motoneurons central integrative components, possibly as a result of imbalance in the subthreshold currents that regulate firing.

Their erratic firing necessarily disturbs steady muscle contraction, motor performance and might lead to the development of movement disorders experienced by patients following chemotherapy (Bennett, Park *et al.* 2012; Tofthagen, Donovan *et al.* 2013). Specifically, effects on motoneurons could degrade task performance at two level. Motoneurons may act directly via altered neuromuscular control and/or indirectly by influencing sensory neuron encoding by altering the mechanical environment that sensory neurons operate in (discussed above). Direct influence of altered active neuromuscular control would be in addition to the potential corruption of intrinsic muscle homeostasis (discussed above). While previous reports have observed deficits consistent with motoneuron involvement, these studies utilized either indirect measures or focused on acute hyper-excitability which in both instances do not necessarily provide insight into the lasting signs and symptoms experienced by cancer survivors (Burakgazi, Messersmith *et al.* 2011; Tofthagen, Overcash *et al.* 2012; Kneis, Wehrle *et al.* 2016; Taleb, Bouzobra *et al.* 2017). In any event, motoneuron involvement would work to compound any effects induced independently from corrupt sensory encoding.

*Evidence for Codependency.*

For many studies, particularly those at the clinical level, decoupling chemotherapy-induced effects and those induced by cancer is difficult. As we have identified, no preclinical study has investigated the synergistic effect of the disease and chemotherapy for CIPN (Currie, Angel-Scott *et al.* 2018) with most opting to investigate each in isolation. Outside of CIPN, one preclinical study did examine fatigue-related behaviors in mice with Lewis Lung Carcinoma cell tumors (Wood, Nail *et al.* 2006) that received Etoposide a topoisomerase II inhibitor and member of the broadly family of alkaloid agents. Etoposide significantly reduced voluntary wheel running activity, an index of fatigue (Novak, Burghardt *et al.* 2012), above control with further reductions in activity noted in animals with tumors. Human studies only allow us to infer exacerbation of symptoms by chemotherapy on existing fatigue in cancer patients. For example, reduced muscle strength and function was observed in individuals with acute lymphoblastic leukemia diagnosis prior to treatment (Ness, Kaste *et al.* 2015). Symptoms worsened following chemotherapy treatment, which suggests a significant role of chemotherapy in the development of these symptoms. A recent large-scale observational study found increased fatigue in a cohort of individuals diagnosed with colorectal cancer that underwent chemotherapy treatment, as opposed to those that did not (Vardy, Dhillon *et al.* 2016). These few reports highlight the fact that little work has been done to investigate and test for the explicit role of interaction effects between cancer and chemotherapy in any side-effect of treatment or disease. Coupled with the abject failure of current treatment approaches for *chronic* CIPN, the above discussion underscores the importance of our findings and necessitate further study of these non-linear interactions and their effects on potential treatments.

*Mechanisms of Codependency*

We have now firmly established that codependent effects of chemotherapy and cancer exist at multiple levels of biological control, e.g. gene and protein expression, control neuron excitability, and behavioral performance, and that their interactions significantly exacerbate deficits at each level. We must now move to determine the underlying mechanisms (sites) of this interaction. More importantly, with the recognition that neither process is stationary with respect to time, e.g. development of cancer, accumulation of chemotherapy, and subsequent suppression of cancer, we must uncouple the temporal pattern by which these two systemic perturbations work together to influence pathophysiology of chronic CIPN (and likely other side effect that remain recalcitrant to treatment). Filling this gap in knowledge is needed to expose the most effective treatment targets or cures for chronic CIPN (Hershman, Lacchetti *et al.* 2014). Barriers to obtaining this information are formidable, given the overwhelming abundance and complexity of possible pathways identified by our multiscale approach. however, given the magnitude and multiple scales of dysregulation we observed leads us to suspect that codependent interactions may be mediated by high-levels of biological control. Such candidates include DNA methylation and hydroxymethylation, histone modification, e.g. acetylation and deacetylation and non-coding RNA regulation, e.g. miRNAs, all of which comprise global regulatory processes known as epigenetic phenomena. While it is clear that perturbation to epigenetic control may lead to alterations in gene expression which results in cellular transformation and ultimately cancer development (Lund and van Lohuizen 2004; Esteller 2008); it is less clear whether cancer itself can cause alterations to epigenetic control either directly or indirectly via systemic signaling pathways (inflammatory). Identifying the existence of such reciprocal relationships may be crucial to determine where feedback loops intersect with the known influences of chemotherapy

on epigenetic control in the nervous system of animals in preclinical study, e.g. increase H3 acetylation and decreased histone deacetylase activity (Briones and Woods 2011; Wang, Walitt *et al.* 2015). While the evidence is far from conclusive, we hypothesize that the administration of chemotherapy agents in the presence of systemic influence of cancer initiates a cascade of biological changes, with transient alterations in low levels of biological control, e.g. hyperexcitability: a positive acute effect observed throughout the nervous system and changes in inflammatory milieu that ultimately converge on high level epigenetic alterations that persist long after treatment cessation and disease free survival. These epigenetic changes would then lead to gene expression changes, altering metabolic activity and neuronal alterations that are responsible for generating clinically relevant *chronic* CIPN. Effects of epigenetic alterations may also help explain heterogeneity in patient populations. A recent study indicated a strong association between the strength of persistent methylation changes and developed persistent neuropsychological symptoms, whereas patients with preserved methylation status were protected from chronic symptoms (Lyon, Elmore *et al.* 2014).

Alternatively, lower levels of biologic control might be the center of codependent interactions between cancer and chemotherapy that ultimately result in exacerbated *chronic* neurologic deficits. Fortunately, our unbiased transcriptional analyses afforded some insight into this possibility. Our data point to changes in oxidative, inflammatory, and metabolic pathways as likely culprits. While previous studies suggest changes to systemic inflammatory milieu are transient (Wang, Walitt *et al.* 2015), our data point to both genetic (Aim 1) and protein (Aim 2) level pathway disruption that persists after treatment cessation. Differences may be attributable to divergence in experimental targets. Our preclinical studies afforded unique tissue specific focus on the sensory nervous system, while prior work was limited to experimental targets accessible in

clinical populations namely minimally invasive sampling from blood. Moreover, the expression of persistent changes in low levels of biologic control simply rules in their potential role and does not rule out the possibility that they emerge from high-level epigenetic alterations that this work cannot currently disentangle.

In summary, innumerable pathways and/or loci exist that could house interaction. It is tempting then to speculate where and when interactions are taking place; however, despite definitive evidence that clinically relevant sensory neuropathy is codependent on cancer and chemotherapy, it is futile to attempt to constrain possibilities at this time because we simply don't have adequate spatiotemporal resolution across the relevant tissue specific domains. That being said, we are hopeful that the trends in big data and powerful computational modeling, some of which we developed in this project, will coincide with the acquisition of the requisite data to answer this most fundamental question.

# Supplemental Tables

*Supplemental Table 1.*

**Supplemental Table 1.** Members of cluster C1a: n=350.

| | | | | |
|---|---|---|---|---|
| 1389043_at | 1371781_at | 1383860_at | 1371785_at | 1382059_at |
| 1369772_at | 1390519_at | 1387558_at | 1384260_at | 1377187_at |
| 1382074_at | 1388812_at | 1369885_at | 1367973_at | 1384147_at |
| 1367499_at | 1371550_at | 1373225_at | 1377340_at | 1387606_at |
| 1378552_at | 1387153_at | 1370023_at | 1393550_at | 1385180_at |
| 1389675_at | 1369352_at | 1374468_at | 1378925_at | 1376645_at |
| 1374806_at | 1367825_at | 1377210_at | 1379935_at | 1377387_a_at |
| 1367715_at | 1390535_at | 1373984_at | 1372520_at | 1377019_at |
| 1392107_at | 1387132_at | 1368353_at | 1372729_at | 1368473_at |
| 1369814_at | 1378005_at | 1372691_at | 1380229_at | 1393553_at |
| 1370928_at | 1371019_at | 1367712_at | 1397437_at | 1375041_at |
| 1374228_at | 1391543_at | 1385869_at | 1377103_at | 1374137_at |
| 1397916_s_at | 1375866_at | 1369191_at | 1391643_at | 1369035_a_at |
| 1376737_at | 1369012_at | 1393456_at | 1379311_at | 1376425_at |
| 1371529_at | 1378126_at | 1388944_at | 1380772_at | 1377380_at |
| 1384389_at | 1391095_at | 1393730_at | 1372211_at | 1383661_at |
| 1371697_at | 1392267_at | 1384294_at | 1371194_at | 1377310_at |
| 1385627_at | 1374626_at | 1388722_at | 1388587_at | 1392640_at |
| 1369778_at | 1372579_at | 1388924_at | 1387343_at | 1388666_at |
| 1373219_at | 1368489_at | 1373224_at | 1382351_at | 1375901_at |
| 1368370_at | 1367721_at | 1378800_at | 1391042_at | 1384993_at |
| 1380414_at | 1371237_a_at | 1376151_a_at | 1382379_at | 1394953_at |
| 1390571_at | 1388271_at | 1392818_at | 1396217_at | 1382275_at |

Supplemental Table 1 continued

| | | | | |
|---|---|---|---|---|
| 1388528_at | 1379910_at | 1369871_at | 1378440_at | 1384381_at |
| 1368585_at | 1398482_at | 1370051_at | 1393563_at | 1369738_s_at |
| 1374857_at | 1371644_at | 1368487_at | 1393316_at | 1382404_at |
| 1367938_at | 1370257_at | 1373623_at | 1372414_at | 1374422_at |
| 1375714_at | 1393728_at | 1376775_at | 1373554_at | 1368947_at |
| 1380972_at | 1376100_at | 1376144_at | 1387610_at | 1386181_at |
| 1371792_at | 1367741_at | 1380110_at | 1383935_at | 1368856_at |
| 1382527_at | 1383486_at | 1368224_at | 1369550_at | 1368527_at |
| 1369055_at | 1370080_at | 1372236_at | 1377768_at | 1370141_at |
| 1371824_at | 1374474_at | 1377049_at | 1388170_at | 1373035_at |
| 1387319_at | 1378420_at | 1381775_at | 1383354_a_at | 1371079_at |
| 1388858_at | 1382154_at | 1376891_at | 1391582_at | 1384507_at |
| 1374570_at | 1368266_at | 1373975_at | 1376628_at | 1373062_at |
| 1383993_at | 1387090_a_at | 1387050_s_at | 1369391_at | 1397848_at |
| 1373499_at | 1372599_at | 1373286_at | 1374911_at | 1374113_at |
| 1382950_at | 1372752_at | 1391026_at | 1373730_at | 1388672_at |
| 1372750_at | 1374758_at | 1386552_at | 1390391_at | 1371988_at |
| 1373421_at | 1392502_at | 1398706_at | 1386611_at | 1387995_a_at |
| 1368420_at | 1389742_at | 1383574_at | 1384063_at | 1388482_at |
| 1387868_at | 1385568_at | 1373989_at | 1377221_at | 1371974_at |
| 1387037_at | 1387769_a_at | 1397304_at | 1376204_at | 1377761_at |
| 1367940_at | 1371713_at | 1384968_at | 1376125_at | 1387959_at |
| 1390969_at | 1368645_at | 1368332_at | 1398455_at | 1388054_a_at |
| 1387202_at | 1386888_at | 1368014_at | 1389569_at | 1371040_at |
| 1389754_at | 1378196_at | 1368361_a_at | 1377688_at | 1389295_at |
| 1369737_at | 1382315_at | 1374473_at | 1387453_at | 1373310_at |

Supplemental Table 1 continued

| | | | | |
|---|---|---|---|---|
| 1376102_at | 1376648_at | 1373590_at | 1383489_at | 1370650_s_at |
| 1388149_at | 1369619_at | 1381923_at | 1370047_at | 1369496_at |
| 1382919_at | 1368892_at | 1369766_at | 1386870_at | 1388686_at |
| 1396163_at | 1376976_at | 1390943_at | 1386660_at | 1376867_at |
| 1376481_at | 1385450_at | 1387389_at | 1393331_at | 1367795_at |
| 1394160_at | 1373403_at | 1368921_a_at | 1382533_at | 1378074_at |
| 1392881_at | 1394047_at | 1393825_at | 1368924_at | 1397527_at |
| 1387759_s_at | 1393516_at | 1370773_a_at | 1368853_at | 1385753_at |
| 1370177_at | 1380318_at | 1369845_at | 1387824_at | 1387585_at |
| 1395765_at | 1369973_at | 1370406_a_at | 1369781_at | 1390801_at |
| 1392946_at | 1370445_at | 1385857_at | 1393480_at | 1380054_at |
| 1371450_at | 1370595_a_at | 1395789_at | 1383180_at | 1369222_at |
| 1370452_at | 1370606_at | 1398273_at | 1385217_at | 1390262_a_at |
| 1385827_at | 1379312_at | 1370781_a_at | 1368980_at | 1380611_at |
| 1388485_at | 1391808_at | 1395620_at | 1384950_at | 1369577_at |
| 1383655_at | 1368931_at | 1395840_at | 1378261_at | 1385808_at |
| 1368015_at | 1379500_at | 1368864_at | 1368941_at | 1368758_a_at |
| 1393477_at | 1387952_a_at | 1382199_at | 1395696_at | 1368962_at |
| 1383949_at | 1393105_at | 1386106_at | 1369421_at | 1370757_at |
| 1368254_a_at | 1383551_at | 1381611_at | 1369069_at | 1369428_a_at |
| 1389380_at | 1370624_at | 1371166_at | 1388233_at | |

*Supplemental Table 2.*

**Supplemental Table 2.** Members of cluster C2b: n=632.

| | | | | |
|---|---|---|---|---|
| 1395359_at | 1383849_at | 1379412_at | 1381958_at | 1367728_at |
| 1377617_at | 1376865_at | 1398217_at | 1384133_at | 1375396_at |
| 1385422_at | 1394079_at | 1378003_at | 1390983_at | 1369628_at |
| 1379338_at | 1385393_at | 1370260_at | 1388167_at | 1380062_at |
| 1393813_at | 1370932_at | 1379578_at | 1370432_at | 1379555_at |
| 1368939_a_at | 1395154_at | 1373566_at | 1387146_a_at | 1382118_at |
| 1396803_at | 1381115_at | 1384182_at | 1368080_at | 1382265_at |
| 1380144_at | 1394243_at | 1376967_at | 1389214_at | 1392840_at |
| 1393596_at | 1388000_at | 1371003_at | 1377923_at | 1397700_x_at |
| 1382312_at | 1383066_at | 1381021_at | 1367860_a_at | 1398716_at |
| 1391689_at | 1391305_at | 1380172_at | 1373432_at | 1396141_at |
| 1383334_at | 1395714_at | 1394347_at | 1394574_at | 1379715_at |
| 1390486_at | 1368858_at | 1375523_at | 1388101_at | 1369044_a_at |
| 1394972_at | 1376194_at | 1369742_at | 1372668_at | 1391758_at |
| 1392738_at | 1383811_at | 1382064_at | 1392166_at | 1368411_a_at |
| 1380475_at | 1385431_at | 1380371_at | 1395535_at | 1380730_at |
| 1377906_at | 1368825_at | 1394746_at | 1386089_at | 1369678_a_at |
| 1395100_at | 1370114_a_at | 1376725_at | 1370948_a_at | 1391838_at |
| 1390706_at | 1375542_at | 1390813_at | 1393702_at | 1397201_at |
| 1395923_at | 1384648_at | 1383053_x_at | 1379485_at | 1384355_at |
| 1396207_at | 1384812_at | 1383455_at | 1382620_at | 1380063_at |
| 1383786_at | 1374780_at | 1370935_at | 1384573_at | 1397241_at |
| 1379615_at | 1391598_at | 1392249_at | 1376299_at | 1395358_at |
| 1397335_at | 1382812_at | 1391170_at | 1387964_a_at | 1382565_at |
| 1381394_at | 1382171_at | 1374803_at | 1378775_at | 1394699_at |

Supplemental Table 2 continued

| | | | | |
|---|---|---|---|---|
| 1396676_at | 1391906_at | 1374708_at | 1390136_at | 1375640_at |
| 1384728_at | 1382658_at | 1374144_at | 1383240_at | 1395201_at |
| 1387406_at | 1393418_at | 1376170_at | 1393368_at | 1374448_at |
| 1397505_at | 1370955_at | 1385887_at | 1391139_at | 1368514_at |
| 1393866_at | 1397851_at | 1387854_at | 1368993_at | 1395794_at |
| 1397573_at | 1392566_at | 1367563_at | 1393576_at | 1373676_at |
| 1392269_at | 1376770_at | 1389546_at | 1390423_at | 1398387_at |
| 1382286_at | 1376733_at | 1373648_at | 1370831_at | 1371518_at |
| 1380195_at | 1394985_at | 1390404_at | 1392799_at | 1398354_at |
| 1389894_at | 1396612_at | 1372758_at | 1372480_at | 1392935_at |
| 1389986_at | 1385087_at | 1375138_at | 1379755_at | 1372101_at |
| 1395092_at | 1376208_at | 1387024_at | 1383827_at | 1373151_at |
| 1381967_at | 1369093_at | 1393663_at | 1385243_at | 1389003_at |
| 1369159_at | 1395105_at | 1387767_a_at | 1386979_at | 1388592_at |
| 1390277_at | 1371361_at | 1372440_at | 1390480_at | 1391556_at |
| 1392730_at | 1368087_a_at | 1390429_at | 1388742_at | 1390411_at |
| 1390340_a_at | 1370946_at | 1388392_at | 1370907_at | 1387040_at |
| 1375739_at | 1377753_at | 1388618_at | 1371430_at | 1398258_at |
| 1391285_at | 1376313_at | 1387897_at | 1373521_at | 1389157_at |
| 1380696_at | 1383013_at | 1375862_at | 1370302_at | 1373122_at |
| 1397666_at | 1389441_at | 1377821_at | 1387112_at | 1373130_at |
| 1369810_at | 1390728_at | 1391848_at | 1374216_at | 1382108_at |
| 1390655_at | 1367968_at | 1390569_at | 1375726_at | 1392597_at |
| 1398125_at | 1375857_at | 1389306_at | 1389711_at | 1382732_at |
| 1382920_at | 1385779_at | 1374535_at | 1376700_at | 1387313_at |
| 1394392_at | 1383222_at | 1384792_at | 1379444_at | 1370956_at |
| 1381644_at | 1374241_at | 1370950_at | 1398362_at | 1370895_at |

Supplemental Table 2 continued

| | | | | |
|---|---|---|---|---|
| 1375266_at | 1372643_at | 1384386_at | 1382524_at | 1374974_at |
| 1368202_a_at | 1379345_at | 1382561_at | 1374283_at | 1385202_at |
| 1391448_at | 1369955_at | 1396255_at | 1378544_at | 1374546_at |
| 1388557_at | 1370951_at | 1395251_at | 1388157_at | 1389562_at |
| 1368671_at | 1368989_at | 1396154_at | 1375444_at | 1374171_at |
| 1380133_at | 1395590_at | 1380363_at | 1373759_at | 1373658_at |
| 1371847_at | 1368388_at | 1384639_at | 1387260_at | 1375030_at |
| 1373538_at | 1372926_at | 1393606_at | 1397884_at | 1385367_at |
| 1391012_at | 1393933_at | 1371173_a_at | 1386935_at | 1372479_at |
| 1375709_at | 1395157_at | 1373358_at | 1368453_at | 1387094_at |
| 1389553_at | 1385191_at | 1369172_at | 1379803_at | 1390159_at |
| 1384707_at | 1385493_at | 1397525_at | 1371104_at | 1390300_at |
| 1371394_x_at | 1379822_at | 1397164_at | 1387793_at | 1379568_at |
| 1385527_at | 1392178_at | 1377445_at | 1375214_at | 1392157_at |
| 1367971_at | 1371186_at | 1369248_a_at | 1375531_at | 1368542_at |
| 1390738_at | 1393558_at | 1385364_at | 1393433_at | 1382914_at |
| 1367517_at | 1385825_at | 1375721_at | 1393860_at | 1389763_at |
| 1393808_at | 1370693_a_at | 1393198_at | 1385641_at | 1391167_at |
| 1382691_at | 1379516_at | 1379397_at | 1398591_at | 1372069_at |
| 1372110_at | 1370032_at | 1395799_at | 1398256_at | 1392785_at |
| 1386943_at | 1386041_a_at | 1369323_at | 1368290_at | 1387454_at |
| 1368090_at | 1395721_at | 1382478_at | 1375043_at | 1384841_at |
| 1371310_s_at | 1388034_at | 1378666_at | 1372389_at | 1392587_at |
| 1373911_at | 1387367_at | 1393910_at | 1386995_at | 1386026_at |
| 1370155_at | 1397983_at | 1387563_at | 1368321_at | 1382134_at |
| 1388422_at | 1371069_at | 1387998_at | 1373401_at | 1382535_at |
| 1368861_a_at | 1387760_a_at | 1368589_at | 1387060_at | 1368728_at |

Supplemental Table 2 continued

| | | | | |
|---|---|---|---|---|
| 1382599_at | 1377781_at | 1380825_at | 1394837_at | 1398020_at |
| 1384617_at | 1384513_at | 1378548_at | 1384890_at | 1382068_at |
| 1389235_at | 1376129_at | 1378628_at | 1396450_at | 1393594_at |
| 1373544_at | 1390351_at | 1398130_at | 1391523_at | 1395030_at |
| 1386947_at | 1377651_at | 1385156_at | 1394416_at | 1397453_at |
| 1392929_at | 1375538_at | 1384692_at | 1375468_at | 1375782_at |
| 1381449_s_at | 1379506_at | 1376388_at | 1382847_at | 1393674_at |
| 1382454_at | 1394834_at | 1380701_at | 1368242_at | 1395264_at |
| 1368146_at | 1381817_at | 1393995_at | 1377151_at | 1381121_at |
| 1387450_at | 1391552_at | 1390302_at | 1396952_at | 1397690_at |
| 1386811_at | 1380685_at | 1392311_at | 1376742_at | 1373972_at |
| 1376569_at | 1385889_at | 1395436_at | 1391863_at | 1389104_s_at |
| 1389974_at | 1390942_at | 1397120_at | 1390733_at | 1394467_at |
| 1376463_at | 1390077_at | 1395130_at | 1371776_at | 1380693_at |
| 1395744_at | 1394727_at | 1396773_at | 1390100_s_at | 1397999_at |
| 1394891_at | 1379511_at | 1378486_at | 1396502_at | 1378062_at |
| 1379763_at | 1398528_at | 1379722_at | 1380738_at | 1391304_at |
| 1377629_at | 1381402_at | 1392650_at | 1377589_at | 1375577_at |
| 1386064_at | 1392182_at | 1377305_at | 1396066_at | 1395365_at |
| 1386707_at | 1380777_at | 1382951_at | 1380882_at | 1397786_at |
| 1379058_at | 1378745_at | 1377212_at | 1392055_at | 1395205_at |
| 1381175_at | 1376531_at | 1397608_at | 1393548_at | 1376938_at |
| 1382413_at | 1390743_at | 1378682_at | 1378161_at | 1378814_at |
| 1390723_at | 1396894_at | 1382911_at | 1371771_at | 1398225_at |
| 1392555_at | 1395521_at | 1397422_at | 1383214_at | 1396775_at |
| 1389996_at | 1382020_at | 1396877_at | 1379089_at | 1396135_at |
| 1398445_at | 1394330_at | 1396957_at | 1390345_at | 1381253_at |

Supplemental Table 2 continued

| | | | | |
|---|---|---|---|---|
| 1368841_at | 1384969_at | 1380154_at | 1385164_at | 1379150_at |
| 1395460_at | 1380168_at | 1381668_at | 1381133_at | 1377377_at |
| 1392026_at | 1368320_at | 1379815_at | 1383479_at | 1380087_at |
| 1376667_at | 1383982_at | 1370991_at | 1394848_at | 1374263_at |
| 1376917_at | 1394714_at | 1391975_at | 1376524_at | 1392368_at |
| 1394778_at | 1391701_at | 1386102_at | 1393029_at | 1395335_at |
| 1387350_at | 1397673_at | 1378099_at | 1385091_at | 1390320_at |
| 1389908_at | 1375449_at | 1395249_at | 1397004_at | 1396965_at |
| 1380541_at | 1384380_at | 1393879_at | 1379594_at | 1397624_at |
| 1376138_at | 1382749_at | 1381125_at | 1375689_at | 1382982_at |
| 1376096_a_at | 1391160_at | 1391841_at | 1392846_at | 1392017_at |
| 1376750_at | 1388604_at | 1397692_at | 1396252_at | 1390671_at |
| 1382229_at | 1377045_at | 1381646_at | 1396850_at | 1391579_at |
| 1379779_at | 1393662_at | 1395772_at | 1385177_at | 1375217_at |
| 1381489_at | 1384146_at | 1397153_at | 1378604_at | 1377208_at |
| 1385453_at | 1392704_at | 1396254_at | 1373534_at | 1391196_at |
| 1381985_at | 1393692_at | 1374786_at | 1378038_at | 1394729_at |
| 1372911_at | 1380097_at | 1378367_at | 1395728_at | 1380940_at |
| 1375767_at | 1368887_at | 1377919_at | 1394283_at | |
| 1391209_at | 1379753_at | 1381472_at | 1397217_at | |
| 1379936_at | 1398131_at | 1396791_at | 1381210_at | |

*Supplemental Table 3.*

**Supplemental Table 3.** Members of cluster C2a: n=636.

| | | | | |
|---|---|---|---|---|
| 1396348_at | 1380050_at | 1382027_at | 1385608_at | 1368154_at |
| 1385668_at | 1374572_at | 1384724_at | 1374565_at | 1370097_a_at |
| 1389172_at | 1377169_at | 1373661_a_at | 1389232_at | 1387093_at |
| 1379971_at | 1386881_at | 1389244_x_at | 1378252_at | 1370333_a_at |
| 1397317_at | 1392234_at | 1390406_at | 1383218_at | 1392569_at |
| 1384996_at | 1380267_at | 1376285_at | 1384971_at | 1388469_at |
| 1381732_at | 1395204_at | 1384515_at | 1382252_at | 1374016_at |
| 1374043_at | 1388725_at | 1389720_at | 1373374_at | 1373725_at |
| 1380941_at | 1393641_at | 1385432_at | 1375654_at | 1373288_at |
| 1386059_at | 1392722_at | 1392521_at | 1376368_at | 1370048_at |
| 1367902_at | 1389697_at | 1389918_at | 1398360_at | 1377353_a_at |
| 1389734_x_at | 1383008_at | 1374615_at | 1388425_at | 1372042_at |
| 1389413_at | 1393552_x_at | 1380312_at | 1375905_at | 1371942_at |
| 1391637_at | 1381902_at | 1377792_at | 1371150_at | 1368344_at |
| 1382173_at | 1387571_at | 1383453_at | 1382072_at | 1376688_a_at |
| 1373740_at | 1382296_at | 1393806_at | 1385200_at | 1368474_at |
| 1398732_at | 1376036_at | 1379075_at | 1393398_at | 1388426_at |
| 1397610_at | 1385252_at | 1384420_at | 1398661_at | 1377637_at |
| 1373748_at | 1378094_at | 1376263_at | 1393012_at | 1393336_at |
| 1385275_at | 1379688_at | 1384864_at | 1379281_at | 1382613_at |
| 1379766_at | 1384392_at | 1382096_at | 1373210_at | 1367922_at |
| 1383020_at | 1397808_at | 1371643_at | 1392971_at | 1377156_at |
| 1389034_at | 1390148_a_at | 1372966_at | 1391911_at | 1377946_at |
| 1379253_at | 1370391_at | 1398578_at | 1373017_at | 1395819_at |
| 1395439_at | 1384869_at | 1374871_at | 1393460_at | 1396833_at |

Supplemental Table 3 continued

| | | | | |
|---|---|---|---|---|
| 1392972_at | 1393228_at | 1384535_at | 1383058_at | 1370414_at |
| 1390436_at | 1375622_at | 1377632_at | 1380387_at | 1370531_a_at |
| 1389586_at | 1391447_at | 1372125_at | 1388569_at | 1397511_at |
| 1392943_at | 1374652_at | 1396383_at | 1376344_at | 1385051_at |
| 1394761_at | 1381190_at | 1395472_at | 1389617_at | 1398250_at |
| 1396009_at | 1388745_at | 1395644_at | 1384310_at | 1392118_at |
| 1376082_at | 1389648_at | 1373659_at | 1379200_at | 1385692_at |
| 1389305_at | 1373270_at | 1368919_at | 1394033_at | 1388385_at |
| 1389229_at | 1384211_at | 1393876_at | 1393691_at | 1367887_at |
| 1374874_at | 1374746_at | 1389612_at | 1390881_at | 1382525_at |
| 1372294_at | 1388949_at | 1383414_at | 1371015_at | 1372672_at |
| 1376105_at | 1373410_at | 1378397_at | 1388298_at | 1372213_at |
| 1382630_at | 1376575_at | 1392928_at | 1388211_s_at | 1383743_at |
| 1378645_at | 1376674_at | 1380822_at | 1368930_at | 1377392_at |
| 1376868_at | 1378049_at | 1390037_at | 1391383_at | 1399019_at |
| 1383840_at | 1393345_at | 1384699_at | 1368381_at | 1384505_at |
| 1384940_at | 1393226_at | 1380810_at | 1396316_at | 1381574_at |
| 1380091_at | 1382458_at | 1381208_at | 1370024_at | 1373903_at |
| 1385798_at | 1391904_at | 1392170_at | 1379374_at | 1370235_at |
| 1375984_at | 1393575_at | 1373484_at | 1390964_at | 1374908_at |
| 1382084_at | 1395410_at | 1383439_at | 1374475_at | 1389221_at |
| 1375001_at | 1376785_at | 1371530_at | 1396001_at | 1386718_at |
| 1379347_at | 1381131_at | 1394678_at | 1378324_at | 1398255_at |
| 1370420_at | 1381591_at | 1383920_at | 1370823_at | 1377375_at |
| 1389705_at | 1383197_at | 1384081_at | 1389622_at | 1393028_at |
| 1377342_s_at | 1382882_x_at | 1395126_at | 1371052_at | 1368674_at |
| 1367989_at | 1367659_s_at | 1374403_at | 1368587_at | 1377455_at |

Supplemental Table 3 continued

| | | | | |
|---|---|---|---|---|
| 1388876_at | 1378601_at | 1376028_at | 1384709_at | 1384178_at |
| 1392215_at | 1379614_at | 1379948_at | 1395000_at | 1382558_at |
| 1368554_at | 1397343_at | 1375369_at | 1390459_at | 1394497_at |
| 1383546_at | 1379669_at | 1372775_at | 1397246_at | 1368703_at |
| 1382358_at | 1379824_at | 1382976_at | 1371363_at | 1380471_at |
| 1377878_at | 1378480_at | 1379300_at | 1380459_at | 1380045_at |
| 1397652_at | 1374104_at | 1380027_at | 1377064_at | 1371429_at |
| 1383225_at | 1375990_a_at | 1391117_at | 1376045_at | 1385912_at |
| 1390283_at | 1370657_at | 1389132_at | 1378878_at | 1374558_at |
| 1370157_at | 1375983_at | 1390940_at | 1382190_at | 1378164_at |
| 1374762_at | 1380577_at | 1395353_at | 1370845_at | 1376878_at |
| 1373908_at | 1368008_at | 1370833_at | 1380563_at | 1375658_at |
| 1370310_at | 1372587_at | 1378155_at | 1390518_at | 1380228_at |
| 1389161_at | 1369133_a_at | 1375305_at | 1369944_at | 1375231_a_at |
| 1370068_at | 1382276_at | 1397194_at | 1388939_at | 1392595_at |
| 1374496_at | 1377914_at | 1394964_at | 1385333_at | 1378048_at |
| 1390138_at | 1376779_at | 1385981_at | 1368005_at | 1387111_at |
| 1373696_at | 1389999_at | 1378409_at | 1368322_at | 1369751_at |
| 1378320_at | 1392932_at | 1370307_at | 1367562_at | 1385876_at |
| 1370530_a_at | 1393491_at | 1398251_a_at | 1380142_at | 1389324_at |
| 1367811_at | 1377908_at | 1391803_at | 1369135_at | 1371045_at |
| 1383086_at | 1389995_at | 1382510_at | 1380248_at | 1368339_at |
| 1376084_a_at | 1379469_at | 1376771_at | 1388116_at | 1376998_a_at |
| 1398453_at | 1367844_at | 1379370_at | 1368612_at | 1376240_at |
| 1384273_at | 1376516_at | 1383284_at | 1379997_at | 1374200_at |
| 1383721_at | 1398351_at | 1385006_at | 1386833_at | 1378802_at |
| 1373818_at | 1376355_at | 1392915_at | 1394375_x_at | 1370106_at |

Supplemental Table 3 continued

| | | | | |
|---|---|---|---|---|
| 1391618_at | 1368555_at | 1387470_at | 1386261_x_at | 1395184_at |
| 1373161_at | 1380088_at | 1393356_at | 1389404_at | 1373065_at |
| 1393974_at | 1380616_at | 1385248_a_at | 1374530_at | 1372585_at |
| 1377840_at | 1384127_at | 1383263_at | 1367700_at | 1373596_at |
| 1371352_at | 1373881_at | 1393210_at | 1370960_at | 1377452_at |
| 1380175_at | 1375247_at | 1367631_at | 1376398_at | 1367939_at |
| 1376063_at | 1387789_at | 1372615_at | 1382905_at | 1373000_at |
| 1368295_at | 1368563_at | 1392510_at | 1383852_at | 1397548_at |
| 1379677_at | 1393259_at | 1372647_at | 1388920_at | 1371475_at |
| 1380405_at | 1389490_at | 1373175_at | 1387348_at | 1393330_at |
| 1387164_at | 1389059_at | 1368380_at | 1389662_at | 1389873_at |
| 1375660_at | 1387323_at | 1369633_at | 1386901_at | 1372297_at |
| 1374257_at | 1368047_at | 1372818_at | 1370816_at | 1377239_at |
| 1373642_at | 1371595_at | 1374273_at | 1379057_at | 1374544_at |
| 1370334_at | 1387655_at | 1375638_at | 1374444_at | 1372870_at |
| 1377943_at | 1382278_at | 1384770_at | 1375856_at | 1386128_at |
| 1388511_at | 1381498_at | 1383946_at | 1382050_at | 1368558_s_at |
| 1389475_at | 1392741_at | 1388176_at | 1396150_at | 1390914_at |
| 1370959_at | 1396152_s_at | 1376708_at | 1370019_at | 1367850_at |
| 1371924_at | 1388201_at | 1376937_at | 1372273_at | 1372305_at |
| 1386899_at | 1381179_at | 1368533_at | 1368170_at | 1373032_at |
| 1392672_at | 1370166_at | 1388880_at | 1372111_at | 1374527_at |
| 1394451_at | 1370131_at | 1379379_at | 1386911_at | 1393227_at |
| 1373240_at | 1393281_at | 1382078_at | 1371815_at | 1389649_at |
| 1372070_at | 1389905_at | 1377642_at | 1373348_at | 1382825_at |
| 1387886_at | 1389423_at | 1375962_at | 1376394_at | 1368270_at |
| 1395003_at | 1369181_at | 1390800_a_at | 1370982_at | 1383189_at |

Supplemental Table 3 continued

| | | | | |
|---|---|---|---|---|
| 1373523_at | 1393249_at | 1367679_at | 1379344_at | 1374247_at |
| 1368482_at | 1379760_at | 1370882_at | 1385047_x_at | 1382184_at |
| 1370987_at | 1397958_at | 1392074_at | 1393109_at | 1384298_at |
| 1384837_at | 1387113_at | 1382531_at | 1376047_at | 1393038_at |
| 1368463_at | 1370516_at | 1379295_at | 1373829_at | 1369725_at |
| 1385213_at | 1381311_at | 1390798_at | 1388784_at | 1373785_at |
| 1392515_at | 1370382_at | 1367912_at | 1382692_at | 1392813_at |
| 1389696_at | 1385465_at | 1397736_at | 1376457_at | 1383658_at |
| 1398467_at | 1389123_at | 1385572_at | 1388730_at | 1390849_at |
| 1393387_at | 1398304_at | 1383708_at | 1370449_at | 1384195_at |
| 1394766_at | 1372299_at | 1389783_s_at | 1370301_at | 1392965_a_at |
| 1388164_at | 1387029_at | 1393688_at | 1391812_at | 1374730_at |
| 1391067_at | 1370883_at | 1372200_at | 1387022_at | 1385682_at |
| 1379404_at | 1370383_s_at | 1398246_s_at | 1370864_at | 1391630_at |
| 1398407_at | 1389006_at | 1370202_at | 1387922_at | 1390510_at |
| 1392655_at | 1373575_at | 1367791_at | 1386912_at | 1371913_at |
| 1377835_at | 1371033_at | 1391977_at | 1389403_at | 1381145_at |
| 1385832_s_at | 1368006_at | 1372029_at | 1391341_at | 1368395_at |
| 1373490_at | 1370822_at | 1368027_at | 1378720_at | |
| 1378193_at | 1390420_at | 1380894_at | 1390348_at | |
| 1374778_at | 1387947_at | 1367749_at | 1385978_at | |
| 1373164_at | 1370154_at | 1373932_at | 1392265_s_at | |

*Supplemental Table 4*

**Supplemental Table 4.** Members of cluster C2c: n=570.

| | | | | |
|---|---|---|---|---|
| 1370949_at | 1391719_at | 1378595_at | 1382308_at | 1381229_at |
| 1384394_at | 1379664_at | 1391794_at | 1395836_at | 1393454_at |
| 1382307_at | 1393564_at | 1392854_at | 1377232_at | 1384509_s_at |
| 1391625_at | 1391416_at | 1398846_at | 1377427_at | 1384766_a_at |
| 1379571_at | 1397535_at | 1392054_at | 1395064_at | 1381410_a_at |
| 1393836_at | 1387199_a_at | 1390704_at | 1394935_at | 1381821_at |
| 1397362_at | 1383063_a_at | 1379232_at | 1378303_at | 1376843_at |
| 1383825_at | 1370607_a_at | 1394784_at | 1376996_at | 1381075_at |
| 1371093_at | 1374463_at | 1377816_at | 1376256_at | 1395762_at |
| 1390398_at | 1383044_at | 1377105_at | 1391852_at | 1395136_at |
| 1379101_at | 1382775_at | 1379130_at | 1384809_at | 1393613_at |
| 1373347_at | 1380069_at | 1380314_at | 1384240_at | 1383194_a_at |
| 1368725_at | 1376562_at | 1376739_at | 1390463_at | 1374350_at |
| 1381850_at | 1394961_at | 1395616_at | 1384335_at | 1385163_at |
| 1375459_at | 1372542_at | 1385041_at | 1385102_at | 1375486_at |
| 1391430_at | 1382130_at | 1381809_at | 1385101_a_at | 1397889_at |
| 1378965_at | 1367652_at | 1385931_at | 1394474_at | 1381515_at |
| 1393795_at | 1396036_at | 1384293_at | 1376490_at | 1383829_at |
| 1384376_at | 1394504_at | 1380981_at | 1393735_at | 1375532_at |
| 1377457_a_at | 1383075_at | 1386525_at | 1395336_at | 1385923_at |
| 1390710_x_at | 1392523_at | 1398483_at | 1384484_at | 1380744_at |
| 1383054_at | 1374593_at | 1389868_at | 1389972_at | 1391222_at |
| 1368401_at | 1379409_at | 1392902_at | 1388015_at | 1393189_at |
| 1369679_a_at | 1390426_at | 1368867_at | 1377556_at | 1398595_at |
| 1375174_at | 1382952_at | 1393881_at | 1382262_at | 1395222_at |

Supplemental Table 4 continued

| | | | | |
|---|---|---|---|---|
| 1391128_at | 1391979_at | 1392231_at | 1380783_at | 1378962_at |
| 1370387_at | 1395333_at | 1377090_at | 1397373_at | 1380325_at |
| 1396437_at | 1375358_at | 1374320_at | 1368255_at | 1384311_at |
| 1383266_at | 1375011_at | 1374779_at | 1381063_at | 1377172_at |
| 1385157_at | 1370072_at | 1380600_at | 1369681_at | 1392144_at |
| 1380446_at | 1370465_at | 1385525_at | 1395395_at | 1385017_at |
| 1377774_at | 1382211_at | 1387154_at | 1391549_at | 1393804_at |
| 1389554_at | 1374676_at | 1379387_at | 1385773_at | 1379077_at |
| 1388999_at | 1393811_at | 1384180_at | 1385974_at | 1375582_at |
| 1383127_at | 1393777_at | 1379055_x_at | 1390797_at | 1372000_at |
| 1396550_at | 1375350_at | 1377051_at | 1376836_at | 1384542_at |
| 1379912_at | 1398500_at | 1383932_at | 1370090_at | 1398582_at |
| 1385638_at | 1370145_at | 1389601_at | 1383064_at | 1378493_at |
| 1378389_at | 1373666_at | 1383644_at | 1391711_at | 1382614_at |
| 1373463_at | 1376610_a_at | 1371483_at | 1394401_at | 1391474_at |
| 1368770_at | 1391428_at | 1377308_a_at | 1392040_at | 1383145_at |
| 1383527_at | 1390687_at | 1377266_at | 1395076_at | 1397779_at |
| 1376755_at | 1370205_at | 1372002_at | 1390777_at | 1380699_at |
| 1370678_s_at | 1368221_at | 1383353_at | 1393901_at | 1377974_at |
| 1383199_at | 1377640_at | 1393589_at | 1370043_at | 1390866_at |
| 1393672_at | 1390782_at | 1387349_at | 1385215_at | 1382913_at |
| 1382452_at | 1371951_at | 1377857_at | 1384181_at | 1384048_at |
| 1392842_at | 1369156_at | 1382301_at | 1378509_at | 1392717_at |
| 1372814_at | 1389632_at | 1385972_at | 1391935_at | 1370570_at |
| 1382776_at | 1368691_at | 1396696_at | 1379062_at | 1369215_a_at |
| 1379724_at | 1398727_at | 1383343_at | 1382705_at | 1378282_at |
| 1384250_a_at | 1377934_at | 1383795_at | 1380523_at | 1392051_at |

Supplemental Table 4 continued

| | | | | |
|---|---|---|---|---|
| 1375785_at | 1397531_at | 1394425_at | 1380824_at | 1384857_at |
| 1387204_at | 1379872_at | 1379416_at | 1370085_at | 1382368_at |
| 1384610_at | 1393622_at | 1376933_at | 1384587_at | 1394436_at |
| 1393505_x_at | 1398440_at | 1385227_at | 1390592_at | 1385108_at |
| 1383219_at | 1393582_at | 1377072_at | 1389998_at | 1394010_at |
| 1394483_at | 1392864_at | 1392660_at | 1394849_at | 1380545_at |
| 1391524_at | 1378624_at | 1395986_at | 1380547_at | 1379645_at |
| 1375469_at | 1376627_at | 1380937_at | 1392453_at | 1375552_at |
| 1380763_at | 1382489_at | 1379286_at | 1391089_at | 1379544_at |
| 1383615_a_at | 1376685_at | 1385519_at | 1373494_at | 1370035_at |
| 1379221_at | 1390858_at | 1389989_at | 1389116_at | 1367884_at |
| 1394578_at | 1391757_at | 1371679_at | 1368824_at | 1375524_at |
| 1382960_at | 1397630_at | 1370830_at | 1379733_at | 1391438_at |
| 1373773_at | 1383726_at | 1377029_at | 1395075_at | 1390048_at |
| 1396225_at | 1377345_at | 1397676_at | 1391297_at | 1370176_at |
| 1394654_at | 1390757_at | 1382268_at | 1392653_at | 1379509_at |
| 1392245_at | 1392806_at | 1378457_at | 1370267_at | 1374066_at |
| 1376744_at | 1374246_at | 1384125_at | 1387165_at | 1370262_at |
| 1391594_at | 1395015_at | 1390266_at | 1368842_at | 1392180_at |
| 1389444_at | 1375763_at | 1398420_at | 1377070_at | 1384759_at |
| 1385350_at | 1383253_at | 1391439_at | 1368958_at | 1381048_at |
| 1382584_at | 1392715_at | 1397179_at | 1390184_at | 1376080_at |
| 1379866_at | 1393643_at | 1392764_at | 1391743_at | 1377526_at |
| 1382898_at | 1385953_at | 1383112_at | 1376419_at | 1379941_at |
| 1384164_at | 1392592_at | 1390506_at | 1375723_at | 1383069_at |
| 1376619_at | 1392198_at | 1374909_at | 1383052_a_at | 1375545_at |
| 1381296_at | 1384115_at | 1393981_at | 1390871_at | 1379313_at |

Supplemental Table 4 continued

| | | | | |
|---|---|---|---|---|
| 1384948_at | 1378325_at | 1378740_at | 1391687_at | 1394493_at |
| 1375278_at | 1398544_at | 1395021_at | 1382939_at | 1395318_at |
| 1382303_at | 1370052_at | 1379886_at | 1378413_at | 1380525_at |
| 1377111_at | 1389957_at | 1385044_at | 1375426_a_at | 1384804_at |
| 1379140_at | 1379398_at | 1389442_at | 1390443_at | 1394576_at |
| 1375119_at | 1391576_at | 1386063_at | 1375303_at | 1383833_at |
| 1369735_at | 1390923_a_at | 1368933_at | 1397286_at | 1397959_at |
| 1397632_at | 1382226_at | 1382551_at | 1378255_at | 1394422_at |
| 1380503_at | 1375699_at | 1376654_at | 1384609_a_at | 1391405_at |
| 1379804_at | 1375259_at | 1391770_at | 1396403_at | 1379603_at |
| 1397552_at | 1392666_at | 1394756_at | 1375215_x_at | 1383632_at |
| 1375453_at | 1380143_at | 1381471_at | 1384339_s_at | 1376523_at |
| 1379461_at | 1382654_at | 1381753_at | 1367958_at | 1388108_at |
| 1391600_at | 1377881_at | 1392675_at | 1382382_at | 1385552_at |
| 1375378_at | 1382953_at | 1382313_at | 1391075_at | 1377513_at |
| 1395711_at | 1379423_at | 1385903_at | 1381100_at | 1388866_at |
| 1396470_at | 1382778_at | 1382258_at | 1385240_at | 1388710_at |
| 1379103_at | 1385888_at | 1385925_at | 1387233_at | 1391436_at |
| 1368871_at | 1375612_at | 1379107_at | 1376853_at | 1379719_at |
| 1375212_at | 1379535_at | 1376226_at | 1375703_at | 1377686_at |
| 1376533_at | 1390467_at | 1379112_at | 1376436_at | 1375343_at |
| 1370063_at | 1382291_at | 1389840_at | 1376644_at | 1380552_at |
| 1370512_at | 1390347_at | 1391968_at | 1383296_a_at | 1378269_at |
| 1392441_at | 1370221_at | 1370810_at | 1378581_at | 1370089_at |
| 1372812_at | 1378453_at | 1371005_at | 1378368_at | 1384478_at |
| 1389836_a_at | 1373497_at | 1391855_at | 1380406_at | 1393585_at |
| 1371202_a_at | 1393752_at | 1375724_at | 1389761_at | 1371024_at |

Supplemental Table 4 continued

| | | | | |
|---|---|---|---|---|
| 1392044_at | 1369404_a_at | 1376848_at | 1369957_at | 1371034_at |
| 1394626_at | 1379126_at | 1384168_at | 1376623_at | 1395255_at |
| 1369654_at | 1398739_at | 1381167_at | 1371541_at | 1371281_at |
| 1378610_at | 1369499_at | 1394824_at | 1393167_at | 1392295_a_at |
| 1396256_at | 1391569_at | 1395361_at | 1398649_at | 1392607_at |
| 1383552_at | 1391187_at | 1369756_a_at | 1385354_at | 1390097_at |
| 1393661_at | 1377508_at | 1379492_at | 1371472_at | 1392582_at |
| 1398202_at | 1395546_at | 1388527_at | 1377675_at | 1378904_at |

*Supplemental Table 5*

**Supplemental Table 5.** Members of cluster C1b: n=313.

| | | | | |
|---|---|---|---|---|
| 1376872_at | 1393283_at | 1368720_at | 1389500_at | 1378539_at |
| 1384393_at | 1393547_at | 1383879_at | 1387951_at | 1387179_at |
| 1382682_at | 1383846_at | 1368311_at | 1391707_at | 1387269_s_at |
| 1375999_at | 1368059_at | 1377453_at | 1371162_at | 1396206_at |
| 1393952_at | 1370361_at | 1383853_at | 1378498_at | 1389177_at |
| 1372004_at | 1387766_a_at | 1368400_at | 1370139_a_at | 1394710_at |
| 1393157_at | 1390912_at | 1371536_at | 1392531_at | 1384034_at |
| 1385559_at | 1390707_at | 1368622_at | 1390828_at | 1368789_at |
| 1389507_at | 1370450_at | 1388663_at | 1380460_at | 1383797_a_at |
| 1378120_at | 1388802_at | 1368085_at | 1371243_at | 1387369_at |
| 1368358_a_at | 1384921_at | 1383692_at | 1376829_at | 1377168_at |
| 1385099_at | 1373085_at | 1381276_at | 1397850_at | 1388077_a_at |
| 1393111_at | 1385587_at | 1374146_at | 1381626_at | 1367925_at |
| 1373267_at | 1369590_a_at | 1387032_at | 1383742_at | 1373559_at |
| 1392206_at | 1369179_a_at | 1393124_at | 1377517_at | 1391106_at |
| 1372423_at | 1368238_at | 1368846_at | 1376579_at | 1368359_a_at |
| 1379814_at | 1378855_a_at | 1380346_at | 1381064_at | 1394908_at |
| 1379757_at | 1374649_at | 1394070_at | 1368313_a_at | 1396387_at |
| 1392999_at | 1396199_at | 1367754_s_at | 1369474_a_at | 1379363_at |
| 1381770_at | 1370944_at | 1368559_at | 1369019_at | 1393729_at |
| 1395456_at | 1373606_at | 1369755_at | 1389092_at | 1368916_at |
| 1374367_at | 1376174_at | 1372832_at | 1390607_at | 1393706_at |
| 1368545_at | 1393747_at | 1371134_at | 1368927_at | 1372590_at |
| 1387660_at | 1370936_at | 1369204_at | 1396176_at | 1369664_at |

Supplemental Table 5 continued

| | | | | |
|---|---|---|---|---|
| 1392948_at | 1379022_at | 1376893_at | 1376098_a_at | 1368692_a_at |
| 1387523_at | 1389007_at | 1391879_at | 1376215_at | 1376988_at |
| 1378400_at | 1368412_a_at | 1396687_at | 1380457_at | 1370694_at |
| 1373783_at | 1368355_at | 1392425_x_at | 1384564_at | 1370336_at |
| 1394855_at | 1374672_at | 1381173_at | 1388544_at | 1389054_at |
| 1378315_at | 1372844_at | 1372885_at | 1386321_s_at | 1367774_at |
| 1374948_at | 1369050_at | 1393147_at | 1367767_at | 1379486_at |
| 1398431_at | 1384667_x_at | 1379425_at | 1379907_at | 1383304_at |
| 1374787_at | 1398623_at | 1378274_at | 1377739_at | 1381341_at |
| 1389350_at | 1371883_at | 1393047_at | 1390042_at | 1387221_at |
| 1388187_at | 1372755_at | 1392274_at | 1373120_at | 1387818_at |
| 1368300_at | 1377885_at | 1375051_at | 1376754_at | 1371259_at |
| 1378470_at | 1395673_at | 1374632_at | 1378586_at | 1368187_at |
| 1393081_at | 1387543_at | 1372808_at | 1367834_at | 1374330_at |
| 1393307_at | 1368194_at | 1376076_at | 1379401_a_at | 1393441_at |
| 1375925_at | 1385176_at | 1393057_at | 1379477_at | 1368072_at |
| 1369717_at | 1390999_at | 1384522_at | 1385464_at | 1367624_at |
| 1388219_at | 1384683_at | 1382739_at | 1387645_at | 1391121_at |
| 1388968_at | 1368197_at | 1373632_at | 1378536_at | 1374819_at |
| 1378557_at | 1378818_at | 1389573_at | 1390114_at | 1378605_at |
| 1372989_at | 1395536_at | 1375052_at | 1387201_at | 1370695_s_at |
| 1377034_at | 1384526_at | 1376195_at | 1382319_at | 1388261_at |
| 1395655_at | 1377867_at | 1388919_at | 1394297_at | 1372013_at |
| 1385434_at | 1384165_at | 1384488_at | 1388659_at | 1368443_at |
| 1371801_at | 1378111_at | 1379493_at | 1372851_at | 1384444_at |
| 1374117_at | 1381080_at | 1398840_at | 1370902_at | 1392082_a_at |
| 1369752_a_at | 1381233_at | 1372642_at | 1385325_at | 1368708_a_at |

Supplemental Table 5 continued

| | | | | |
|---|---|---|---|---|
| 1367762_at | 1383220_at | 1373987_at | 1382002_at | 1391586_at |
| 1369137_at | 1393957_at | 1387065_at | 1370805_at | 1394522_at |
| 1391074_at | 1393190_at | 1369475_x_at | 1387063_at | 1385229_at |
| 1383887_at | 1392077_at | 1387578_a_at | 1370922_at | 1367888_at |
| 1382541_at | 1369165_at | 1388891_at | 1378479_at | 1370850_at |
| 1386679_at | 1376417_at | 1369632_a_at | 1374724_at | 1368667_at |
| 1384863_at | 1390473_at | 1368595_at | 1387360_at | 1393163_at |
| 1387208_at | 1374095_at | 1377176_at | 1379545_at | 1391656_at |
| 1376410_at | 1387799_at | 1373782_a_at | 1380016_at | 1376345_at |
| 1368037_at | 1371049_at | 1388099_a_at | 1389461_at | 1370964_at |
| 1387395_at | 1374818_at | 1377056_at | 1382975_at | |
| 1376788_at | 1375868_at | 1371908_at | 1376443_at | |

# Appendix

***Data availability***

Microarray datasets supporting the conclusions of this article are available in the Gene Expression Omnibus (GEO) repository under accession code: GSE126773. Other datasets supporting the conclusions of this article are included within the article and its Supplementary Files or have been deposited in the public repository https://github.com/nickh89/Stephen-N.-Housley-Public-Repository-for-Publication-Code-and-Data.

***Code***

All code and models used can be accessed in the public repository https://github.com/nickh89/Stephen-N.-Housley-Public-Repository-for-Publication-Code-and-Data

# References


**Aaronson, N. K., V. Mattioli, O. Minton, J. Weis, C. Johansen, S. O. Dalton, I. M. Verdonck-de Leeuw, K. D. Stein, C. M. Alfano and A. Mehnert** (2014). "Beyond treatment–psychosocial and behavioural issues in cancer survivorship research and practice." European Journal of Cancer Supplements **12**(1): 54-64.

**Abadi, M., A. Agarwal, P. Barham, E. Brevdo, Z. Chen, C. Citro, G. S. Corrado, A. Davis, J. Dean and M. Devin** (2016). "Tensorflow: Large-scale machine learning on heterogeneous distributed systems." arXiv preprint arXiv:1603.04467.

**Abelew, T. A., M. D. Miller, T. C. Cope and T. R. Nichols** (2000). "Local loss of proprioception results in disruption of interjoint coordination during locomotion in the cat." Journal of neurophysiology **84**(5): 2709-2714.

**Adelsberger, H., S. Quasthoff, J. Grosskreutz, A. Lepier, F. Eckel and C. Lersch** (2000). "The chemotherapeutic oxaliplatin alters voltage-gated Na+ channel kinetics on rat sensory neurons." European journal of pharmacology **406**(1): 25-32.

**Ahles, T. A.** (2012). "Brain vulnerability to chemotherapy toxicities." Psycho-Oncology **21**(11): 1141-1148.

**Ahles, T. A. and A. J. Saykin** (2007). "Candidate mechanisms for chemotherapy-induced cognitive changes." Nature Reviews Cancer **7**(3): 192.

**Akay, T., W. G. Tourtellotte, S. Arber and T. M. Jessell** (2014). "Degradation of mouse locomotor pattern in the absence of proprioceptive sensory feedback." Proceedings of the National Academy of Sciences **111**(47): 16877-16882.

**Akemann, W. and T. Knöpfel** (2006). "Interaction of Kv3 potassium channels and resurgent sodium current influences the rate of spontaneous firing of Purkinje neurons." Journal of Neuroscience **26**(17): 4602-4612.

**Alcindor, T. and N. Beauger** (2011). "Oxaliplatin: a review in the era of molecularly targeted therapy." Current oncology **18**(1): 18.

**Amos-Landgraf, J. M., L. N. Kwong, C. M. Kendziorski, M. Reichelderfer, J. Torrealba, J. Weichert, J. D. Haag, K.-S. Chen, J. L. Waller and M. N. Gould** (2007). "A target-selected Apc-mutant rat kindred enhances the modeling of familial human colon cancer." Proceedings of the National Academy of Sciences **104**(10): 4036-4041.

**Anderson, V., M. Spencer-Smith and A. Wood** (2011). "Do children really recover better? Neurobehavioural plasticity after early brain insult." Brain **134**(8): 2197-2221.

**Ando, T. and R. Tsay** (2010). "Predictive likelihood for Bayesian model selection and averaging." International Journal of Forecasting **26**(4): 744-763.

**André, T., C. Boni, L. Mounedji-Boudiaf, M. Navarro, J. Tabernero, T. Hickish, C. Topham, M. Zaninelli, P. Clingan and J. Bridgewater** (2004). "Oxaliplatin, fluorouracil, and leucovorin as adjuvant treatment for colon cancer." New England Journal of Medicine **350**(23): 2343-2351.

**Aoyagi, T., K. P. Terracina, A. Raza, H. Matsubara and K. Takabe** (2015). "Cancer cachexia, mechanism and treatment." World journal of gastrointestinal oncology **7**(4): 17.

**Argüelles, M., C. Benavides and I. Fernández** (2014). "A new approach to the identification of regional clusters: hierarchical clustering on principal components." Applied Economics **46**(21): 2511-2519.

**Argyriou, A. A., J. Bruna, A. A. Genazzani and G. Cavaletti** (2017). "Chemotherapy-induced peripheral neurotoxicity: management informed by pharmacogenetics." Nature Reviews Neurology **13**(8): 492.

**Argyriou, A. A., A. P. Kyritsis, T. Makatsoris and H. P. Kalofonos** (2014). "Chemotherapy-induced peripheral neuropathy in adults: a comprehensive update of the literature." Cancer management and research **6**: 135.

**Argyriou, A. A., P. Polychronopoulos, G. Iconomou, E. Chroni and H. P. Kalofonos** (2008). "A review on oxaliplatin-induced peripheral nerve damage." Cancer treatment reviews **34**(4): 368-377.

**Avan, A., T. J. Postma, C. Ceresa, A. Avan, G. Cavaletti, E. Giovannetti and G. J. Peters** (2015). "Platinum-induced neurotoxicity and preventive strategies: past, present, and future." The oncologist: theoncologist. 2014-0044.

**Ballion, B., D. Morin and D. Viala** (2001). "Forelimb locomotor generators and quadrupedal locomotion in the neonatal rat." European Journal of Neuroscience **14**(10): 1727-1738.

**Barbosa, C., Y. Xiao, A. J. Johnson, W. Xie, J. A. Strong, J.-M. Zhang and T. R. Cummins** (2017). "FHF2 isoforms differentially regulate Nav1. 6-mediated resurgent sodium currents in dorsal root ganglion neurons." Pflügers Archiv-European Journal of Physiology **469**(2): 195-212.

**Barlow, H.** (2001). "Redundancy reduction revisited." Network: computation in neural systems **12**(3): 241-253.

**Becker, R., J. Chambers and A. Wilks** (1988). "The New S Language Pacific Grove CA: Wadsworth & Brooks/Cole." BeckerThe New S Language1988.

**Beijers, A., F. Mols and G. Vreugdenhil** (2014). "A systematic review on chronic oxaliplatin-induced peripheral neuropathy and the relation with oxaliplatin administration." Supportive Care in Cancer **22**(7): 1999-2007.

**Bennett, B. K., S. B. Park, C. S.-Y. Lin, M. L. Friedlander, M. C. Kiernan and D. Goldstein** (2012). "Impact of oxaliplatin-induced neuropathy: a patient perspective." Supportive Care in Cancer **20**(11): 2959-2967.

**Bergstra, J., D. Yamins and D. D. Cox** (2013). "Making a science of model search: Hyperparameter optimization in hundreds of dimensions for vision architectures."

**Bewick, G. S. and R. W. Banks** (2015). "Mechanotransduction in the muscle spindle." Pflügers Archiv-European Journal of Physiology **467**(1): 175-190.

**Bienz, M. and H. Clevers** (2000). "Linking colorectal cancer to Wnt signaling." Cell **103**(2): 311-320.

**Bishop, C. M.** (1996). "Neural networks: a pattern recognition perspective."

**Bosetti, C., F. Levi, V. Rosato, P. Bertuccio, F. Lucchini, E. Negri and C. La Vecchia** (2011). "Recent trends in colorectal cancer mortality in Europe." International journal of cancer **129**(1): 180-191.

**Boyette-Davis, J. A., C. Eng, X. S. Wang, C. S. Cleeland, G. Wendelschafer-Crabb, W. R. Kennedy, D. A. Simone, H. Zhang and P. M. Dougherty** (2012). "Subclinical peripheral neuropathy is a common finding in colorectal cancer patients prior to chemotherapy." Clinical Cancer Research **18**(11): 3180-3187.

**Boyette-Davis, J. A., E. T. Walters and P. M. Dougherty** (2015). "Mechanisms involved in the development of chemotherapy-induced neuropathy." Pain **5**(4): 285-296.

**Breschi, A., T. R. Gingeras and R. Guigó** (2017). "Comparative transcriptomics in human and mouse." Nature Reviews Genetics **18**(7): 425.

**Briones, T. L. and J. Woods** (2011). "Chemotherapy-induced cognitive impairment is associated with decreases in cell proliferation and histone modifications." BMC neuroscience **12**(1): 124.

**Brooks, S., A. Gelman, G. Jones and X.-L. Meng** (2011). Handbook of markov chain monte carlo, CRC press.

**Browne, M. W.** (2000). "Cross-validation methods." Journal of mathematical psychology **44**(1): 108-132.

**Bullinger, K. L., P. Nardelli, M. J. Pinter, F. J. Alvarez and T. C. Cope** (2011). "Permanent central synaptic disconnection of proprioceptors after nerve injury and regeneration. II. Loss of functional connectivity with motoneurons." Journal of neurophysiology **106**(5): 2471-2485.

**Burakgazi, A., W. Messersmith, D. Vaidya, P. Hauer, A. Hoke and M. Polydefkis** (2011). "Longitudinal assessment of oxaliplatin-induced neuropathy." Neurology **77**(10): 980-986.

**Burke, D., K.-E. Hagbarth and L. Löfstedt** (1978). "Muscle spindle activity in man during shortening and lengthening contractions." The Journal of physiology **277**(1): 131-142.

**Button, D. C., J. M. Kalmar, K. Gardiner, T. Marqueste, H. Zhong, R. R. Roy, V. R. Edgerton and P. F. Gardiner** (2008). "Does elimination of afferent input modify the changes in rat motoneurone properties that occur following chronic spinal cord transection?" J Physiol **586**(2): 529-544.

**Cai, J., D. Fang, X.-D. Liu, S. Li, J. Ren and G.-G. Xing** (2015). "Suppression of KCNQ/M (Kv7) potassium channels in the spinal cord contributes to the sensitization of dorsal horn WDR neurons and pain hypersensitivity in a rat model of bone cancer pain." Oncology reports **33**(3): 1540-1550.

**Cain, D. M., P. W. Wacnik, M. Turner, G. Wendelschafer-Crabb, W. R. Kennedy, G. L. Wilcox and D. A. Simone** (2001). "Functional interactions between tumor and peripheral nerve: changes in excitability and morphology of primary afferent fibers in a murine model of cancer pain." Journal of Neuroscience **21**(23): 9367-9376.

**Carpenter, B., A. Gelman, M. D. Hoffman, D. Lee, B. Goodrich, M. Betancourt, M. Brubaker, J. Guo, P. Li and A. Riddell** (2017). "Stan: A probabilistic programming language." Journal of statistical software **76**(1).

**Carrasco, D. I., J. A. Vincent and T. C. Cope** (2017). "Distribution of TTX-sensitive voltage-gated sodium channels in primary sensory endings of mammalian muscle spindles." Journal of Neurophysiology **117**(4): 1690-1701.

**Cavaletti, G., G. Bogliun, L. Marzorati, A. Zincone, M. Marzola, N. Colombo and G. Tredici** (1995). "Peripheral neurotoxicity of taxol in patients previously treated with cisplatin." Cancer **75**(5): 1141-1150.

**Cavaletti, G. and P. Marmiroli** (2010). "Chemotherapy-induced peripheral neurotoxicity." Nature Reviews Neurology **6**(12): 657.

**Center, M. M., A. Jemal and E. Ward** (2009). "International trends in colorectal cancer incidence rates." Cancer Epidemiology and Prevention Biomarkers **18**(6): 1688-1694.

**Chalfie, M.** (2009). "Neurosensory mechanotransduction." Nature reviews Molecular cell biology **10**(1): 44.

**Chen, R., L. Cohen and M. Hallett** (2002). "Nervous system reorganization following injury." Neuroscience **111**(4): 761-773.

**Chollet, F.** (2018). Deep Learning mit Python und Keras: Das Praxis-Handbuch vom Entwickler der Keras-Bibliothek, MITP-Verlags GmbH & Co. KG.

**Currie, G. L., H. Angel-Scott, L. Colvin, F. Cramond, K. Hair, L. Khandoker, J. Liao, M. R. Macleod, S. K. McCann and R. Morland** (2018). "Animal models of chemotherapy-induced peripheral neuropathy: a machine-assisted systematic review and meta-analysis A comprehensive summary of the field to inform robust experimental design." bioRxiv: 293480.

**Damrauer, J. S., M. E. Stadler, S. Acharyya, A. S. Baldwin, M. E. Couch and D. C. Guttridge** (2018). "Chemotherapy-induced muscle wasting: association with NF-κB and cancer cachexia." European journal of translational myology **28**(2).

**de Nooij, J. C., C. M. Simon, A. Simon, S. Doobar, K. P. Steel, R. W. Banks, G. Z. Mentis, G. S. Bewick and T. M. Jessell** (2015). "The PDZ-domain protein Whirlin facilitates mechanosensory signaling in mammalian proprioceptors." Journal of Neuroscience **35**(7): 3073-3084.

**DeBerardinis, R. J., J. J. Lum, G. Hatzivassiliou and C. B. Thompson** (2008). "The biology of cancer: metabolic reprogramming fuels cell growth and proliferation." Cell metabolism **7**(1): 11-20.

**Desai, N. S., L. C. Rutherford and G. G. Turrigiano** (1999). "Plasticity in the intrinsic excitability of cortical pyramidal neurons." Nature neuroscience **2**(6): 515-520.

**Devor, M., R. Govrin-Lippmann and K. Angelides** (1993). "Na+ channel immunolocalization in peripheral mammalian axons and changes following nerve injury and neuroma formation." Journal of Neuroscience **13**(5): 1976-1992.

**Dietrich, J., R. Han, Y. Yang, M. Mayer-Pröschel and M. Noble** (2006). "CNS progenitor cells and oligodendrocytes are targets of chemotherapeutic agents in vitro and in vivo." Journal of biology **5**(7): 22.

**Dodson, S., V. E. Baracos, A. Jatoi, W. J. Evans, D. Cella, J. T. Dalton and M. S. Steiner** (2011). "Muscle wasting in cancer cachexia: clinical implications, diagnosis, and emerging treatment strategies." Annual review of medicine **62**: 265-279.

**Driver, J. and C. Spence** (1998). "Cross–modal links in spatial attention." Philosophical Transactions of the Royal Society of London. Series B: Biological Sciences **353**(1373): 1319-1331.

**Edwards, B. K., E. Ward, B. A. Kohler, C. Eheman, A. G. Zauber, R. N. Anderson, A. Jemal, M. J. Schymura, I. Lansdorp-Vogelaar and L. C. Seeff** (2010). "Annual report

to the nation on the status of cancer, 1975-2006, featuring colorectal cancer trends and impact of interventions (risk factors, screening, and treatment) to reduce future rates." Cancer **116**(3): 544-573.

**Epifani, I., S. N. MacEachern and M. Peruggia** (2008). "Case-deletion importance sampling estimators: Central limit theorems and related results." Electronic Journal of Statistics **2**: 774-806.

**Espinosa, F., M. A. Torres-Vega, G. A. Marks and R. H. Joho** (2008). "Ablation of Kv3. 1 and Kv3. 3 potassium channels disrupts thalamocortical oscillations in vitro and in vivo." Journal of Neuroscience **28**(21): 5570-5581.

**Esteller, M.** (2008). "Epigenetics in cancer." New England Journal of Medicine **358**(11): 1148-1159.

**Fearon, K., F. Strasser, S. D. Anker, I. Bosaeus, E. Bruera, R. L. Fainsinger, A. Jatoi, C. Loprinzi, N. MacDonald and G. Mantovani** (2011). "Definition and classification of cancer cachexia: an international consensus." The lancet oncology **12**(5): 489-495.

**Feather, C. E., J. G. Lees, P. G. Makker, D. Goldstein, J. B. Kwok, G. Moalem-Taylor and P. Polly** (2018). "Oxaliplatin induces muscle loss and muscle-specific molecular changes in Mice." Muscle & nerve **57**(4): 650-658.

**Femia, A. P., C. Luceri, P. V. Soares, M. Lodovici and G. Caderni** (2015). "Multiple mucin depleted foci, high proliferation and low apoptotic response in the onset of colon carcinogenesis of the PIRC rat, mutated in Apc." International journal of cancer **136**(6).

**Ferlay, J., I. Soerjomataram, R. Dikshit, S. Eser, C. Mathers, M. Rebelo, D. M. Parkin, D. Forman and F. Bray** (2015). "Cancer incidence and mortality worldwide: sources, methods and major patterns in GLOBOCAN 2012." International journal of cancer **136**(5): E359-E386.

**Figueroa, K. P., N. A. Minassian, G. Stevanin, M. Waters, V. Garibyan, S. Forlani, A. Strzelczyk, K. Bürk, A. Brice and A. Dürr** (2010). "KCNC3: phenotype, mutations, channel biophysics—a study of 260 familial ataxia patients." Human mutation **31**(2): 191-196.

**Frigon, A.** (2017). "The neural control of interlimb coordination during mammalian locomotion." Journal of neurophysiology **117**(6): 2224-2241.

**Fukuda, Y., Y. Li and R. A. Segal** (2017). "A mechanistic understanding of axon degeneration in chemotherapy-induced peripheral neuropathy." Frontiers in neuroscience **11**: 481.

**Gabry, J. and B. Goodrich** (2018). "rstanarm: Bayesian applied regression modeling via Stan." R package version **2.18.1**.

**Gal, Y. and Z. Ghahramani** (2016). A theoretically grounded application of dropout in recurrent neural networks. Advances in neural information processing systems.

**Galanski, M., M. A. Jakupec and B. K. Keppler** (2005). "Update of the preclinical situation of anticancer platinum complexes: novel design strategies and innovative analytical approaches." Current medicinal chemistry **12**(18): 2075-2094.

**Geisser, S. and W. F. Eddy** (1979). "A predictive approach to model selection." Journal of the American Statistical Association **74**(365): 153-160.

**Gelfand, A. E.** (1996). "Model determination using sampling-based methods." Markov chain Monte Carlo in practice: 145-161.

Gelfand, A. E., D. K. Dey and H. Chang (1992). Model determination using predictive distributions with implementation via sampling-based methods, STANFORD UNIV CA DEPT OF STATISTICS.

**Gelman, A. and D. B. Rubin** (1992). "Inference from iterative simulation using multiple sequences." Statistical science **7**(4): 457-472.

**Goodfellow, I., Y. Bengio and A. Courville** (2016). Deep learning, MIT press.

**Grisold, W., G. Cavaletti and A. J. Windebank** (2012). "Peripheral neuropathies from chemotherapeutics and targeted agents: diagnosis, treatment, and prevention." Neuro-oncology **14**(suppl_4): iv45-iv54.

**Grolleau, F., L. Gamelin, M. Boisdron-Celle, B. Lapied, M. Pelhate and E. Gamelin** (2001). "A possible explanation for a neurotoxic effect of the anticancer agent oxaliplatin on neuronal voltage-gated sodium channels." Journal of neurophysiology **85**(5): 2293-2297.

**Grubb, M. S. and J. Burrone** (2010). "Activity-dependent relocation of the axon initial segment fine-tunes neuronal excitability." Nature **465**(7301): 1070-1074.

**Gu, Y., D. Servello, Z. Han, R. R. Lalchandani, J. B. Ding, K. Huang and C. Gu** (2018). "Balanced Activity between Kv3 and Nav Channels Determines Fast-Spiking in Mammalian Central Neurons." iScience **9**: 120-137.

**Haftel, V. K., E. K. Bichler, T. R. Nichols, M. J. Pinter and T. C. Cope** (2004). "Movement reduces the dynamic response of muscle spindle afferents and motoneuron synaptic potentials in rat." Journal of neurophysiology **91**(5): 2164-2171.

**Hasan, Z.** (1983). "A model of spindle afferent response to muscle stretch." Journal of neurophysiology **49**(4): 989-1006.

**Hay, N.** (2016). "Reprogramming glucose metabolism in cancer: can it be exploited for cancer therapy?" Nature Reviews Cancer **16**(10): 635.

**Hershman, D. L., C. Lacchetti, R. H. Dworkin, E. M. Lavoie Smith, J. Bleeker, G. Cavaletti, C. Chauhan, P. Gavin, A. Lavino and M. B. Lustberg** (2014). "Prevention and management of chemotherapy-induced peripheral neuropathy in survivors of adult cancers: American Society of Clinical Oncology clinical practice guideline." Journal of Clinical Oncology **32**(18): 1941-1967.

**Hershman, D. L., C. Lacchetti, R. H. Dworkin, E. M. Lavoie Smith, J. Bleeker, G. Cavaletti, C. Chauhan, P. Gavin, A. Lavino, M. B. Lustberg, J. Paice, B. Schneider, M. L. Smith, T. Smith, S. Terstriep, N. Wagner-Johnston, K. Bak, C. L. Loprinzi and O. American Society of Clinical** (2014). "Prevention and management of chemotherapy-induced peripheral neuropathy in survivors of adult cancers: American Society of Clinical Oncology clinical practice guideline." J Clin Oncol **32**(18): 1941-1967.

**Hochreiter, S. and J. Schmidhuber** (1997). "Long short-term memory." Neural computation **9**(8): 1735-1780.

**Hoffman, M. D. and A. Gelman** (2014). "The No-U-turn sampler: adaptively setting path lengths in Hamiltonian Monte Carlo." Journal of Machine Learning Research **15**(1): 1593-1623.

**Hong, G., W. Zhang, H. Li, X. Shen and Z. Guo** (2014). "Separate enrichment analysis of pathways for up-and downregulated genes." Journal of the Royal Society Interface **11**(92): 20130950.

**Housley, S. N., P. Nardelli, D. Carrasco, E. Pfahl, L. Matyunina, J. F. McDonald and T. C. Cope** (2019). "Cancer Exacerbates Chemotherapy Induced Sensory Neuropathy." bioRxiv: 667105.

**Huang, D. W., B. T. Sherman and R. A. Lempicki** (2008). "Bioinformatics enrichment tools: paths toward the comprehensive functional analysis of large gene lists." Nucleic acids research **37**(1): 1-13.

**Huang, D. W., B. T. Sherman and R. A. Lempicki** (2008). "Systematic and integrative analysis of large gene lists using DAVID bioinformatics resources." Nature protocols **4**(1): 44.

**Husson, F., J. Josse and J. Pages** (2010). "Principal component methods-hierarchical clustering-partitional clustering: why would we need to choose for visualizing data." Applied Mathematics Department.

**Ionta, S., M. Villiger, C. R. Jutzeler, P. Freund, A. Curt and R. Gassert** (2016). "Spinal cord injury affects the interplay between visual and sensorimotor representations of the body." Scientific reports **6**: 20144.

**Irving, A. A., K. Yoshimi, M. L. Hart, T. Parker, L. Clipson, M. R. Ford, T. Kuramoto, W. F. Dove and J. M. Amos-Landgraf** (2014). "The utility of Apc-mutant rats in modeling human colon cancer." Disease models & mechanisms **7**(11): 1215-1225.

**Ishibashi, K., N. Okada, T. Miyazaki, M. Sano and H. Ishida** (2010). "Effect of calcium and magnesium on neurotoxicity and blood platinum concentrations in patients receiving mFOLFOX6 therapy: a prospective randomized study." International journal of clinical oncology **15**(1): 82-87.

**Ivanenko, Y., N. Dominici, E. Daprati, D. Nico, G. Cappellini and F. Lacquaniti** (2011). "Locomotor body scheme." Human movement science **30**(2): 341-351.

**Johnstone, T. C., G. Y. Park and S. J. Lippard** (2014). "Understanding and improving platinum anticancer drugs–phenanthriplatin." Anticancer research **34**(1): 471-476.

**Juvin, L., J. Simmers and D. Morin** (2005). "Propriospinal circuitry underlying interlimb coordination in mammalian quadrupedal locomotion." Journal of Neuroscience **25**(25): 6025-6035.

**Kaczmarek, L. K. and Y. Zhang** (2017). "Kv3 channels: enablers of rapid firing, neurotransmitter release, and neuronal endurance." Physiological reviews **97**(4): 1431-1468.

**Kagiava, A., E. K Kosmidis and G. Theophilidis** (2013). "Oxaliplatin-induced hyperexcitation of rat sciatic nerve fibers: an intra-axonal study." Anti-Cancer Agents in Medicinal Chemistry (Formerly Current Medicinal Chemistry-Anti-Cancer Agents) **13**(2): 373-379.

**Kanat, O., H. Ertas and B. Caner** (2017). "Platinum-induced neurotoxicity: A review of possible mechanisms." World Journal of Clinical Oncology **8**(4): 329.

**Kassambara, A. and F. Mundt** (2016). "Factoextra: extract and visualize the results of multivariate data analyses." R package version **1**(3).

**Klampfer, L.** (2011). "Cytokines, inflammation and colon cancer." Current cancer drug targets **11**(4): 451-464.

**Kneis, S., A. Wehrle, K. Freyler, K. Lehmann, B. Rudolphi, B. Hildenbrand, H. H. Bartsch, H. Bertz, A. Gollhofer and R. Ritzmann** (2016). "Balance impairments and neuromuscular changes in breast cancer patients with chemotherapy-induced peripheral neuropathy." Clinical neurophysiology **127**(2): 1481-1490.

**Kovalchuk, A., Y. Ilnytskyy, R. Rodriguez-Juarez, S. Shpyleva, S. Melnyk, I. Pogribny, A. Katz, D. Sidransky, O. Kovalchuk and B. Kolb** (2017). "Chemo brain or tumor brain-that is the question: the presence of extracranial tumors profoundly affects molecular processes in the prefrontal cortex of TumorGraft mice." Aging (Albany NY) **9**(7): 1660.

**Krishnan, A. V., D. Goldstein, M. Friedlander and M. C. Kiernan** (2006). "Oxaliplatin and axonal Na+ channel function in vivo." Clinical cancer research **12**(15): 4481-4484.

**Kruschke, J.** (2014). Doing Bayesian data analysis: A tutorial with R, JAGS, and Stan, Academic Press.

**Kruschke, J. K.** (2013). "Bayesian estimation supersedes the t test." Journal of Experimental Psychology: General **142**(2): 573.

**Kuo, J. J., T. Siddique, R. Fu and C. J. Heckman** (2005). "Increased persistent Na(+) current and its effect on excitability in motoneurones cultured from mutant SOD1 mice." J Physiol **563**(Pt 3): 843-854.

**Kwong, L. N. and W. F. Dove** (2009). APC and its modifiers in colon cancer. APC Proteins, Springer**:** 85-106.

**Lili, L. N., L. V. Matyunina, L. Walker, B. B. Benigno and J. F. McDonald** (2013). "Molecular profiling predicts the existence of two functionally distinct classes of ovarian cancer stroma." BioMed research international **2013**.

**Loprinzi, C. L., R. Qin, S. R. Dakhil, L. Fehrenbacher, K. A. Flynn, P. Atherton, D. Seisler, R. Qamar, G. C. Lewis and A. Grothey** (2013). "Phase III randomized, placebo-controlled, double-blind study of intravenous calcium and magnesium to prevent oxaliplatin-induced sensory neurotoxicity (N08CB/Alliance)." Journal of Clinical Oncology **32**(10): 997-1005.

**Lund, A. H. and M. van Lohuizen** (2004). "Epigenetics and cancer." Genes & development **18**(19): 2315-2335.

**Lyon, D., L. Elmore, N. Aboalela, J. Merrill-Schools, N. McCain, A. Starkweather, R. Elswick Jr and C. Jackson-Cook** (2014). "Potential epigenetic mechanism (s) associated with the persistence of psychoneurological symptoms in women receiving chemotherapy for breast cancer: a hypothesis." Biological research for nursing **16**(2): 160-174.

**Mager, L. F., M.-H. Wasmer, T. T. Rau and P. Krebs** (2016). "Cytokine-induced modulation of colorectal cancer." Frontiers in oncology **6**.

**Maksimovic, S., M. Nakatani, Y. Baba, A. M. Nelson, K. L. Marshall, S. A. Wellnitz, P. Firozi, S.-H. Woo, S. Ranade and A. Patapoutian** (2014). "Epidermal Merkel cells are mechanosensory cells that tune mammalian touch receptors." Nature **509**(7502): 617.

**Marshall, T. F., G. P. Zipp, F. Battaglia, R. Moss and S. Bryan** (2017). "Chemotherapy-induced-peripheral neuropathy, gait and fall risk in older adults following cancer treatment." Journal of Cancer Research and Practice.

**Matthews, P. B.** (1972). "Mammalian muscle receptors and their central actions."

**Metz, G. A. and I. Q. Whishaw** (2002). "Cortical and subcortical lesions impair skilled walking in the ladder rung walking test: a new task to evaluate fore-and hindlimb stepping, placing, and co-ordination." Journal of neuroscience methods **115**(2): 169-179.

**Metz, G. A. and I. Q. Whishaw** (2009). "The ladder rung walking task: a scoring system and its practical application." JoVE (Journal of Visualized Experiments)(28): e1204.

**Mols, F., T. Beijers, V. Lemmens, C. J. van den Hurk, G. Vreugdenhil and L. V. van de Poll-Franse** (2013). "Chemotherapy-induced neuropathy and its association with quality of life among 2-to 11-year colorectal cancer survivors: results from the population-based PROFILES registry." Journal of Clinical Oncology **31**(21): 2699-2707.

**Monfort, S. M., X. Pan, C. L. Loprinzi, M. B. Lustberg and A. M. Chaudhari** (2019). "Impaired Postural Control and Altered Sensory Organization During Quiet Stance Following Neurotoxic Chemotherapy: A Preliminary Study." Integrative cancer therapies **18**: 1534735419828823.

**Montagnani, F., G. Turrisi, C. Marinozzi, C. Aliberti and G. Fiorentini** (2011). "Effectiveness and safety of oxaliplatin compared to cisplatin for advanced, unresectable gastric cancer: a systematic review and meta-analysis." Gastric Cancer **14**(1): 50-55.

**Murtagh, F. and P. Legendre** (2014). "Ward's hierarchical agglomerative clustering method: which algorithms implement Ward's criterion?" Journal of classification **31**(3): 274-295.

**Nair, A. B. and S. Jacob** (2016). "A simple practice guide for dose conversion between animals and human." Journal of basic and clinical pharmacy **7**(2): 27.

**Nardelli, P., R. Powers, T. C. Cope and M. M. Rich** (2017). "Increasing motor neuron excitability to treat weakness in sepsis." Annals of neurology **82**(6): 961-971.

**Nelson, T. E., C. L. Ur and D. L. Gruol** (2002). "Chronic interleukin-6 exposure alters electrophysiological properties and calcium signaling in developing cerebellar purkinje neurons in culture." Journal of neurophysiology **88**(1): 475-486.

**Ness, K. K., S. C. Kaste, L. Zhu, C.-H. Pui, S. Jeha, P. C. Nathan, H. Inaba, K. Wasilewski-Masker, D. Shah and R. J. Wells** (2015). "Skeletal, neuromuscular and fitness impairments among children with newly diagnosed acute lymphoblastic leukemia." Leukemia & lymphoma **56**(4): 1004-1011.

**Nichols, T. R., T. C. Cope and T. A. Abelew** (1999). "8 Rapid Spinal Mechanisms of Motor Coordination." Exercise and sport sciences reviews **27**(1): 255-284.

**Novak, C. M., P. R. Burghardt and J. A. Levine** (2012). "The use of a running wheel to measure activity in rodents: relationship to energy balance, general activity, and reward." Neuroscience & Biobehavioral Reviews **36**(3): 1001-1014.

**Ochala, J. and L. Larsson** (2008). "Effects of a preferential myosin loss on Ca2+ activation of force generation in single human skeletal muscle fibres." Experimental physiology **93**(4): 486-495.

**Panatier, A. and R. Robitaille** (2012). "The soothing touch: microglial contact influences neuronal excitability." Developmental cell **23**(6): 1125-1126.

**Pardillo-Díaz, R., L. Carrascal, A. Ayala and P. Nunez-Abades** (2015). "Oxidative stress induced by cumene hydroperoxide evokes changes in neuronal excitability of rat motor cortex neurons." Neuroscience **289**: 85-98.

**Park, S. B., D. Goldstein, A. V. Krishnan, C. S. Y. Lin, M. L. Friedlander, J. Cassidy, M. Koltzenburg and M. C. Kiernan** (2013). "Chemotherapy-induced peripheral neurotoxicity: A critical analysis." CA: a cancer journal for clinicians **63**(6): 419-437.

**Park, S. B., C. S. Lin, A. V. Krishnan, D. Goldstein, M. L. Friedlander and M. C. Kiernan** (2011). "Long-term neuropathy after oxaliplatin treatment: challenging the dictum of reversibility." Oncologist **16**(5): 708-716.

**Phipson, B., S. Lee, I. J. Majewski, W. S. Alexander and G. K. Smyth** (2016). "Robust hyperparameter estimation protects against hypervariable genes and improves power to detect differential expression." The annals of applied statistics **10**(2): 946.

**Porporato, P.** (2016). "Understanding cachexia as a cancer metabolism syndrome." Oncogenesis **5**(2): e200.

**Prochazka, A. and P. Ellaway** (2012). "Sensory systems in the control of movement." Comprehensive Physiology **2**(4): 2615-2627.

**Proske, U. and S. C. Gandevia** (2009). "The kinaesthetic senses." The Journal of physiology **587**(17): 4139-4146.

**Proske, U. and S. C. Gandevia** (2012). "The proprioceptive senses: their roles in signaling body shape, body position and movement, and muscle force." Physiological reviews **92**(4): 1651-1697.

**Quasthoff, S. and H. P. Hartung** (2002). "Chemotherapy-induced peripheral neuropathy." Journal of neurology **249**(1): 9-17.

**Reagan-Shaw, S., M. Nihal and N. Ahmad** (2008). "Dose translation from animal to human studies revisited." The FASEB journal **22**(3): 659-661.

**Reimand, J., M. Kull, H. Peterson, J. Hansen and J. Vilo** (2007). "g: Profiler—a web-based toolset for functional profiling of gene lists from large-scale experiments." Nucleic acids research **35**(suppl_2): W193-W200.

**Rekling, J. C., G. D. Funk, D. A. Bayliss, X.-W. Dong and J. L. Feldman** (2000). "Synaptic control of motoneuronal excitability." Physiological reviews **80**(2): 767-852.

**Reuter, S., S. C. Gupta, M. M. Chaturvedi and B. B. Aggarwal** (2010). "Oxidative stress, inflammation, and cancer: how are they linked?" Free Radical Biology and Medicine **49**(11): 1603-1616.

**Ritchie, M. E., J. Silver, A. Oshlack, M. Holmes, D. Diyagama, A. Holloway and G. K. Smyth** (2007). "A comparison of background correction methods for two-colour microarrays." Bioinformatics **23**(20): 2700-2707.

**Roberts, B., G. Frye, B. Ahn, L. Ferreira and A. Judge** (2013). "Cancer cachexia decreases specific force and accelerates fatigue in limb muscle." Biochemical and biophysical research communications **435**(3): 488-492.

**Rudy, B., A. Chow, D. Lau, Y. Amarillo, A. Ozaita, M. Saganich, H. Moreno, M. S. Nadal, R. HERNANDEZ-PINEDA and A. HERNANDEZ-CRUZ** (1999). "Contributions of Kv3 channels to neuronal excitability." Annals of the New York Academy of Sciences **868**(1): 304-343.

**Rudy, B. and C. J. McBain** (2001). "Kv3 channels: voltage-gated K+ channels designed for high-frequency repetitive firing." Trends in neurosciences **24**(9): 517-526.

**Rumelhart, D. E., G. E. Hinton and R. J. Williams** (1988). "Learning representations by back-propagating errors." Cognitive modeling **5**(3): 1.

**Saif, M. W., K. Syrigos, K. Kaley and I. Isufi** (2010). "Role of pregabalin in treatment of oxaliplatin-induced sensory neuropathy." Anticancer research **30**(7): 2927-2933.

**Sakai, H., A. Sagara, K. Arakawa, R. Sugiyama, A. Hirosaki, K. Takase, A. Jo, K. Sato, Y. Chiba and M. Yamazaki** (2014). "Mechanisms of cisplatin-induced muscle atrophy." Toxicology and applied pharmacology **278**(2): 190-199.

**Schmidt, S. F., M. Rohm, S. Herzig and M. B. Diaz** (2018). "Cancer Cachexia: More Than Skeletal Muscle Wasting." Trends in cancer.

**Schneidman, E., W. Bialek and M. J. Berry** (2003). "Synergy, redundancy, and independence in population codes." Journal of Neuroscience **23**(37): 11539-11553.

**Seretny, M., G. L. Currie, E. S. Sena, S. Ramnarine, R. Grant, M. R. MacLeod, L. A. Colvin and M. Fallon** (2014). "Incidence, prevalence, and predictors of chemotherapy-induced peripheral neuropathy: a systematic review and meta-analysis." PAIN® **155**(12): 2461-2470.

**Sghirlanzoni, A., D. Pareyson and G. Lauria** (2005). "Sensory neuron diseases." The Lancet Neurology **4**(6): 349-361.

**Sharma, V. and J. H. McNeill** (2009). "To scale or not to scale: the principles of dose extrapolation." British journal of pharmacology **157**(6): 907-921.

**Shemmell, J., M. A. Krutky and E. J. Perreault** (2010). "Stretch sensitive reflexes as an adaptive mechanism for maintaining limb stability." Clinical Neurophysiology **121**(10): 1680-1689.

**Shenton, J. T., J. Schwoebel and H. B. Coslett** (2004). "Mental motor imagery and the body schema: evidence for proprioceptive dominance." Neuroscience letters **370**(1): 19-24.

**Shimojo, S. and L. Shams** (2001). "Sensory modalities are not separate modalities: plasticity and interactions." Current opinion in neurobiology **11**(4): 505-509.

**Simon, A., F. Shenton, I. Hunter, R. W. Banks and G. S. Bewick** (2010). "Amiloride-sensitive channels are a major contributor to mechanotransduction in mammalian muscle spindles." The Journal of physiology **588**(1): 171-185.

**Sisignano, M., R. Baron, K. Scholich and G. Geisslinger** (2014). "Mechanism-based treatment for chemotherapy-induced peripheral neuropathic pain." Nat Rev Neurol **10**(12): 694-707.

**Sittl, R., A. Lampert, T. Huth, E. T. Schuy, A. S. Link, J. Fleckenstein, C. Alzheimer, P. Grafe and R. W. Carr** (2012). "Anticancer drug oxaliplatin induces acute cooling-aggravated neuropathy via sodium channel subtype Na(V)1.6-resurgent and persistent current." Proc Natl Acad Sci U S A **109**(17): 6704-6709.

**Sittl, R., A. Lampert, T. Huth, E. T. Schuy, A. S. Link, J. Fleckenstein, C. Alzheimer, P. Grafe and R. W. Carr** (2012). "Anticancer drug oxaliplatin induces acute cooling-aggravated neuropathy via sodium channel subtype NaV1. 6-resurgent and persistent current." Proceedings of the National Academy of Sciences **109**(17): 6704-6709.

**Smyth, G. K.** (2004). "Linear models and empirical bayes methods for assessing differential expression in microarray experiments." Statistical applications in genetics and molecular biology **3**(1): 1-25.

**Smyth, G. K.** (2005). Limma: linear models for microarray data. Bioinformatics and computational biology solutions using R and Bioconductor, Springer**:** 397-420.

**Sorensen, J. C., A. C. Petersen, C. A. Timpani, D. G. Campelj, J. Cook, A. J. Trewin, V. Stojanovska, M. Stewart, A. Hayes and E. Rybalka** (2017). "BGP-15 protects against Oxaliplatin-induced skeletal myopathy and mitochondrial reactive oxygen species production in mice." Frontiers in pharmacology **8**: 137.

**Srivastava, N., G. Hinton, A. Krizhevsky, I. Sutskever and R. Salakhutdinov** (2014). "Dropout: a simple way to prevent neural networks from overfitting." The journal of machine learning research **15**(1): 1929-1958.

**Stein, B. E.** (2012). The new handbook of multisensory processing, Mit Press.

**Stein, R. B., D. Weber, Y. Aoyagi, A. Prochazka, J. Wagenaar, S. Shoham and R. Normann** (2004). "Coding of position by simultaneously recorded sensory neurones in the cat dorsal root ganglion." The Journal of physiology **560**(3): 883-896.

**Stone, J. B. and L. M. DeAngelis** (2016). "Cancer-treatment-induced neurotoxicity—focus on newer treatments." Nature reviews Clinical oncology **13**(2): 92.

**Stone, M.** (1974). "Cross-validatory choice and assessment of statistical predictions." Journal of the Royal Statistical Society: Series B (Methodological) **36**(2): 111-133.

**Taleb, O., F. Bouzobra, H. Tekin-Pala, L. Meyer, A. Mensah-Nyagan and C. Patte-Mensah** (2017). "Behavioral and electromyographic assessment of oxaliplatin-induced motor dysfunctions: Evidence for a therapeutic effect of allopregnanolone." Behavioural brain research **320**: 440-449.

Team, R. C. (2018). R: A Language and Environment for Statistical Computing, R Foundation for Statistical Computing, Austria, 2015, ISBN 3-900051-07-0.

**Tieleman, T. and G. Hinton** (2012). "Lecture 6.5-rmsprop: Divide the gradient by a running average of its recent magnitude." COURSERA: Neural networks for machine learning **4**(2): 26-31.

**Tisdale, M. J.** (2002). "Cachexia in cancer patients." Nature Reviews Cancer **2**(11): 862.

**Tofthagen, C., K. A. Donovan, M. A. Morgan, D. Shibata and Y. Yeh** (2013). "Oxaliplatin-induced peripheral neuropathy's effects on health-related quality of life of colorectal cancer survivors." Supportive Care in Cancer **21**(12): 3307-3313.

**Tofthagen, C., J. Overcash and K. Kip** (2012). "Falls in persons with chemotherapy-induced peripheral neuropathy." Supportive care in cancer **20**(3): 583-589.

**Torre, L. A., F. Bray, R. L. Siegel, J. Ferlay, J. Lortet-Tieulent and A. Jemal** (2015). "Global cancer statistics, 2012." CA: a cancer journal for clinicians **65**(2): 87-108.

**Tulleuda, A., B. Cokic, G. Callejo, B. Saiani, J. Serra and X. Gasull** (2011). "TRESK channel contribution to nociceptive sensory neurons excitability: modulation by nerve injury." Molecular pain **7**(1): 30.

**Tzour, A., H. Leibovich, O. Barkai, Y. Biala, S. Lev, Y. Yaari and A. M. Binshtok** (2017). "KV7/M channels as targets for lipopolysaccharide-induced inflammatory neuronal hyperexcitability." The Journal of physiology **595**(3): 713-738.

**van Erning, F. N., M. L. Janssen-Heijnen, J. A. Wegdam, G. D. Slooter, J. H. Wijsman, A. Vreugenhil, T. A. Beijers, L. V. van de Poll-Franse and V. E. Lemmens** (2016). "The course of neuropathic symptoms in relation to adjuvant chemotherapy among elderly patients with stage III colon cancer: a longitudinal study." Clinical colorectal cancer.

**VanderVeen, B. N., J. P. Hardee, D. K. Fix and J. A. Carson** (2017). "Skeletal muscle function during the progression of cancer cachexia in the male ApcMin/+ mouse." Journal of Applied Physiology **124**(3): 684-695.

**Vardy, J., H. Dhillon, G. Pond, C. Renton, A. Dodd, H. Zhang, S. Clarke and I. Tannock** (2016). "Fatigue in people with localized colorectal cancer who do and do not receive chemotherapy: a longitudinal prospective study." Annals of Oncology **27**(9): 1761-1767.

**Vehtari, A., A. Gelman and J. Gabry** (2017). "Practical Bayesian model evaluation using leave-one-out cross-validation and WAIC." Statistics and Computing **27**(5): 1413-1432.

**Vehtari, A. and J. Lampinen** (2002). "Bayesian model assessment and comparison using cross-validation predictive densities." Neural computation **14**(10): 2439-2468.

**Vehtari, A. and J. Ojanen** (2012). "A survey of Bayesian predictive methods for model assessment, selection and comparison." Statistics Surveys **6**: 142-228.

Venables, W. and B. Ripley (2002). Modern applied statistics (Fourth S., editor) New York, Springer.

**Vezzani, A. and B. Viviani** (2015). "Neuromodulatory properties of inflammatory cytokines and their impact on neuronal excitability." Neuropharmacology **96**: 70-82.

**Vichaya, E. G., G. S. Chiu, K. Krukowski, T. E. Lacourt, A. Kavelaars, R. Dantzer, C. J. Heijnen and A. K. Walker** (2015). "Mechanisms of chemotherapy-induced behavioral toxicities." Frontiers in neuroscience **9**: 131.

**Vincent, J. A., H. M. Gabriel, A. S. Deardorff, P. Nardelli, R. E. Fyffe, T. Burkholder and T. C. Cope** (2017). "Muscle proprioceptors in adult rat: mechanosensory signaling and synapse distribution in spinal cord." Journal of neurophysiology **118**(5): 2687-2701.

**Vincent, J. A., P. Nardelli, H. M. Gabriel, A. S. Deardorff and T. C. Cope** (2015). "Complex impairment of IA muscle proprioceptors following traumatic or neurotoxic injury." Journal of anatomy **227**(2): 221-230.

**Vincent, J. A., K. B. Wieczerzak, H. M. Gabriel, P. Nardelli, M. M. Rich and T. C. Cope** (2016). "A novel path to chronic proprioceptive disability with oxaliplatin: distortion of sensory encoding." Neurobiology of disease **95**: 54-65.

**Wagenmakers, E.-J.** (2007). "A practical solution to the pervasive problems ofp values." Psychonomic bulletin & review **14**(5): 779-804.

**Wang, J., X.-S. Zhang, R. Tao, J. Zhang, L. Liu, Y.-H. Jiang, S.-H. Ma, L.-X. Song and L.-J. Xia** (2017). "Upregulation of CX3CL1 mediated by NF-κB activation in dorsal root ganglion contributes to peripheral sensitization and chronic pain induced by oxaliplatin administration." Molecular pain **13**: 1744806917726256.

**Wang, X.-M., B. Walitt, L. Saligan, A. F. Tiwari, C. W. Cheung and Z.-J. Zhang** (2015). "Chemobrain: a critical review and causal hypothesis of link between cytokines and epigenetic reprogramming associated with chemotherapy." Cytokine **72**(1): 86-96.

**Warnes, M. G. R., B. Bolker, L. Bonebakker and R. Gentleman** (2016). "Package 'gplots'." Various R Programming Tools for Plotting Data.

**Washington, M. K., A. E. Powell, R. Sullivan, J. P. Sundberg, N. Wright, R. J. Coffey and W. F. Dove** (2013). "Pathology of rodent models of intestinal cancer: progress report and recommendations." Gastroenterology **144**(4): 705-717.

**Watanabe, S.** (2010). "Asymptotic equivalence of Bayes cross validation and widely applicable information criterion in singular learning theory." Journal of Machine Learning Research **11**(Dec): 3571-3594.

**Waxman, S. G. and G. W. Zamponi** (2014). "Regulating excitability of peripheral afferents: emerging ion channel targets." Nature neuroscience **17**(2): 153.

**Weber, D., R. Stein, D. Everaert and A. Prochazka** (2007). "Limb-state feedback from ensembles of simultaneously recorded dorsal root ganglion neurons." Journal of Neural Engineering **4**(3): S168.

**Webster, R. G., K. L. Brain, R. H. Wilson, J. L. Grem and A. Vincent** (2005). "Oxaliplatin induces hyperexcitability at motor and autonomic neuromuscular junctions through effects on voltage-gated sodium channels." Br J Pharmacol **146**(7): 1027-1039.

**West, N. R., S. McCuaig, F. Franchini and F. Powrie** (2015). "Emerging cytokine networks in colorectal cancer." Nature reviews Immunology **15**(10): 615-629.

**Woo, S.-H., V. Lukacs, J. C. De Nooij, D. Zaytseva, C. R. Criddle, A. Francisco, T. M. Jessell, K. A. Wilkinson and A. Patapoutian** (2015). "Piezo2 is the principal mechanotransduction channel for proprioception." Nature neuroscience **18**(12): 1756.

**Wood, L. J., L. M. Nail, N. A. Perrin, C. R. Elsea, A. Fischer and B. J. Druker** (2006). "The Cancer Chemotherapy Drug Etoposide (VP-16) Induces Proinflammatory Cytokine Production and Sickness Behavior–like Symptoms in a Mouse Model of Cancer Chemotherapy–Related Symptoms." Biological research for nursing **8**(2): 157-169.

**Yamamoto, K., M. Tsuboi, T. Kambe, K. Abe, Y. Nakatani, K. Kawakami, I. Utsunomiya and K. Taguchi** (2016). "Oxaliplatin administration increases expression of the voltage-dependent calcium channel alpha2delta-1 subunit in the rat spinal cord." J Pharmacol Sci **130**(2): 117-122.

**Yamamoto, S., H. Ono, K. Kume and M. Ohsawa** (2016). "Oxaliplatin treatment changes the function of sensory nerves in rats." J Pharmacol Sci **130**(4): 189-193.

**Zheng, Q., D. Fang, J. Cai, Y. Wan, J.-S. Han and G.-G. Xing** (2012). "Enhanced excitability of small dorsal root ganglion neurons in rats with bone cancer pain." Molecular pain **8**(1): 24.